COMPOSITE RIGHT/LEFT HANDED ANTENNAS FOR WIRELESS LAN APPLICATIONS

Sheeja K. L.

Department of Electrical Engineering
National Institute of Technology
Rourkela, India
April, 2014

COMPOSITE RIGHT/LEFT HANDED ANTENNAS FOR WIRELESS LAN APPLICATIONS

Thesis submitted
in partial fulfillment of the requirement for the degree of

Doctor of Philosophy

in

Electrical Engineering

By

Sheeja K. L.
(Roll No. 509EE109)

Under the guidance of

Dr. Prasanna Kumar Sahu
Department of Electrical Engineering

and

Dr. Santanu Kumar Behera
Department of Electronics and Communication Engineering

Department of Electrical Engineering
National Institute of Technology
Rourkela, India
April, 2014

Dedicated To

Devi Kali Maa

Declaration

I certify that

- The work contained in this thesis is original and has been done by me under the guidance of my supervisor (s).
- The work has not been submitted to any other Institute for the reward of any other degree or diploma.
- I have followed the guidelines provided by the Institute in preparing the thesis.
- I have confirmed to the norms and guidelines in the Ethical Code of Conduct of the Institute.
- Whenever I used materials (data, theoretical analysis, figures and text) from other sources, I have given due credit to them by citing them in the text of the thesis and giving their details in the references. Further, I have taken permission from the copyright owners of the sources, whenever necessary.

April 2014

Sheeja K. L.
(509EE109)

Department of Electrical Engineering
National Institute of Technology Rourkela
Rourkela-769008, Orissa, India

CERTIFICATE

This is to certify that the thesis entitled "**COMPOSITE RIGHT/LEFT HANDED ANTENNAS FOR WIRELESS LAN APPLICATIONS**" being submitted by **Sheeja K. L.** for the degree of Doctor of Philosophy in Engineering from N.I.T. Rourkela is a record of bonafide research work carried out by her under our supervision at the Department of Electrical Engineering. In our opinion, this is an authentic piece of work for submission for the degree of Doctor of Philosophy. To the best of our knowledge, the work has not been submitted to any other University or Institute for the award of any degree or diploma.

Supervisor:

Dr. P. K. Sahu
Associate Professor,
Department of Electrical Engineering,
N. I. T. Rourkela,
Rourkela-769008.
E-mail id: pksahu@nitrkl.ac.in
Phone No: +91-661-2462413 (O),

Co-Supervisor:

Dr. S. K. Behera
Associate Professor,
Department of Electronics and
Communication Engineering,
N. I. T. Rourkela,
Rourkela-769008.
E-mail id: skbehera@nitrkl.ac.in
Phone No: +91-661-2462462 (O),

Acknowledgements

The hardest arithmetic to master is that which enables us to count our blessings.

~ Eric Hoffer

First and foremost, I would like to express my deep and sincere regards for my supervisor, *Prof. Prasanna Kumar Sahu* for providing me the opportunity, support and freedom to carry on this research work. His passion, guidance, and discipline have been indispensable to my growth as a scientist and as a person over these past four years. I am especially grateful for his devotion to his students' education and success. I would also like to express my heartfelt gratitude to my co supervisor *Prof. Santanu Kumar Behera* for his painstaking patience in correcting all the articles. I am grateful for his advice and guidance which is simply exemplary.

Special thanks to *Prof. S. K. Sarangi*, Director, NIT Rourkela for providing all the facilities. I would like to express my gratitude to the Head of Department, *Prof. A. K. Panda* for extending kind support and cooperation in my thesis work, despite his hectic schedules. Heartfelt thanks to my Doctoral Scrutiny Members *Prof.B. D. Subudhi*, *Prof. S. K. Patra, Prof. S. Meher, Prof. D. Patra* and *Prof. S. K. Jena*.

I would also like to thank *Prof. D. R. Poddar*, Jadavpur University, Kolkata, India for providing simulation facilities at his laboratory. Thanks are also due to *Mr. K. Srinivas Reddy*, General Manager, Atlantic Circuits, Hyderabad for fabrication of the antennas proposed in this thesis at his organisation and for his continued support throughout the research period. I thank from the bottom of my heart, *Prof. R. K. Mishra*, Dept. of Electronic science, Berhampur University, Orissa, for his support and good will through all my years.I am especially indebted to *Mr. R. K.Malaviya*, Secretary of Antenna Testing and Measurement Society (ATMS), *Mr. Rajeev Jyoti*, Group Director, *Mr. H.C. Sanandiya*, Head AMF and *Antenna System Group members of Space Application Centre, ISRO, Ahmedabad* for carrying out measurement facilities in their laboratory towards furtherance of this research work. Thanks to *Prof. Vasudevan Kesavath*, CUSAT, Cochin, Kerala for providing measurement facility in his antenna and microwave lab. Also, thanks are due to *Mr. Nijas Muhammed*, CUSAT for his support during the measurement of antenna.Special thanks are extended to *Mr. Kishore Kujur*, senior technical assistant, Electronics and Communication Department for giving a final touch to the fabricated antennas.

I would like to acknowledge my Laptop and Desktop. I want to thank 'them' for their essential support in this project, as, without them, all of my work, from the thought process, to the simulations, to the actual writing up, would not have been possible. They have granted me the possibility to do whatever I want, to experiment on my thoughts, to write my ideas down, and to share them with the world. I know they are just pieces of hardware to anybody else, but to me, they are an extension of my being and without them, it is hard to be me.

Last, but not the least I would express my sincere gratitude to my *family* for their love, sacrifice and moral support for without their continued support this work would never have been possible. Also my sincere gratitude goes to *Mr. Nabil Dakhli,* Research Unit of Telecommunication Systems (6Tel) at Sup'Com, Tunisia whose initial help and encouragement motivated me in this work. Finally my gratitude goes to the lizard who kept me company throughout day and night in our microwave and antenna lab which ultimately succumbed to death due to heat stroke during the summer of my third year of research work. It inspired me to carry my work diligently and we have yet to learn so many things from our mother nature and metamaterials is one such inspired beautiful gift.

I would finally like to thank the almighty for making this experience possible with the following verses

'O Mother, I am the machine and Thou art the Operator.

I am the house and Thou art the indweller.

I am the chariot and Thou art the Charioteer.

I do as Thou makest me do. I speak as Thou makest me speak;

I move as Thou makest me move. It is not I !

It is all Thou ! It is all Thou !'

Hers is the glory; we are only Her instruments

Sheeja K. L.

ABSTRACT

The term ‘metamaterial’ has become a buzzword in electromagnetics over the past decade. In recent years, advancement in this new scientific area has given birth to numerous discoveries and inventions based on the exotic properties exhibited by these materials. Some of the exotic properties like negative permittivity, negative permeability, and infinite propagation at a particular non-zero resonant frequency are shown by these artificial materials especially called as Composite Right Left Handed structures. Metamaterials gain these properties from their structural configuration rather than from their material constitution. The electromagnetic characteristics of metamaterials can be exploited to meet the ever increasing demand for lighter, compact, size reduced, multiband antennas. One of the most exciting applications of these CRLH transmission lines (TL) is the Zeroth Order Resonant Antennas. CRLH TL metamaterials when open or short ended produce standing waves and thus behave as resonant antennas. Miniaturization of antennas is possible through these structures as the resonant frequency is independent of the parameters of the antenna aperture. Due to their infinite wavelength propagation property; reduced size, quarter wavelength antennas can be designed.

This thesis focuses on realization of different structural designs of CRLH based zeroth order resonant (ZOR) antennas with enhanced bandwidth. Its applicability in wireless LAN applications is investigated. Three novel ZOR antennas with enhanced bandwidth for wireless LAN applications are proposed. As a stepping stone, the performance attributes of a conventional microstrip based CRLH ZOR antenna is studied. The effect of parametric analysis and optimization using Ansoft Optimetrics is presented. The antennas are simulated using Ansoft HFSSv12, consequent to which they are fabricated and experimentally validated at Space application Centre (SAC), ISRO, Ahmedabad, India. The bandwidth is enhanced to almost 9% in the proposed structures, which is quite remarkable in comparison to just 0.75% in the case of microstrip based CRLH resonant antennas. Wide bandwidth radiation pattern in the E-plane and an omni-directional one in H-plane is achieved. The proposed ZOR antennas are germane for multiband wireless LAN communications with wide coverage areas and holds high promise in the realm of small antennas.

BIO-DATA

Sheeja K. L.

Date of Birth: 28th November, 1977

Correspondence:

PhD Scholar, Department of Electronics and Communication Engineering,
National Institute of Technology, Rourkela, India – 769 008.
Ph: +91 9438168522 (M)
e-mail: sheejakl@gmail.com

Qualification

• Ph.D. (Continuing)
National Institute of Technology, Rourkela, India

• M.Tech. (Electrical Engineering)
National Institute of Technology, Rourkela, India.

• B.E.
Biju Patnaik University of Technology, Rourkela, Odisha, India.

• B.Sc
Sambalpur University, Sambalpur, Odisha.

• 12th (Science)
Central Board of Secondary Education, Rourkela, Odisha, India.

• 10th
Central Board of Secondary Education, Rourkela, Odisha, India.

Publications

• 3 Journal articles;
• 1 Journal article communicated;
• 11 Conference articles.

Awards

Young Scientists Travel Grant award from DST
Best paper award
Institute Fellowship

CONTENTS

List of Figures

List of Tables

Acronyms and Abbreviations

1D	One Dimensional
2D	Two Dimensional
3D	Three Dimensional
AMF	Antenna Measurement Facility
BE	Backfire-to-endfire
BZ	Brillouin zone
CRLH	Composite Right/Left Handed
CUSAT	Cochin University of Science and Technology
D	Directivity
DGS	Defected Ground Structures
DNM	Double Negative Material
FEM	Finite Element Method
G	Gain
GSM	Global System for Mobile
HFSS	High Frequency Structure Simulator
ISRO	Indian Space Research Organisation
LW	Leaky-Wave
LH	Left-handed
LHM	Left Handed Material
MIM	Metal-insulator-metal
MTM	Metamaterial
NRI	Negative refractive index
PBCs	Periodic boundary conditions
PBG	Photonic band-gap
PLH	Purely left-handed
PRH	Purely right-handed
PCB	Printed Circuit Board
Q	Quality Factor
RF	Radio Frequency
RH	Right-handed
RHM	RH Material
RFID	Radio Frequency Identification
SRR	Split-Ring Resonator
SMT	Surface-Mount Technology
SAC	Space Application Centre
TL	Transmission Line
TM	Transverse Magnetic
TE	Transverse Electric
TEM	Transverse Electro-Magnetic
UMTS	Universal Mobile Telecommunications System
VNA	Vector Network Analyzer
VSWR	Voltage Standing Wave Ratio
WLAN	Wireless Local Area Network
WiMax	World-wide interoperability for Microwave access
ZOR	Zeroth Order Resonator

List of Symbols

η	refractive index
c	velocity of light in vacuum
ε	permittivity
ε_r	relative permittivity
μ	permeability
μ_r	relative permeability
M_s	magnetic current densities
J_s	electric current densities
ρ_m	magnetic charge densities
ρ_e	electric charge densities
$\overline{E}$	electric field intensity
$\overline{H}$	magnetic field intensity
$\overline{D}$	electric flux density
$\overline{B}$	magnetic flux density
β	wave vector/ phase constant
γ	propagation constant
α	attenuation constant
$\overline{S}$	Poynting vector
θ_1	angle of incidence
θ_2	angle of refraction
λ_g	guided wavelength
v_p	phase velocity
v_g	group velocity

Z' per unit length impedance

Y' per unit length admittance

C_R right handed capacitance

L_R right handed inductance

C_L left handed capacitance

L_L left handed inductance

ω_{se} series resonance

ω_{sh} shunt resonance

Z_L load impedance

Z_{in} input impedance

θ electrical length

m resonance index

Chapter 1

Introduction

"Antennas form the core of all wireless systems". Low profile, multiband antennas have been one of the most significant and interesting subjects in antenna and related fields. Since the beginning of radio communication, the desire for small and versatile antennas has been increasing. Today's needs for more multifunctional systems further drive requirements for small mobile terminals including cell-phones, handheld portable wireless devices for internet connection, short and long range communication equipments, Radio Frequency Identification (RFIDs), etc. Similarly small equipments and devices used for data transmission and navigation (GPS systems) require small antennas with omni-directional radiation patterns [1]. These applications along with continuing growth of wireless devices continue to challenge the community to create low profile multifrequency antennas.

For reducing antenna size and volume, traditional miniaturisation methods such as shorting pins [2], meandering [3] and dielectric loading [4] are adopted. This often results in low radiation efficiency, narrow bandwidth and undesired radiation patterns. Therefore, in recent years, a strong interest has been generated on using periodic structures to lower antenna profile as a method to optimize or enhance antenna performance. These designs exploit resonance phenomena which are unique to the makeup of periodic (planar or volumetric) structure and not necessarily the constituent materials. The latter are referred to as "metamaterials" (from the Greek as "next" materials, i.e. next generation materials), engineered or simply artificial materials. Metamaterials are typically constructed from periodic arrangements of conventional materials to exhibit electromagnetic properties not found in any of their bulk individual constituents. Over the last decade, theory and practical implementation of metamaterials at microwave frequencies have been an extensive area for research. An early boost to this research was the initial experimental verifications of electromagnetic band gap structures (EBG's) [5] and negative refractive index media (NRI or equivalently $\varepsilon<0 and \mu<0$ media) [6, 7]. Since then, NRI metamaterials were studied to demonstrate sub-wavelength focusing for greater sensitivity [8] in lens systems. Printed circuit realizations of metamaterials led to smaller radio frequency (RF) devices such as phase shifters, couplers and antennas [9, 10].

Latest technology to achieve the purpose is made possible through scientific breakthroughs in the field of Composite Right/Left Handed (CRLH) Metamaterials especially the *Zeroth Order mode Resonators* (ZOR) which is the basis of the research done in this thesis. The radiation principle of ZOR antennas is based on a *resonance mechanism* where the operating wave is a *standing wave* exhibiting uniform-phase field distribution along the structure which leads to broadside radiation and constructive field interference above the structure further allows this radiation. In fact in these antennas, the overall structure resonates due to open/short boundary conditions rather than its structural elements or unit cells. Due to the unique nature of this zeroth order mode, the size of the resonator does not depend on its

physical length but only on the amount of reactance provided by its unit cells. The size of the resonator is thus limited just by the minimal size of its constituent cells. This property is extensively studied to realize wide variety of miniature and multiband antennas over recent years. Metamaterials when introduced into an antenna system to guide specifics of a design provide exciting challenges for antenna engineers to meet the need for an increasing demand for wireless products [11].

1.1 Modern Wireless Communication Services

Antennas have wide range of applications throughout the electromagnetic spectrum. In order to avoid the congestion during the communication process and to reduce the interference from multiple users, Federal Communications Commission (FCC) allocated frequency bands for different applications. The different frequency bands allocated by the governing council is given in Table.1.1 with corresponding category of antennas commonly used.

Table 1.1 Wireless Communication [12-15]

Name of the Wireless Communication service	**FCC Allocated Frequency Band**	**Commonly used Antennas**
Digital Video Broadcasting (DVB-H)	470MHZ-702MHz	Compact printed Antennas
Radio Frequency Identification (RFID)	865-868MHz, 2.446-2.454GHz	Loops, Folded-F, Patch and Monopole
Global System for Mobile (GSM 900)	890MHz-960MHz	Dipole, patch arrays and Monopoles.
Global Positioning System (GPS1400, GPS1575)	1227MHz -1575MHz, 1565MHz-1585MHz	Microstrip patch or bifilar helix
Personal Communication System (PCS 1900)	1850MHz-1990MHz	
International Mobile Telecommunication-2000 (3G IMT-2000)	1885MHz-2200MHz	
Universal Mobile Telecommunication Systems (UMTS 2000)	1920MHz-2170MHz	
WLAN ISM-2.4 (Bluetooth), ISM-5.2, ISM-5.8 *Industrial ,Scientific, Medical (ISM)*	2400MHz-2484MHz, 5150MHz-5350MHz, 5725MHz-5825MHz	

1.2 Antennas for Wireless LAN Applications: An Overview

A major development in antenna technology is the WLAN applications and will continue to grow in the foreseeable future. In the evolution of the Wireless LAN (WLAN) communications (Figure 1.1), different frequency bands have been allocated with the release of newly developed standards. Under IEEE 802.11n standard, it is required to include the MIMO techniques, which implies that more than one antenna has to be equipped in one device [16]. Enhancements to 802.11n are under development as part of the newer released IEEE 802.11ac.

With newer wireless technologies, the selection of operating frequencies is widening and allocated frequency bands are getting lower which creates demand for more antenna area and volume on the device, especially with handheld and portable devices. Therefore, physical size has taken an increased importance in antenna design. It is a growing trend in antenna engineering to design compact antennas or antenna arrays that can operate at multiple commercial frequency bands including GSM, UMTS, WLAN and WiMAX applications. Size reduction, adequate bandwidth, multimode operation etc. are the essential design consideration for practical applications.

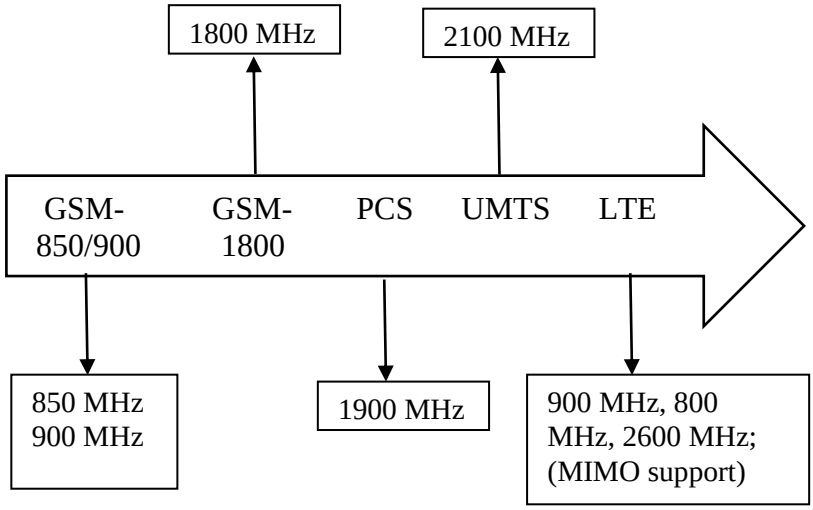

Figure 1.1 The evolution of the Wireless LAN standards [19].

For instance, in case of mobile phone communication system, the first mobile phone antennas were simple monopole or spiral antennas, operating at a single frequency band, located outside the shell of mobile devices. Modern mobile phones or laptop dongles might have almost ten operating bands that all need to be implemented in one device. To support different mobile networks, it is required to have the handset be equipped with a multiband antenna, a quad-band or even penta-band antenna for example, or multiple antennas. Long Term Evolution systems require Multiple Input Multiple Output techniques to be employed on mobile devices [17, 18]. To enable one mobile device to support all of these wireless protocols, at the physical layer, it is imperative to have one multiband antenna or even a multiband array antenna integrated on this mobile device [19].

Various multiband antennas have also received considerable attention for multimode communication systems such as dipole, monopole [20], cylindrical patch array [1] and planar dipole antenna [21, 22]. However, these antennas are very complicated in structure and their large size needs to be miniaturized in order to meet the demands of portable devices. Currently popular antenna structures suitable for applications to wireless local area network (WLAN) and world-wide interoperability for microwave access (WiMax) have been reported [23-26]. The challenge in designing a WLAN/WiMax system is to design a compact, low-cost, lightweight and low profile antennas so as to fit into the limited space of WLAN and WiMax devices. The planar microstrip antenna is considered a good candidate for multiband WLAN applications because of its low profile and etched on a single substrate [27], [28]. To achieve multi-band operation, the traditional method is to employ multi-resonator elements [20], which often leads to a large volume [29-31] or requires a large ground-plane [32]. In [23], Kuo et al. proposed a dual-band double T-monopole antenna, which achieves a certain miniaturization factor but with a narrow bandwidth at the upper WLAN band. Other processes normally employed for multiband monopole antennas is the use of slots, such as half-wavelength slots [33] or quarter-wavelength open slots, and due to size advantage over the half-wavelength slots, quarter-wavelength open slots are more preferred for multiband antenna designs. The L-shaped [34], double T-shaped [35], Z-shaped [36] and C-shaped [37] slots are reported to provide multiband solutions. In [45, 46], the dual-band operation is achieved by etching annular-ring slots in ground or adding U-shaped strips to wide slot. Although these antennas exhibit multiband property but are too large in size to be used in small communication terminals. Slot antennas also suffer from back radiations if the substrate is relatively thin and surface wave losses if the substrate is relatively thick thus reducing the efficiency of these antennas.

Latest technique to achieve multiband is to use Defected Ground Structure (DGS) with parasitic stubs [42-44] or metallic holes [40, 41] to introduce additional resonant modes. Hybrid antennas composed of a simple monopole and parasitic element are reported in [38, 39], [28] to achieve dual or triple bands. But these structures lead to large antenna apertures and fails to exhibit stable omni-directional radiation patterns which is a major requirement in WLAN applications. Furthermore, designing a multiband antenna by including an extra antenna element to make an antenna array will lead to an increase of the overall antenna volume. However, the fact is that the available volume for antenna design keeps on decreasing as it is desirous to have one wireless device, especially a portable one, as compact as possible.

It is well known fact that theoretically the antenna's performance degrades when the size of the antenna is reduced. Some of the parameters that suffer in this process are:

- Reduced efficiency (or gain),
- Shorter range,
- Smaller useful bandwidth,
- More critical tuning,
- Increased sensitivity to component and PCB spread,

• Increased sensitivity to external factors.

Current internal antenna designs are already pushing the limit of fundamental performance of electrically small antennas. Metamaterials (MTM), in turn, allows a conceptual path for implementing small multiband resonant antennas [24, 25]. Since a zeroth order resonating antenna supports infinite propagation at the zeroth mode and dissipative losses are minimum. Therefore, designing compact, multiband antennas using metamaterials for WLAN applications further needs to be explored.

1.3 Metamaterials

There has been growing interest theoretically as well as experimentally in the scientific community for the study of metamaterials. Materials simultaneously exhibiting negative permittivity and permeability is referred to as double negative material (DNM) or left-handed metamaterials (LHM). These materials belong to the fourth quadrant of the constituent parameter based material landscape illustrated in Figure 1.2. Science magazine even named Left Handed Metamaterials (LHM) as the top 10 scientific breakthroughs of 2003. Electromagnetic metamaterials (MTMs) are artificially structured composite materials whose average cell size should be at least smaller than a quarter of wavelength ($p\langle\lambda_g/4$) [9]. This condition $p=\lambda_g/4$ otherwise known as the *effective-homogeneity condition,* when satisfied ensures predominance of *refractive phenomena* over *scattering/ diffraction* phenomena when a wave propagates inside such a media. The material then behaves as a real material in the sense that electromagnetic waves are essentially *myopic to the lattice* or are effectively macroscopic with well-defined *constitutive parameters*. Since, these parameters depends on the nature of the unit cell, therefore it renders the structure to be electromagnetically uniform along the direction of propagation. The constitutive parameters are the permittivity ε and permeability μ, which are related to the refractive index n by $n=\pm\sqrt{\varepsilon_r\mu_r}$, where ε_r and μ_r are the relative permittivity and permeability.

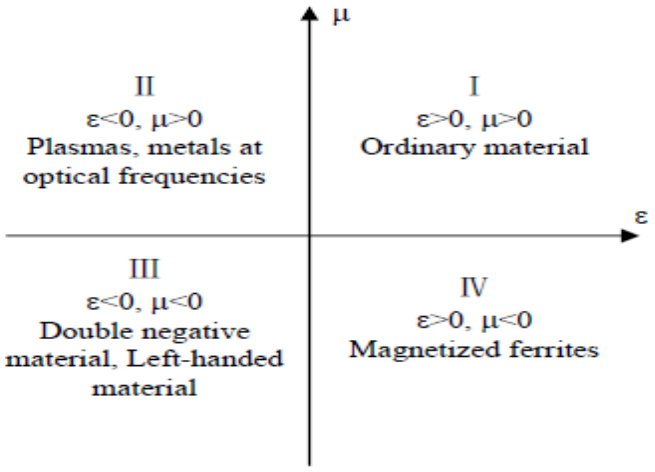

Figure 1.2 All possible combinations of permittivity and permeability [9].

In 1898 J. C., Bose [47] first attempted to explore the concept of artificial materials with twisted structures; geometries that were essentially artificial chiral elements by today's terminology. In 1905, Lamb [48] suggested the existence of backward waves from reflection directions based on the signs of permittivity and permeability. In late 1940s W. E. Kock developed the first artificial dielectric materials with metal-lens antennas [49] and metallic delay lenses [50]. General properties of wave propagation in metamaterial structures were first outlined by Victor Veselago in 1968 who predicted its properties [51] of exhibiting simultaneously existing negative permittivity (ε) and permeability (μ) from physics point of view. He theoretically analysed and concluded that the direction of Poynting vector in such materials is anti-parallel to the direction of phase velocity. Therefore, he first coined the term Left handed (LH); as $\overline{E}$, $\overline{H}$ *and* $\overline{\beta}$ vectors of the electromagnetic wave form a left- handed triad. He also predicted the existence of other unique properties such as reversal of Snell's law, Doppler Effect, negative refraction and amplification of evanescent waves.

In 1999, Pendry at Imperial College, London introduced the *plasmonic-type* (negative-ε/positive-μ or positive-ε/negative-μ) structures, which can be engineered to have their *plasmonic frequency in the microwave range.* Both these structures have their average cell size much smaller than the guided wavelength λ_g and are therefore effectively homogeneous structures [7, 52].

In 2000 Smith et al., at the University of California, San Diego (UCSD) first experimentally verified LH material phenomena [6]. They used metal split ring resonators and a bundle of thin straight metal wires to practically verify the existence of simultaneous negative values of ε and μ and thus obtained negative refractive index over a finite band of frequencies in the microwave region. Thereafter repeated research continued in this area which confirmed UCSD's findings [53-56]. However due to the lossy and narrow bandwidth characteristics, they are hard to implement in the range of microwave frequencies. This drawback restricted their use in many different applications.

An alternative approach pertaining to transmission line approach of metamaterials popularly named as Left Handed Materials (LHM) was developed. This idea of using the transmission line theory to describe and design LH material was first introduced in June 2002 by Caloz group [57]. From TL approach, it was concluded that a physical existence of LH material is in fact Composite Right/Left Handed (CRLH) in nature, exhibiting left handedness in low frequencies and right handedness in high frequencies due to inevitable parasitic right handed effects. It is implemented on non-resonant structures with low loss and wider bandwidth and engineered in planar configurations so as to integrate it with modern microwave integrated circuits (MICs). Further exploration in metamaterial application led to the development of several microwave devices such as superlenses [58], microwave couplers [59] and leaky wave antennas [60]. Wide varieties of beam steerers, modulators, band-pass filters, and antenna radomes could be developed in the near future.

1.4 Special Properties of Left-Handed Metamaterials

There has been tremendous interest in LH metamaterials ever since they were experimentally verified. The main reason for this interest is the extraordinary properties that they exhibit. Some of the physical phenomena which occur in natural (right-handed) materials are seen to be totally reversed in LH materials. This makes the LH materials very useful for a lot of existing and novel applications. Some of the special properties of LH materials are explained in this section.

1.4.1 Backward Wave Propagation

Backward wave propagation is essentially the origin of the term 'left-handed' materials by Veselago [51]. It can be better explained by initially considering the wave form of Maxwell's equations:

$$\left(\nabla^2 - \frac{\eta^2}{c^2}\frac{\partial^2}{\partial t^2}\right)\psi = 0 \tag{1.1}$$

where, η is the refractive index and c is the velocity of light in vacuum, which are related as:

$$\frac{\eta^2}{c^2} = \varepsilon\mu \tag{1.2}$$

Hence when the square of the refractive index is considered, there is no effect due to the simultaneous negative values of ε and μ. The intuition from this is that the solutions to the Maxwell's equation in wave form do not change even with simultaneously negative values of ε and μ.

However considering Maxwell's equations in time harmonic form:

$$\nabla \times \overline{E} = -j\omega\mu\overline{H} - \overline{M}_s, \quad \text{(Faraday's law)} \tag{1.3}$$

$$\nabla \times \overline{H} = j\omega\varepsilon\overline{E} + \overline{J}_s, \text{(Ampere's law)} \tag{1.4}$$

$$\nabla \cdot \overline{D} = \rho_{e,} \quad \text{(Electric Gauss' law)} \tag{1.5}$$

$$\nabla \cdot \overline{B} = \rho_{m,} \quad \text{(Magnetic Gauss'law)} \tag{1.6}$$

and

$$\overline{D} = \varepsilon\overline{E}, \tag{1.7}$$

$$\overline{B} = \mu\overline{H} \tag{1.8}$$

where M_s (V/m^2) and J_s (A/m^2) are the magnetic and electric current densities, respectively. Also, ρ_m (Wb/m^3) and ρ_e (C/m^3) are respectively, magnetic and electric charge densities. As usual, $\overline{E}$ stands for electric field intensity (V/m), $\overline{H}$ denotes the magnetic field intensity (A/m), $\overline{D}$ is the electric flux density (C/m^2) and $\overline{B}$ is the magnetic flux density (Wb/m^2). It

is predictable that for simultaneous negative values of ε and μ the solutions are quite different. The electric and magnetic field vectors for a planar wave are given as:

$$\overline{E} = \overline{E}_0 e^{(-j\overline{\beta}r + j\omega t)} \tag{1.9}$$

$$\overline{H} = \overline{H}_0 e^{(-j\overline{\beta}r + j\omega t)} = \frac{\overline{E}_0}{\eta} e^{(-j\overline{\beta}r + j\omega t)} \tag{1.10}$$

where, $\eta = \left|\overline{E}\right| \Big/ \left|\overline{H}\right|$ denotes the wave impedance. For simplicity, let us consider a loss-less medium in regions without sources ($\overline{M}_s = \overline{J}_s = 0$). In the case of RH medium, therefore

$$\overline{\beta} \times \overline{E} = \omega\mu\overline{H} \tag{1.11a}$$

$$\overline{\beta} \times \overline{H} = -\omega\varepsilon\overline{E} \tag{1.11b}$$

It is evident from these two equations that for positive values of $\varepsilon and \mu,$ the electric field, magnetic field and wave vectors form a right-handed triplet.

For negative values of $\varepsilon and \mu,$

$$\overline{\beta} \times \overline{E} = -\omega|\mu|\overline{H} \tag{1.12a}$$

$$\overline{\beta} \times \overline{H} = \omega|\varepsilon|\overline{E} \tag{1.12b}$$

which indicates that the $\overline{E}$, $\overline{H}$ *and* $\overline{\beta}$ vectors now form a left-handed triplet.

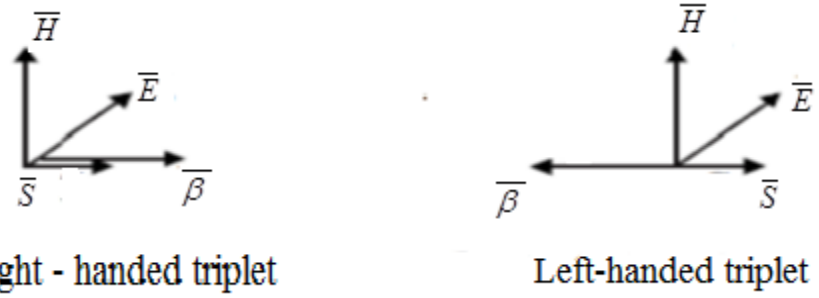

Figure 1.3 System of vector $\overline{E}$, $\overline{H}$, $\overline{S}$ and $\overline{\beta}$ in conventional and Left-Handed media.

The impact of the above result can be seen in Figure 1.3. The propagation of the wave is now seen to be in a direction opposite to that of the direction in a normal (right-handed) material. It is also important to note that the direction of the Poynting vector S does not change. This phenomenon is referred to as *Backward-wave* propagation.

1.4.2 Negative Refractive Index

One of the most interesting properties of LH materials is the reversal of the fundamental Snell's law of refraction. According to Snell's law:

$$\frac{\sin\theta_1}{\sin\theta_2} = \frac{\eta_2}{\eta_1} \rangle 0 \tag{1.13}$$

where η_1 is the refractive index of the incident medium, η_2 is the refractive index of the refracted medium, θ_1 is the angle of incidence, and θ_2 is the angle of refraction.

When both the incident and the refracted media are conventional materials, the angle of incidence and the angle to refraction have the same signs. However, when the refracted medium is a LH material, θ_1 and θ_2, have opposite signs. This follows directly from the concept of Backward wave propagation in LH materials which has been explained in the previous section. Hence it follows that when the refracted medium is a LH material,

$$\frac{\sin\theta_1}{\sin\theta_2} = \frac{\eta_2}{\eta_1} \langle 0 \tag{1.14}$$

Since the refractive index of any conventional material is positive, $\eta_1 \rangle 0.$ This implies that the refractive index of the LH metamaterial, $\eta_2 \langle 0.$ The implication of this result is that when LH are used, convex lenses which are normally convergent become divergent and concave lenses which are normally divergent become convergent [51].

1.4.3 Reversal of Doppler Effect

A popular concept useful in many applications is the Doppler Effect which is the shift in the frequency of the wave observed from a source depending on the relative velocity of the observer and the source. For any medium this implies that when the observer is moving towards the source, the wave and the observer are moving in opposite directions and hence the frequency of the wave shifts upwards. The frequency shifts downwards when the observer moves away from the source.

However in a LH medium, backward wave propagation occurs and hence when the observer moves towards the source the wave propagates in the same direction and hence the frequency shifts downwards. The frequency shifts upwards when the observer moves towards the source. This is a reversal of the Doppler Effect described above. This has been proven both theoretically [51, 9] and experimentally [61].

1.5 Motivation

The urge of the antenna designers to reduce the size and to improve the radiation characteristics are satisfied by the introduction of metamaterials. Metamaterials have been widely researched for antenna applications. Compact multiband antennas for Wireless Local Area Network (WLAN) applications with omni-directional radiation patterns are in huge demand nowadays. In recent years, metamaterials in particular as zeroth order resonant antennas have drawn considerable attention for the design of compact antennas [62-64]. Compact metamaterial antennas with omni-directional radiation patterns serve the above purpose. Since these antennas are inherently multiband, so it will be an asset to employ these antennas for WLAN applications. Conventional patch antennas if loaded with metamaterials can increase the radiated power of an antenna. Lighter, cheaper and more energy efficient broadband antennas on communication satellites are possible by using metamaterials. Less cost is incurred to boost lighter antennas into space. Energy efficient antennas reduces the size of storage batteries and solar cells thereby reducing large volumetric spaces occupied by these cells. Metamaterial antennas possess higher potential to overcome restrictive efficiency and bandwidth limitations suffered by conventionally constructed electrically small antennas. Metamaterial antennas can be engineered to cover a wider frequency range, thus making better use of available space for small platforms by allowing smaller antenna elements. Metamaterial antennas satisfy this aspect by enabling the antennas to be sized on the order of one-tenth the signal's wavelength and yet providing performance at par or better than conventional half wavelength antennas. Thereby providing five times the size reduction in comparison to conventional patch antennas. Metamaterial antennas employed in the ground planes offers improved isolation between radio frequency and MIMO antenna arrays. These high-impedance ground planes can also be used to improve the radiation efficiency and axial ratio performance of low-profile antennas located near the ground plane. By using the backward wave and forward wave concept of metamaterials, beam-scanning range of Leaky Wave antennas can remarkably be enhanced. Metamaterial antennas have proven to exhibit unparalleled performance and is continuously being researched by the researchers to open up the gates for various other possibilities, which seemed to have been unachievable even a few years back.

In this thesis different types CRLH based zeroth order resonant antennas are proposed with operating frequency ranging from 0.5 GHz to 5 GHz. They are designed to be compact with additional features to provide multifrequency and multifunctionality bands. They exhibit omni-directional radiation pattern with wide coverage area thus making it highly suitable for IEEE 802.11 a/b/g/n standards of Wireless Local Area Network applications. Some of the drawbacks often suffered by these antennas such as narrow bandwidth, fabrication complexity and low antenna gain problem have been addressed.

1.6 Problem Statement

To design and develop CRLH TL antennas based on zeroth order resonance concept for wireless applications in the frequency range of 2.4 GHz to 5 GHz (specifically for WLAN).

- Investigation of bandwidth, gain and radiation efficiency characteristic of CRLH TL antennas using microstrip technique.
- Investigation of gain, radiation efficiency and bandwidth enhancement of CRLH TL antennas using coplanar waveguide technique by incorporating structures such as
  (i) Spirals with via based rectangular radiating patch (using single and double unit cells).
  (ii) Spiral and anti-Spiral with via-less rectangular and elliptical radiating patch.

1.7 Organization of the Dissertation

This dissertation provides a complete review of the methods for **analyzing, designing, fabricating, measuring** and **optimizing** different types of **CRLH TL** antennas. The content of this thesis is divided into five chapters.

Chapter-1 is devoted to the background of metamaterials, literature review and development of metamaterial antennas for wireless communication. The motivation and problem statement are also included in this chapter.

Chapter-2 of this thesis gives a detailed review on the Composite Right/Left Handed Transmission Line theory starting with transmission line concepts and progressing gradually to zeroth order resonant antenna theory and its basic characteristics. Successively moving on to radiation application of metamaterials and thereby leading to microstrip implementation of Zeroth Order Resonant antennas and delineating on prior art that motivates the present work.

In **Chapter-3**, microstrip based zeroth order resonant antenna is investigated and experimentally verified. The radiation properties, bandwidth, efficiency and gain at different modes are analyzed. The simulated results are validated through experimental verification. The dispersion diagram and surface wave modes supported by the structure are also discussed.

Chapter-4 introduces a method using coplanar waveguide to enhance the bandwidth of zeroth order resonant antennas. The bandwidth, gain, radiation pattern and efficiency of three different antenna structures are investigated and their possibilities for multiband wireless applications are explored. Methodologies adopted in these designs are introduced. The simulated results are validated through experimental verification.

Chapter-5 focusses on enhancing the gain of zeroth order resonant antennas proposed in chapter 4. Optimization process is carried out through HFSS software to achieve optimum antenna design with enhanced bandwidth and gain.

In **Chapter-6**, summary and suggestions for future research work is suggested.

Appendix deals with the techniques used for the design, fabrication and measurement of antennas proposed in this thesis. The design and simulations are performed using the FEM based Ansoft High Frequency Structure Simulator (HFSS). The antennas are fabricated using photolithographic process and a detailed description of this process is mentioned.

1.8 Summary

This chapter begins with an overview of NRI metamaterials. Subsequently, it lays insight into the evolution of theory of metamaterials and its properties. Further it is illustrated how Left Handed Metamaterial properties can be harnessed to realize novel multiband and more energy efficient broadband antennas for wireless applications. Brief emphasis is laid on the research work carried out in subsequent chapters. To sum up, this chapter highlights the work carried out in this thesis.

Chapter 2

Composite Right/ Left Handed Metamaterials: A State of the Art

2.1 Introduction

Left Handed Materials form a wider topic of research under metamaterials. It was first been studied and verified based on SRR's and thin wire structures. Since these resonant structures are lossy and narrow-banded, an alternative approach based on transmission line theory of LHM's has been developed. The Transmission Line approach was first introduced in 2002 by Caloz et al [57]. Based on this idea, several 1D-, 2D-, or even 3D- CRLH metamaterials can be designed. In the following sections, the TL approach to CRLH metamaterials are reviewed. First, the CRLH metamaterial is analysed from its equivalent TL representation to gain insight into its fundamental characteristics. Then, a practical LC network implementation of the homogeneous TL is developed. The LC network provides a realistic description of the CRLH metamaterial existing in nature. Finally, physical realizations of the LC network is discussed. For ease of analysis, only the loss-less TL is examined.

2.2 Theory and Analysis of Left Handed Materials

The fundamental electromagnetic properties of LH materials is presented in this section based on a general TL approach. Law of nature cannot be violated it will always play its role when any artificial composite material is engineered. Similarly, in the practical realization of the LH transmission line, parasitic effects come into effect to create Composite Right/Left Handed TL. A CRLH TL exhibits LH properties at low frequencies while RH properties at high frequencies. Transmission line theory can be used to analyze and design CRLH TL metamaterials. Metamaterials are designed by engineering a periodic array of unit cells. These unit cell represented by its equivalent circuit model consisting of series capacitance and shunt inductance, was first used by Brillouin and Pierce in late 1940s [65, 66]. They demonstrated wave propagation with negative phase and group velocity and coined the term *Backward Waves*. Brillouin and Pierce's periodic structures shown in Figure 2.1, typically had a unit cell size of the order of half or multiple of half the guided wavelength ($p \approx \lambda_g/2$ *or* $p \approx n\lambda_g/2$). Such structures supported backward waves in negative space harmonics in Fourier series expansion of fields [67] or higher order modes, due to diffraction and scattering phenomenon. So these structures are not related to their constitutive parameters (ε_r *and* μ_r) and refractive index (n) and hence cannot be characterized as artificial materials or metamaterials. Pierce *et al.* also demonstrated backward wave amplification in Travelling Wave Tubes [68].

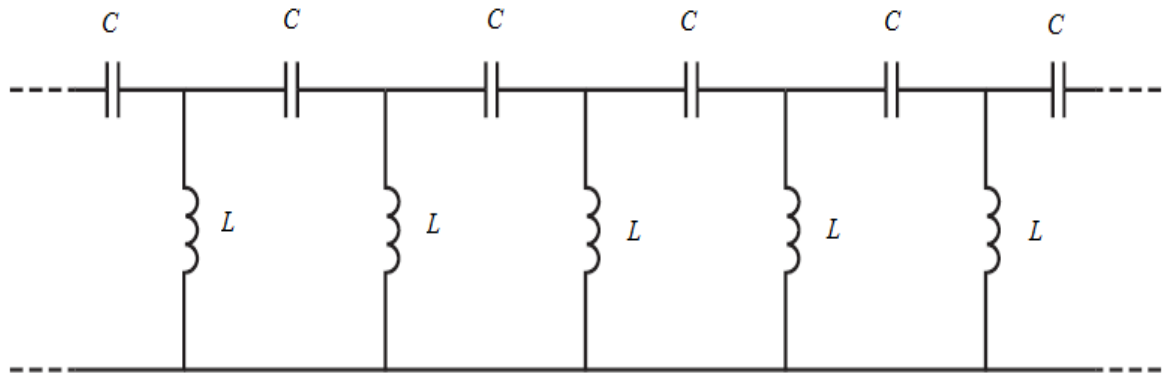

Figure 2.1 Equivalent circuit model of Brillouin and Pierce's *backward wave* TL.

Based on Brillouin and Pierce's equivalent circuit model, in 2002 several research groups, viz. Caloz *et al.* [69, 70], Oliner [71] and Eleftheriades *et al.* [72], proposed a similar Transmission Line (TL) approach for electromagnetic metamaterials.

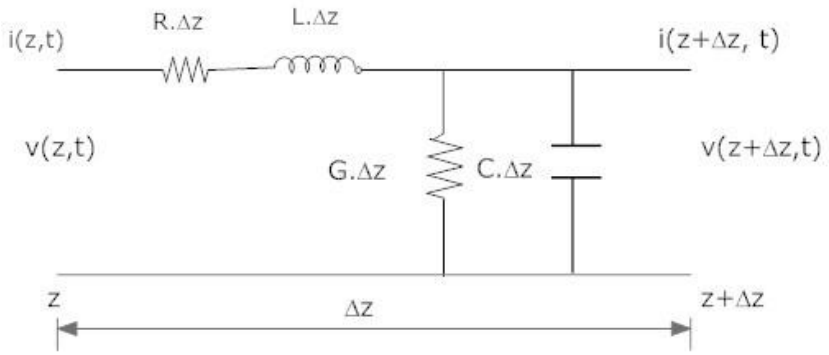

Figure 2.2 Lumped element equivalent circuit for purely RH lossy TL [9].

Figure 2.2 shows an incremental circuit model for a homogeneous purely lossy RH transmission line. For simplicity sake, only the loss-less line is considered as shown in Figure 2.3

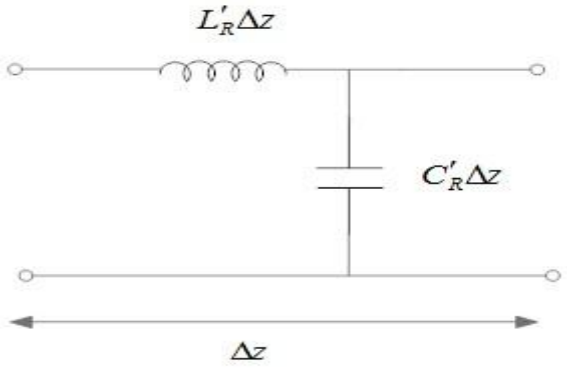

Figure 2.3 Lumped element equivalent circuit for purely lossless RH TL [9].

The dual of Figure 2.3, a pure RH TL, is a left - handed transmission line (LH TL) with series capacitance and shunt inductance is shown in Figure 2.4. Subscripts *R* and *L* are used to denote left or right-handedness of the lines.

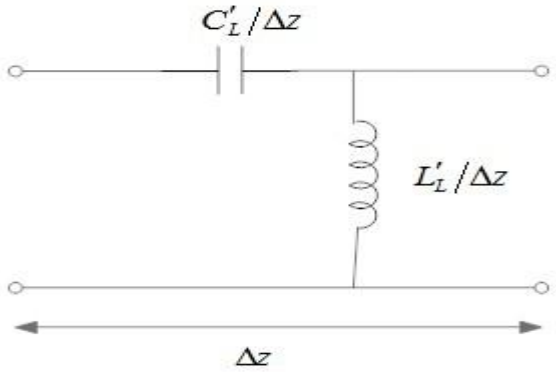

Figure 2.4 Lumped element equivalent circuit for purely lossless LH TL [9].

The complex propagation constant of an incremental circuit model for a hypothetical uniform lossless LH TL (Figure 2.4) is given by,

$$\gamma = j\beta = \sqrt{Z'Y'}$$

where Z' and Y' are, respectively, the per-unit length impedance and per-unit length admittance.

$$\gamma = \frac{1}{j\omega\sqrt{C'_L L'_L}} = -\frac{j}{\omega\sqrt{C'_L L'_L}} \tag{2.1}$$

Wave vector or phase constant $$\beta = \frac{-1}{\omega\sqrt{C'_L L'_L}} \tag{2.2}$$

From Equation (2.2), it can be seen that wave propagation is backwards.

Characteristic Impedance $$Z_C = \sqrt{\frac{Z'}{Y'}} = \sqrt{\frac{L'_L}{C'_L}} \tag{2.3}$$

Phase velocity $\left(v_p\right) = \frac{\omega}{\beta} = -\omega^2\sqrt{C'_L L'_L} < 0$ (2.4)

Group velocity $\left(v_g\right) = \frac{\partial\beta^{-1}}{\partial\omega} = \omega^2\sqrt{C'_L L'_L} > 0$ (2.5)

$$\Rightarrow v_p - \| v_g \tag{2.6}$$

Equations (2.4) and (2.5) shows that the phase velocity and group velocity in LH TL are anti-parallel. The phase velocity v_p denotes direction of phase propagation. The group velocity v_g denotes direction of power flow (Poynting vector). Equation (2.1) through Equation (2.6) shows that the transmission line in Figure 2.4 is purely left handed (LH TL).

Pure LH TL when subjected to practical conditions, had the presence of parasitic (series inductance due to current flow in metallization and shunt capacitance due to voltage gradient) elements. So pure LH TL is not practically possible and led to a more realistic Composite Right/Left Handed (CRLH) transmission line shown in Figure 2.5.

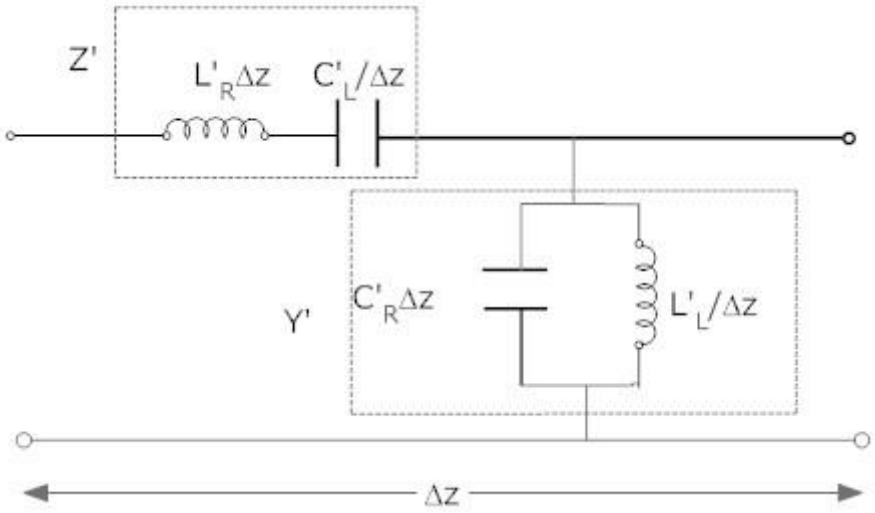

Figure 2.5 Lumped element equivalent circuit for CRLH TL [9].

The propagation constant of the above transmission line (Figure 2.5) is given by;

$$\gamma = \alpha + j\beta = \sqrt{Z'Y'} \tag{2.7}$$

where per unit length impedance Z' and per unit length admittance Y' are defined as

$$\begin{aligned} Z'(\omega) &= j(\omega L'_R - 1/\omega C'_L) \\ Y'(\omega) &= j(\omega C'_R - \frac{1}{\omega L'_L}) \end{aligned} \tag{2.8}$$

Therefore, the phase constant β is given by,

$$\beta(\omega) = s(\omega)\sqrt{\left[\omega^2 L'_R C'_R + \frac{1}{\omega^2 L'_L C'_L} - \left(\frac{L'_R}{L'_L} + \frac{C'_R}{C'_L}\right)\right]} \tag{2.9}$$

$$s(\omega) = \begin{Bmatrix} -1 if \omega < \omega_{\tau_1} = \min\left(\frac{1}{\sqrt{L'_R C'_L}}, \frac{1}{\sqrt{L'_L C'_R}}\right) \\ +1 if \omega > \omega_{\tau_2} = \max\left(\frac{1}{\sqrt{L'_R C'_L}}, \frac{1}{\sqrt{L'_L C'_R}}\right) \end{Bmatrix} \tag{2.10}$$

The phase constant β in Equation (2.9) can either be purely real or purely imaginary depending on whether the radicand $s(\omega)$ is positive or negative, respectively. When β is purely real, in that frequency range wave propagation takes place so a pass-band is present

since $\gamma = j\beta$. On the contrary, a stop-band in those frequency range occurs where β is purely imaginary since $\gamma = \alpha$. This stop-band is a unique characteristic of the CRLH TL, and is not present either in the PRH or the PLH cases. In general, when the series and shunt resonances of the CRLH TL are different, then it is known as unbalanced CRLH TL. However, when the series and shunt resonances are equal [70], then

$$L'_R C'_L = L'_L C'_R \tag{2.11}$$

and the CRLH TL becomes a balanced CRLH structure.

Characteristic impedance of a transmission line is given by,

$$Z_C = \sqrt{\frac{Z'}{Y'}}\ . \tag{2.12}$$

In case of an unbalanced CRLH TL, the characteristic impedance is

$$Z_C = Z_L \sqrt{\frac{(\omega/\omega_{se})^2 - 1}{(\omega/\omega_{sh})^2 - 1}}$$

or,
$$Z_C = Z_L \sqrt{\frac{L'_R C'_L \omega^2 - 1}{L'_L C'_R \omega^2 - 1}}\ . \tag{2.13}$$

In case of balanced CRLH TL, this reduces to $Z_C = Z_L = Z_R$ (2.14)

where the purely LH impedance is $Z_L = \sqrt{\frac{L'_L}{C'_L}}$ (2.15(a))

and the purely RH impedance is $Z_R = \sqrt{\frac{L'_R}{C'_R}}$ (2.15 (b))

2.2.1 Relation between Constitutive Parameters and CRLH TL Parameters

The characteristic impedance of the CRLH TL can be related to the constitutive parameters as follows [9, 70].

Propagation Constant

The propagation constant γ for a CRLH transmission line is

$$\gamma = j\beta = \sqrt{Z'Y'} \tag{2.16}$$

In case of a CRLH metamaterial, propagation constant is expressed as

$$\beta = \omega\sqrt{\mu\varepsilon} \tag{2.17}$$

Squaring and equating the two expressions given in equations (2.16) and (2.17), we get,

$$-\omega^2 \mu\varepsilon = Z'Y' \tag{2.18}$$

Characteristic Impedance

The characteristic impedance of a CRLH TL is

$$Z_C = \sqrt{Z'/Y'} \tag{2.19}$$

The intrinsic impedance of the metamaterial is $\eta = \sqrt{\frac{\mu}{\varepsilon}}$ (2.20)

Equating (2.18) and (2.19) we get $\frac{Z'}{Y'} = \frac{\mu}{\varepsilon}$ (2.21)

Hence the permittivity and permeability of the metamaterial in terms of impedance and admittance of the TL is

$$\mu = \frac{Z'}{j\omega} = L'_R - \frac{1}{\omega^2 C'_L} \tag{2.22}$$

$$\varepsilon = \frac{Y'}{j\omega} = C'_R - \frac{1}{\omega^2 L'_L} \tag{2.23}$$

2.3 Applications of CRLH Metamaterials as Antenna

The ability of the CRLH metamaterial structures as antenna is of tremendous interest and leads to a variety of microwave applications. When a metamaterial structure is open to free space, it radiates and supports a fast-wave called as a leaky wave (LW) mode [9]. This property is utilized as antennas or as reflectors (by reciprocity). Unique radiation properties are obtained with CRLH structures due to their rich and unusual propagation characteristics. In addition to novel resonant type metamaterial antennas based on resonators, there have been many antenna-reflector applications of CRLH metamaterials. Some such applications are CRLH LW backfire-to-endfire (including broadside) radiation with a frequency-scanned antenna application [73-74], a fixed frequency electronically scanned BE antenna [75-77], reflecto-directive systems [78-81], 2D leaky-wave structures such as conical beam antenna [82, 83], full-space scanning antenna [84], dual frequency CRLH TL resonating ring antenna and zeroth order (size-independent) resonant CRLH antenna [60, 61]. The prime focus of this thesis is on the design, implementation and application of Zeroth Order Resonating (ZOR) antenna whose radiation is based on a resonance mechanism.

2.3.1 Zeroth Order Resonant Antenna Theory

A homogeneous metamaterial structure when open- or short-ended, produces radiation based on *resonance mechanism*, where, the operating wave is a *standing wave* exhibiting constant-phase and constant- magnitude field distribution along the structure, which give rise to broadside radiation. Constructive field interference above the structure further allows the radiation [9]. In these antennas the overall structure resonates rather than its structural elements or unit cells. Zeroth order resonating antenna is based on zeroth order resonator concepts which is essentially a CRLH TL structure with either short or open coupling terminations. When designed to operate at any transition frequency, it corresponds to infinite wavelength propagation (zeroth order mode) according to the resonance condition $l = |n|\lambda/2$ discussed in the next section. Due to the unique nature of this zeroth-order mode, the size of the resonator does not depend on its physical length but only on the amount of reactance provided by its unit cells. In terms of antenna, this represents a potential interest for miniaturisation. Reduction in size of an antenna, by whatever methods, necessarily results in the decrease of its Directivity *D* and thereby of its Gain *G*, assuming a constant efficiency factor $k = G/D$ [85]. A potential advantage of the ZOR antenna lies in its constant-magnitude field distribution. The corresponding uniform repartition of energy along the antenna structure results in smaller ohmic losses than in other conventional microstrip patch antennas where ohmic losses are quite large due to high current concentrations near discontinuities. As a result, higher efficiency factor *k* is obtained in the ZOR antennas, which mitigates to some extent, the reduction in gain subsequent to size reduction. This forms the fundamental basis of the antenna designed in this thesis.

2.3.2 Zeroth Order Resonance Principle

In case of conventional (PRH) distributed resonator, the resonant frequencies correspond to the frequencies where the physical length l of the structure is a multiple of half a wavelength or, equivalently, the electrical length $\theta = \beta l$ is a multiple of π,

$$l = n\frac{\lambda}{2} \quad \text{or} \quad \theta_n = \beta_n l = \left(\frac{2\pi}{\lambda}\right)\cdot\left(\frac{n\lambda}{2}\right) = n\pi, \tag{2.24}$$

with $n = +1,+2,.....,+\infty.$

Since the phase constant of a PRH TL is always positive $(\beta > 0)$, so the electrical length $(\theta = \beta l)$ can only have positive values. This implies that only non zero and positive resonances are allowed in PRH TL resonators. On the contrary, CRLH TL can have $\beta = 0$ (transition frequency) and $\beta < 0$ (LH range). Therefore, the electrical length $\theta = \beta l$ can be zero and negative. Therefore we have,

$$l = |n|\frac{\lambda}{2} \quad \text{or} \quad \theta_n = \beta_n l = \left(\frac{2\pi}{\lambda}\right)\cdot\left(\frac{n\lambda}{2}\right) = n\pi, \tag{2.25}$$

with $n = 0, \pm 1, \pm 2, \ldots\ldots\ldots, \pm\infty.$

2.3.3 Zeroth Order Resonant Antenna Characteristics

Considering an open-ended CRLH TL, where $Z_L = \infty$, the input impedance (Z_{in}) seen from one end of the resonator towards the other end is given by [9, 86],

$$\begin{aligned} Z_{in}^{\ open} &= -jZ_C \cot(\beta l) \overset{\beta \to 0}{\approx} -jZ_C \frac{1}{\beta \ell} \\ &= -j\sqrt{\frac{Z'_{series}}{Y'_{shunt}}}\left(\frac{1}{-j\sqrt{Z'_{series}Y'_{shunt}}}\right)\frac{1}{\ell} = \frac{1}{Y'_{shunt}\ell} \\ &= \frac{1}{Y'_{shunt}(Np)} = \frac{1}{NY_{shunt}}, \end{aligned} \tag{2.26}$$

where, N is the number of unit cell and Y_{shunt} is the admittance of the CRLH unit cell, given by Equation (2.8).

Now from Equation (2.26), the input impedance is equal to 1/N times $1/Y_{shunt}$ of the unit cell. Since, N is a simple integer, not affecting the susceptance; the resonance of the whole resonator is the same as the resonance of the admittance Y_{shunt} [9]. Therefore, there is a single resonant frequency,

$$\omega_{res}^{open} = \omega_{sh} = \frac{1}{\sqrt{L_L C_R}}. \tag{2.27}$$

In contrast, no resonance occurs at $\omega_{se} = 1/\sqrt{L_R C_L}$.

In the *short-ended* case, the input impedance Z_{in} seen from one end of the resonator towards the other end is given by [9],

$$Z_{in}^{\ short} = jZ_C \tan(\beta l) \overset{\beta \to 0}{\approx} -jZ_C \beta l.$$

$$= -j\sqrt{\frac{Z'_{series}}{Y'_{shunt}}}\left(j\sqrt{Z'_{series}Y'_{shunt}}\right)\ell = Z'_{series}\ell = Z'_{series}(Np) = NZ_{series}, \tag{2.28}$$

where, N is the number of unit cell and Z_{series} is the impedance of the CRLH unit cell, given by Equation (2.8).

This result shows that the input impedance of a short-ended is equal to N times Z_{series} of the unit cell. Since, N is a simple integer, not affecting the reactance; the resonance of the

whole resonator is the same as the resonance of the series impedance Z_{series} [9]. Therefore, there is a single resonant frequency,

$$\omega_{res}^{short} = \omega_{se} = \frac{1}{\sqrt{L_R C_L}}. \tag{2.29}$$

In contrast, no resonance occurs at $\omega_{sh} = 1/\sqrt{L_L C_R}$.

In the particular case of balanced resonances, the zeroth-order resonance occurs for both the open-ended and the short-ended resonators, since $\omega_0^{bal} = \omega_{se} = \omega_{sh}$.

The remarkable feature of the zeroth-order resonator is that, either for an open-ended or a short-ended configuration, *the resonance frequency depends only on the circuit elements* L_R/C_L *or* L_L/C_R *of the unit cell and not on the physical length* ℓ *of the resonator.* This implies that a zeroth-order resonator can be made arbitrarily small, the limitation in size reduction being the minimum footprint required by the LC elements for the required LC values in a given technology.

The *loss mechanism* in the CRLH TL resonator at the zeroth-order resonant state is also different from that of conventional resonators due to infinite wavelength. In case of an open-ended resonator, the input impedance is equal to $1/N$ times the impedance of the shunt tank circuit of the unit cell. The unloaded *Q*-factor is then obtained as

$$\begin{aligned} Q_0^{open} &= \frac{1/NG}{\omega_{sh}(L_L/N)} = \frac{1/G}{\omega_{sh} L_L} \\ &= \omega_{sh}(1/NG)\cdot NC_R = \omega_{sh}(1/G)C_R \\ &= \frac{1}{G}\sqrt{\frac{C_R}{L_L}}. \end{aligned} \tag{2.30}$$

It is thus inferred that the unloaded *Q*-factor depends only on the loss G in the shunt tank circuit and not on the loss R in the series tank circuit of the unit cell.

Similarly, for the short ended case the unloaded *Q*-factor is obtained as

$$\begin{aligned} Q_0^{short} &= \frac{NR}{\omega_{se} N L_R} = \frac{R}{\omega_{se} L_R} \\ &= \omega_{se} NR \cdot C_L/N = \omega_{se} RC_L \\ &= R\sqrt{\frac{C_L}{L_R}}. \end{aligned} \tag{2.31}$$

In this case, the unloaded *Q*-factor depends only on the loss *R* in the series tank circuit and not on the loss *G* in the shunt tank circuit of the unit cell.

A notable feature of the zeroth-order resonator, whether open-ended or short-ended configurations, is that *the unloaded Q-factor is independent of the number of unit cells* (and therefore length ℓ) of the resonator, according to Equations (2.30) and (2.31). A zeroth-order resonator seems therefore to have the potential to exhibit a higher *Q* than that of conventional resonators, since only one of the two possible (series and shunt) loss contributions is present.

2.3.4 Eigen frequency (EIG) Method of Analysis of a single CRLH unit cell

Microstrip is used most commonly as a host transmission line to realize ZOR antennas. It is a class of electromagnetic waveguide consisting of a strip conductor and a back-plane, separated by a thin dielectric. It has been reported that "the nature of propagation in microstrip based CRLH TL structures is quasi-TEM" which implies that the electromagnetic field distribution in such a structure is essentially the same as conventional microstrip structures except at zeroth order resonance due to high impedance as it does not support any surface waves. Applying periodic boundary conditions (PBCs) related to the Bloch-Floquet theorem to Equation (2.14), the CRLH TL unit cell's dispersion relation along the Brillouin zone is determined to be

$$\beta = \frac{1}{a}\cos^{-1}\left\{1-\frac{1}{2}\left[\frac{\omega_L{}^2}{\omega_0{}^2}+\frac{\omega_0{}^2}{\omega_R{}^2}-\left(\frac{\omega_L{}^2}{\omega_{se}{}^2}+\frac{\omega_L{}^2}{\omega_{sh}{}^2}\right)\right]\right\} \tag{2.32}$$

where ω_L and ω_R are the resonant frequencies of the equivalent LH and RH unit cells. All the eigen frequencies satisfy the following resonant condition [87]:

$$\beta_n L = n\pi \tag{2.33}$$

where, L is the total length of the open ended CRLH TL and n is a whole number. If the CRLH TL is composed of M unit-cells $(L = Ma)$, the eigen frequencies can be computed as

$$\frac{n\pi}{M} = \cos^{-1}\left\{1-\frac{1}{2}\left[\frac{\omega_L{}^2}{\omega_n{}^2}+\frac{\omega_n{}^2}{\omega_R{}^2}-\left(\frac{\omega_L{}^2}{\omega_{se}{}^2}+\frac{\omega_L{}^2}{\omega_{sh}{}^2}\right)\right]\right\}$$
$$n = 0,\pm1,\pm2.....\pm(M-1). \tag{2.34}$$

It can be seen that Equation (2.34) depends only on the unit-cell characteristics and not on the total length of the TL. Besides, equivalent resonance conditions can be achieved for the corresponding LH and RH modes (i.e., -1 and +1 modes). These two conclusions, from the antenna point of view, yield the possibility of designing a) resonators smaller than λ/2 or b) multi-frequency antennas.

The operating modes can be obtained by determining eigen frequencies (EIG method) of a CRLH TL [18, 19]. For a pair of resonant frequencies Equation (2.34) can be rewritten as

$$\frac{n\pi}{M} = \cos^{-1}\left\{1-\frac{1}{2}\left[\frac{\omega_L{}^2}{\omega_{+n}{}^2}+\frac{\omega_{+n}{}^2}{\omega_R{}^2}-\left(\frac{\omega_L{}^2}{\omega_{se}{}^2}+\frac{\omega_L{}^2}{\omega_{sh}{}^2}\right)\right]\right\}$$
$$\frac{-n\pi}{M} = \cos^{-1}\left\{1-\frac{1}{2}\left[\frac{\omega_L{}^2}{\omega_{-n}{}^2}+\frac{\omega_{-n}{}^2}{\omega_R{}^2}-\left(\frac{\omega_L{}^2}{\omega_{se}{}^2}+\frac{\omega_L{}^2}{\omega_{sh}{}^2}\right)\right]\right\} \quad (2.35)$$

where the positive sign is used for the RH mode and the negative sign corresponds to the LH mode. If it is taken into account that the cosine function is an even function $[\cos(-x)=\cos(x)]$.

$$\frac{\omega_L{}^2}{\omega_{+n}{}^2}+\frac{\omega_{+n}{}^2}{\omega_R{}^2} = \frac{\omega_L{}^2}{\omega_{-n}{}^2}+\frac{\omega_{-n}{}^2}{\omega_R{}^2} \quad (2.36)$$

Therefore, all the eigen frequencies are related by

$$\omega_L\ \omega_R = \omega_{+n}\ \omega_{-n} = \omega_{sh}\ \omega_{se} \quad (2.37)$$

To obtain the dispersion diagram as a function of the frequency ω, the unknowns ω_L, ω_R, ω_{se} and ω_{sh} will have to be obtained. By solving Equations 2.34 and 2.37 simultaneously, the frequencies ω_L and ω_R can be computed as

$$\omega_R^2 = \frac{1}{2\left[1-\cos\left(\frac{n\pi}{M}\right)\right]}(\omega_{-n}^2+\omega_{+n}^2-\omega_{se}^2-\omega_{sh}^2) \quad (2.38)$$

$$\omega_L^2 = \frac{2\left[1-\cos\left(\frac{n\pi}{M}\right)\right]}{\frac{1}{\omega_{-n}^2}+\frac{1}{\omega_{+n}^2}-\frac{1}{\omega_{se}^2}-\frac{1}{\omega_{sh}^2}} \quad (2.39)$$

The previous Equations (2.38) and (2.39) depend on the unknowns ω_{sh} and ω_{se}. Solving Equations (2.32) or (2.34) by using (2.37) for the zeroth resonant order mode and considering a general unbalanced CRLH transmission line ($(L_L/C_L \neq L_R/C_R)$ without losses; results in the following biquadratic equation in ω_0^2:

$$\frac{\omega_L^2}{\omega_0^2}+\frac{\omega_0^2}{\omega_R^2} = \frac{\omega_{sh}^2}{\omega_R^2}+\frac{\omega_{se}^2}{\omega_R^2} \quad (2.40)$$

This equation has two solutions for ω_0^2, one for the open ended zeroth order resonator

$$\omega_0^2 = \omega_{sh}^2 \quad (2.41)$$

and the other for the short ended zeroth order resonator

$$\omega_0^2 = \omega_{se}^2 \tag{2.42}$$

As we are considering an open ended CRLH TL zeroth order resonator antenna, using (2.41) and (2.37), ω_{se} is computed as

$$\omega_{se} = \frac{\omega_{+n}\omega_{-n}}{\omega_0} \tag{2.43}$$

Finally, the parameters ω_R and ω_L can be obtained using only three eigen frequencies (ω_0 and $\omega_{\pm n}$, being n any whole number) as follows:

$$\omega_L = \frac{\omega_{+n}\omega_{-n}}{\omega_R} \tag{2.44}$$

$$\omega_R^2 = \frac{\omega_{+n}^2 + \omega_{-n}^2 - \omega_0^2 - \frac{\omega_{+n}^2\omega_{-n}^2}{\omega_0^2}}{2\left[1-\cos\left(\frac{n\pi}{M}\right)\right]} \tag{2.45}$$

Once ω_R, ω_L, ω_{se} and ω_{sh} have been found without a Full Wave analysis, Equation (2.42) can be applied to extract the dispersion diagram.

Cut off LH Frequency, $\omega_{CL} = \omega_R\left|1-\sqrt{1+\frac{\omega_L}{\omega_R}}\right|$ (2.46)

Cut off RH Frequency, $\omega_{CR} = \omega_R\left|1+\sqrt{1+\frac{\omega_L}{\omega_R}}\right|$ (2.47)

2.4 Microstrip Implementation

The LC-based model discussed in the previous section needs to be physically implemented to design a CRLH TL structure. The two popular methods for physically implementing the LC network are through surface-mount technology (SMT) chip components or by using distributed components. A popular method of implementing LC network by distributed components is the microstrip implementation. This method is chosen because it is easy to meet the design specifications such as the frequency of operation and phase responses.

- Caloz et al. in 2002 introduced the first distributed microstrip CRLH TL metamaterial structure.It consisted of *interdigital capacitors* and *stub inductors* shorted to the ground by a via [69, 88] and subsequently used in various applications [89, 70].

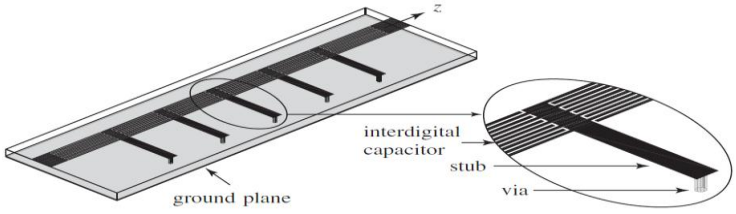

Figure 2.6 Microstrip CRLH TL with Interdigital capacitors and stub inductors [69, 88].

The unit cell, centered in the plane defined by the axis of the stub, represents a *T*- network constituted by two impedance branches with capacitance $2C_L$ and inductance $L_R/2$ and by an admittance branch with inductance L_L and capacitance C_R. The structure shown in Figure 2.7 is *open* to air. As a result the line is potentially radiative, a characteristic exploited in leaky-wave (LW) antenna applications.

- The concept of Zeroth Order Resonance was first demonstrated in 2003 by A. Sanada et al [86]. A microstrip based open-ended CRLH TL structure was designed. The antenna was implemented incorporating vias, which suffered from narrow bandwidth and fabrication difficulties. Later, a via free microstrip based CRLH TL antenna was proposed [90, 91]. Such a via-less configuration is advantageous in processes where fabrication of vias is problematic. The direct connection of the inductor L_L to the ground is replaced by a capacitive coupling through the *virtual-ground capacitance* C_g, which is a high value capacitance obtained by a large metal patch area. Thus the virtual ground leads to a little change of the resonant frequencies. The microstrip-based unit cell consists of an interdigital capacitor and a shunt meander line connected to a rectangular patch. The rectangular patch behaves as a virtual ground plane. Since resonance is independent of physical dimensions for the ZOR, the size of the antenna can be smaller than a half-wavelength. Instead, the antenna's size is determined by the reactive loadings in its unit cells. About 75% footprint reduction is achieved in comparison with that of the $\lambda/2$ patch antenna. A much more drastic size reduction can be obtained by using vias instead of virtual-ground capacitors.

- L. Liu et al. in 2009, showed that when optimally matched to the air impedance the balanced CRLH TL can be used as an efficient, frequency-scanned leaky wave antenna [73]. A 30-cell leaky-wave antenna structure, incorporating both series and shunt varactors for optimal impedance matching and maximal tuning was reported [75]. The CRLH TL realized by interdigital capacitor and short stub inductor cannot provide a large series capacitance and inductance in small area. Several electrically small CRLH antennas based on the modified mushroom structure was reported [92]. A metal insulator metal (MIM) with high dielectric constant and thin substrate height can increase C_L. The inductance L_L is realized by a metallic via with additional CPW stub connected to the ground. The via length and CPW length can be enlarged to increase the shunt inductance. A small unit cell can be developed by combining the MIM capacitor and via plus CPW stub with large values of C_L and L_L. Even though lower resonances occur, the $n=-1$ mode is of most interest in the design of the antenna prototype. Low antenna gains are expected because of the small antenna size. In addition, the radiation efficiency including the impedance mismatch of the $n=-1$ mode was measured to be around 2% and $n=-2$, $n=-3$ mode are less than 1%. The low radiation efficiency implies the radiation power is much less than the power loss in the antenna. In this case, a large current concentrates

at the vias which are lossy conductors. As a result, the large loss in the structure is generated, thus reducing the antenna efficiency.

2.5 Prior Art

Although the above discussed Zeroth Order Resonator (ZOR) antennas are more compact and offer the advantage of size reduction than conventional half-wavelength antennas [93-94], it is difficult to apply them to modern wireless LAN communication systems because of their narrow bandwidth. The main objective of this present research work is to propose efficient technique for extending bandwidth while maintaining high radiation efficiency. Recently many researchers have attempted to solve the bandwidth problem of ZOR antennas [95-98]. To date, nearly all demonstrations of ZOR antennas have been achieved either by using a stacked multi-layer structure or by adopting a microstripline fed implementation of ZOR antennas. For example:

- A metamaterial ring antenna was reported by F. Qureshi et al [95]. This antenna was implemented on a multi-layer structure in which a thick substrate with low permittivity is used. The substrate is supported by holding brackets and its bandwidth is increased up to 6.8% by means of a sleeve balun.

- Alternatively, the bandwidth of the ZOR antenna is increased by a strip matching ground as proposed by C. J. Lee et al [96]. It is also built on a multiple substrate where a thin substrate with high permittivity is stacked on a thick substrate with low permittivity. In this method, fractional bandwidth of antennas is increased up to 8%.

- The other method is to have two resonant frequencies close to each other as propounded by J. Zhu et al [97]. Such an antenna consists of two resonators whose frequencies are slightly different. In this method, the bandwidth is increased by up to 3.1%.

- By realizing ZOR antenna using CPW technology, will allow design freedom for the shunt parameters in the equivalent circuit mode. Thus, bandwidth of ZOR antenna is extended up to 6.8% by realizing high shunt inductance and small shunt capacitance using CPW technology as put forth by T. Jang et al [99].

2.6 Summary

This chapter deals exclusively with the fundamental TL theory and analysis of CRLH TL metamaterials. Indeed the resonance mechanism of CRLH metamaterials is promising for various radiative antenna applications especially zeroth order resonant antennas and its microstrip implementation. This thesis also focuses on progression of research work leading to state of the art ZOR antenna examples from the recent literature. In passing, it provides enough motivation to design and develop microstrip based ZOR monopole antenna for multiband wireless application, which is investigated in chapter 3.

Chapter 3
Microstripline based Zeroth Order Resonant Monopole Antenna

3.1 Introduction

In the previous chapter, an overview of the CRLH TL antennas implemented in microstrip technology incorporating vias was discussed. It was shown that the antennas exhibited zeroth mode (m=0) or infinite wavelength ($\lambda_g = \infty$) resonant frequency are independent of the size of the structure $l = Np$. While most of the antennas presented in the previous sections were exhibiting 1D rectilinear structures, with strong difference between the sizes l in the longitudinal direction (direction of propagation or resonance) and w in the transverse direction ($w << l$), thereby leading to a typical planar dipole like radiation patterns. Alternatively, the 2D dimensions of the structure when made identical ($w = l$), the structure is rendered azimuthally quasi-symmetrical, like the mushroom structure used for 2D conical leaky-wave radiation.

In this chapter a conceptual model and the electromagnetic properties of the microstrip based Zeroth Order Resonant (ZOR) monopole antenna operating at the mode β=0, which were propounded by A. Lai et al will be reviewed. Its experimental demonstrations are presented as a starting point for further developments in subsequent chapters. This chapter is organized as follows. Section 3.2 deals with the radiation principle of CRLH TL monopole antenna. Section 3.3 elucidates on the practical realization of this antenna. Subsequently, a parametric study is carried out to show the dependence of via radius on resonant frequency. Finally, pattern search optimization using HFSS optimizer on inductive via radius parameter is performed to determine optimum via radius and is investigated in different subsections. The performance characteristics of the ZOR antenna is discussed. Simulated and measured results are shown and compared. Finally, conclusions and summary are stated in Section 3.6.

3.2 CRLH Monopole Antenna Principle

The principle of a CRLH TL monopole antenna is illustrated in Figure 3.1 A. It is well known that a conventional patch antenna may be considered as a rectangular cavity with perfect magnetic conducting (PMC) walls at its fundamental resonance mode $l = \lambda_g / 2$ (l is the resonant length). At its fundamental mode, the patch antenna supports a half-wavelength along its resonant length. Hence in this case, the non-zero equivalent magnetic current density at each radiating edge is given by $\overline{M}_s = -2\hat{n} \times \overline{E}$ (where, $\hat{n}$ is the unit normal to the edge, $\overline{E}$ is the electric field at the edge, and the factor of 2 is due to the ground plane) which has the direction shown in the top LH side of Figure 3.1 A (a), thus producing a dipole like radiation pattern. If the electric field is perfectly uniform that is in phase within the substrate, as is the case at the infinite-wavelength frequencies ω_{se} and ω_{sh} of a CRLH structure, then the magnetic current density $\overline{M}_s = -2\hat{n} \times \overline{E}$ follows a continuous loop around the patch, as

depicted in the top RH side of Figure 3.1 A (b). In this case, monopolar radiation is produced with the electric field polarized along the z-direction.

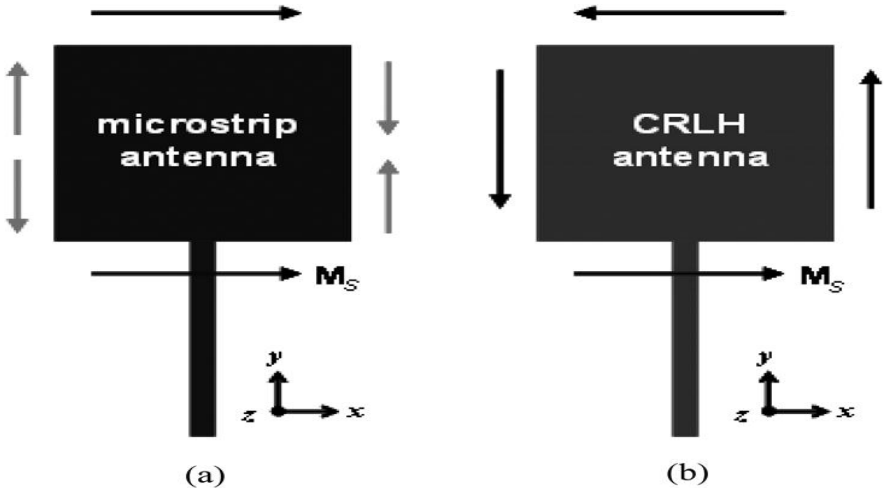

Figure 3.1 A CRLH infinite-wavelength ω_{sh} microstrip monopole antenna. (a) Magnetic current distribution compared to the case of a conventional patch antenna and (b) Mushroom type CRLH- patch implementation [9].

3.2.1 Electric Field/Current Analysis of a CRLH TL

Another (more precise) method employed to examine left handedness of a CRLH structure is the analysis of electric field distribution in the structure. This method is undertaken in the present work although the previous EIG method of analysis is reviewed for the sake of completeness. This is usually done using full-wave electromagnetic simulations and examined for areas where phase and group velocities are anti-parallel, similar to Figure 3.1 B. It is usually done more efficiently using animated graphs in full-wave simulators.

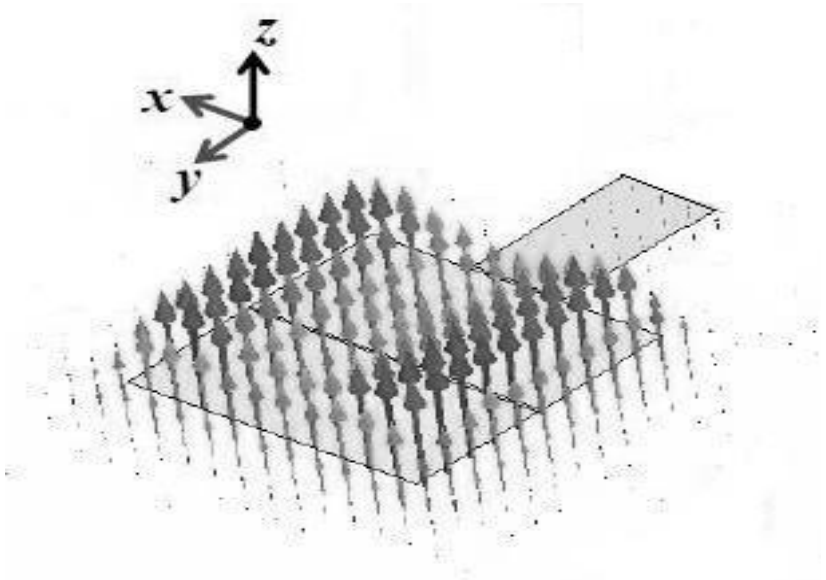

Figure 3.1 B Study of E-field distribution for a CRLH TL antenna for *n=0* mode.

3.3 Realization of CRLH Antenna

A practical realization of a LH TL, which includes unavoidable RH effects; commonly known as a CRLH TL, is the general model for the CRLH based monopolar unit cell. To realize the required capacitances and inductances of the CRLH TL unit-cell model, a physical realization has to be chosen. These can theoretically be implemented with either lumped or distributed structures, though lumped components would be impractical, for radiation type applications due to their inability to radiate. A popular choice of microstrip-type implementation of the CRLH TL is the "Sievenpiper Mushroom" (SM) structures. The resonant structure consists of a rectangular metallic patch which is shorted to a ground plane with a via (or shorting post). It further led to the implementation of CRLH TL based zeroth order resonant antennas. Figure 3.2 pictorially shows a zeroth order resonant monopole antenna consisting of three unit cells when arranged in a periodic fashion adequately represent the CRLH TL.

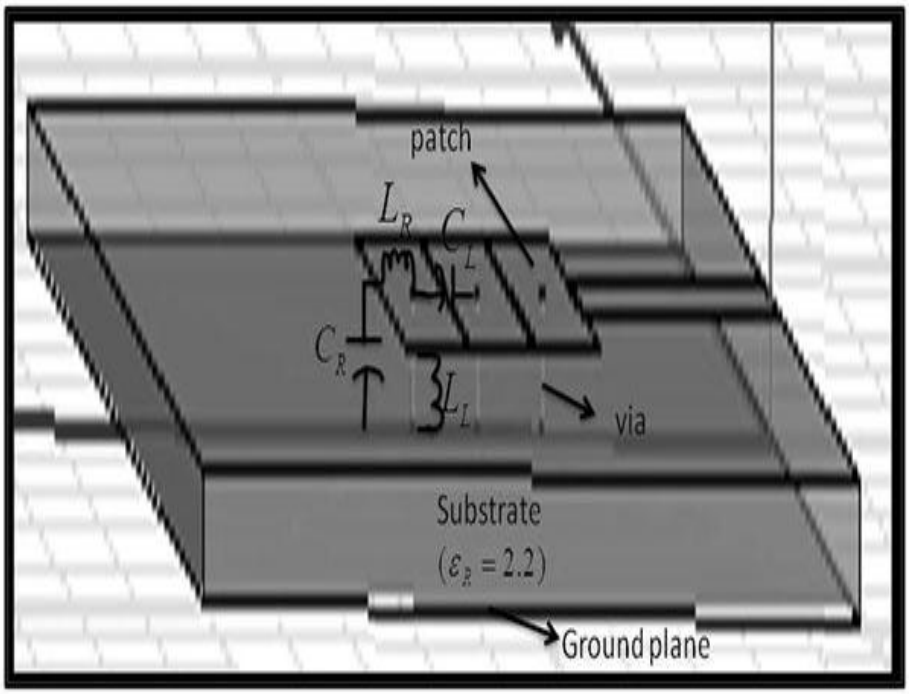

Figure 3.2 Realization of the infinite wavelength CRLH Transmission Line resonant antenna.

It is shown that RH components are derived from the patch structure; the series inductor (L_R) is due to the self-inductance of the patch and the shunt capacitor (C_R) stems from the parallel plate effects between the patch and the ground plane. The LH components result from introduction of the shorting post which gives rise to the shunt inductor (L_L) and a series capacitor (C_L) due to coupling between adjacent unit cells. Thus by altering the physical dimensions (or properties) of the resonant CRLH TL structure the equivalent components can be tuned.

3.4 Antenna Design

A compact microstrip monopole antenna based on composite right/left handed (CRLH) metamaterial transmission line is studied in this section. The software simulation includes the design of CRLH TL based metamaterial antennas using High Frequency Structure Simulator (Ansoft HFSSv12). A conceptual flow chart of the process of antenna design is shown in Figure 3.3.

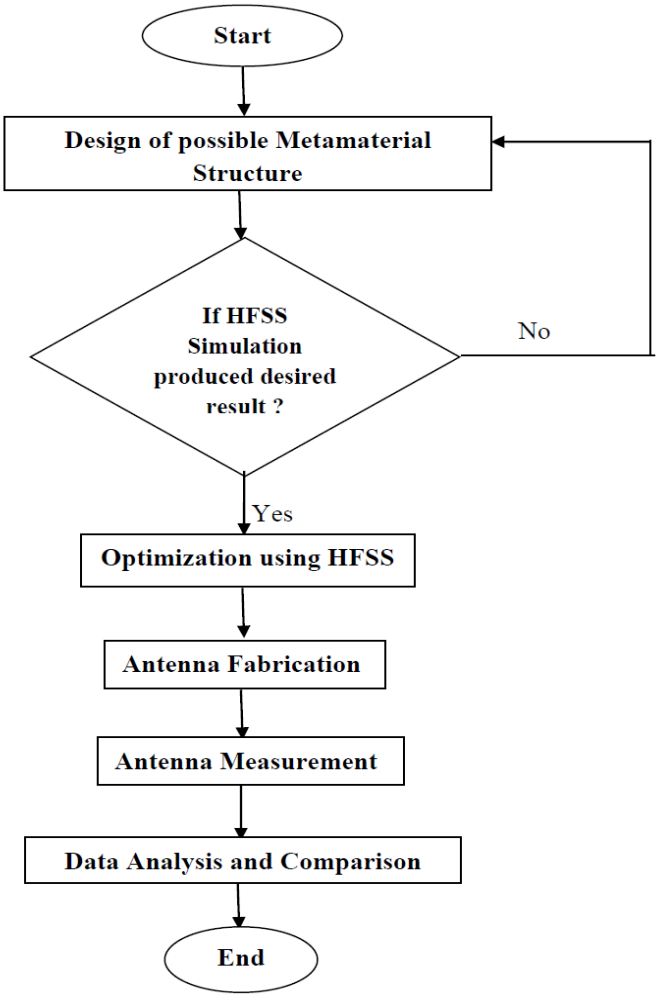

Figure 3.3 Flow Chart for Antenna Design.

3.4.1 Design Guidelines

Typical guidelines for the design of CRLH TL structure may be the following:

1. Appropriate transition frequency is selected as defined by the relation:

$$\omega_0 = \frac{1}{\sqrt[4]{L_R C_R L_L C_L}} = \sqrt{\omega_R \omega_L} = \sqrt{\omega_{se} \omega_{sh}} \qquad (3.1)$$

where

$$\omega_R = \frac{1}{\sqrt{L_R C_R}}, \omega_L = \frac{1}{\sqrt{L_L C_L}}, \omega_{se} = \frac{1}{\sqrt{L_R C_L}}, \omega_{sh} = \frac{1}{\sqrt{L_L C_R}} \quad (3.2)$$

2. Applying the matching condition of Equation (2.14) to ports of impedance, calculation of Z_c is done using the following equations: 3.3 (a) and 3.3 (b).

$$Z_R = \sqrt{\frac{L_R}{C_R}} = Z_c \quad (3.3(a))$$

$$Z_L = \sqrt{\frac{L_L}{C_L}} = Z_c \quad (3.3(b))$$

3. Equations (3.1) and (3.3) consists of four unknowns $L_R, C_R, L_L and C_L$ which can be calculated using eigen frequency method as detailed in Section 2.3.4.

4. Number of unit cells are set to three.

Once the constitutive lumped element values of the CRLH TL are known, depending on whether RH or LH, it is then multiplied or divided by the length of unit-cell (cell size), to obtain the associated per-unit-length and times unit-length component values:

$$L_R^{'} = \frac{L_R}{p}, C_R^{'} = \frac{C_R}{p}, L_L^{'} = L_L.p, C_L^{'} = C_L.p \quad (3.4)$$

The determined values is C_L= 0.46pF, L_L= 1.50nH, C_R= 0.82pF, L_R= 0.29pF at f_0 = 3.62GHz.

3.4.2 Antenna Geometry and Simulation Results

Figure 3.4 shows the simulated geometry of the designed antenna. The entire structure is implemented on a RT Duroid™ substrate of size 50mm x 50mm x 1.57mm, having a substrate loss tangent (tan δ) of about 0.0009. The dielectric constant of the substrate chosen is quite low ($\varepsilon_R = 2.2$) in order to achieve high efficiency. The radiating patch consists of three unit cells separated by a gap of 0.2mm. This gap provides the series LH capacitance C_L while the magnetic flux produced by the current flow along the radiating patch provides the parasitic series RH inductance L_R. The overall area of the substrate contributes to the shunt parasitic capacitance C_R. Each unit cell of size 15 mm x 4.8 mm, is shorted by an inductive via stub of radius 0.3 mm and height 1.57 mm which contributes to the shunt inductance L_L. The proposed antenna is designed to have its zeroth order mode at 4.505 GHz using Ansoft

HFSSv12 simulator. Antenna parameters are adjusted according to the general design guideline that the electrical size of the unit cell is approximately less than $\lambda_g/4$ where λ_g is the guided wavelength at zeroth order resonance. The electrical size of the unit cell of the antenna is $0.225\lambda_0$ x $0.072\lambda_0$ (15 mm x 4.8 mm) at 4.505 GHz. The overall area of the antenna aperture is approximately $0.751\lambda_0$ x $0.751\lambda_0$ x $0.024\lambda_0$ (50.0 mm x 50.0 mm x 1.6 mm) at 4.505 GHz. A single feed line of size 15 mm x 4.8 mm is used to excite the antenna. The feed line parameter is adjusted to achieve good impedance matching. The antenna is excited by shunt mode of resonance as it is an unbalanced open ended TL. The physical size and operational frequencies of the antenna are determined by the shunt elements of the unit cell. The gap between the feed line and the radiating patch is about 0.1mm and it contributes to the coupling capacitance C_C. This helps in matching the antenna input impedance to 42 ohms.

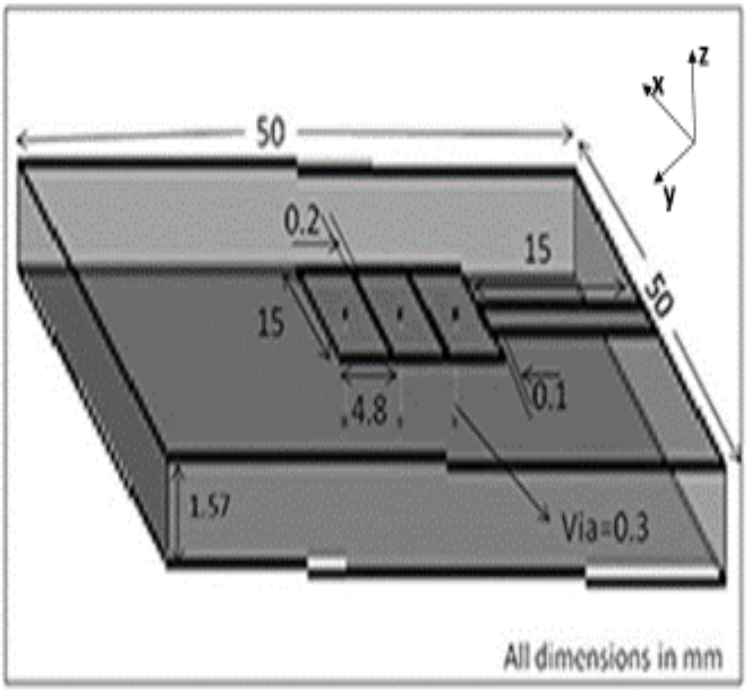

Figure 3.4 Simulated model of CRLH dual-mode ZOR antenna.

The full-wave simulated reflection coefficient of ZOR antenna corresponds to two modes at 4.505GHz and 3.62 GHz with a low reflection coefficient of -10.6151dB and -16.0843dB respectively as shown in Figure 3.5. VSWR less than 2 is obtained at each resonant frequency as shown in Figure 3.6. These two modes correspond to two distinct field modes as shown in Figure 3.7(b) and Figure 3.10 (b). At 4.505GHz an in-phase electric field distribution pattern corresponding to zeroth order mode is obtained but with low reflection coefficient, while, at 3.62 GHz an out-of–phase electric field distribution pattern is realised.

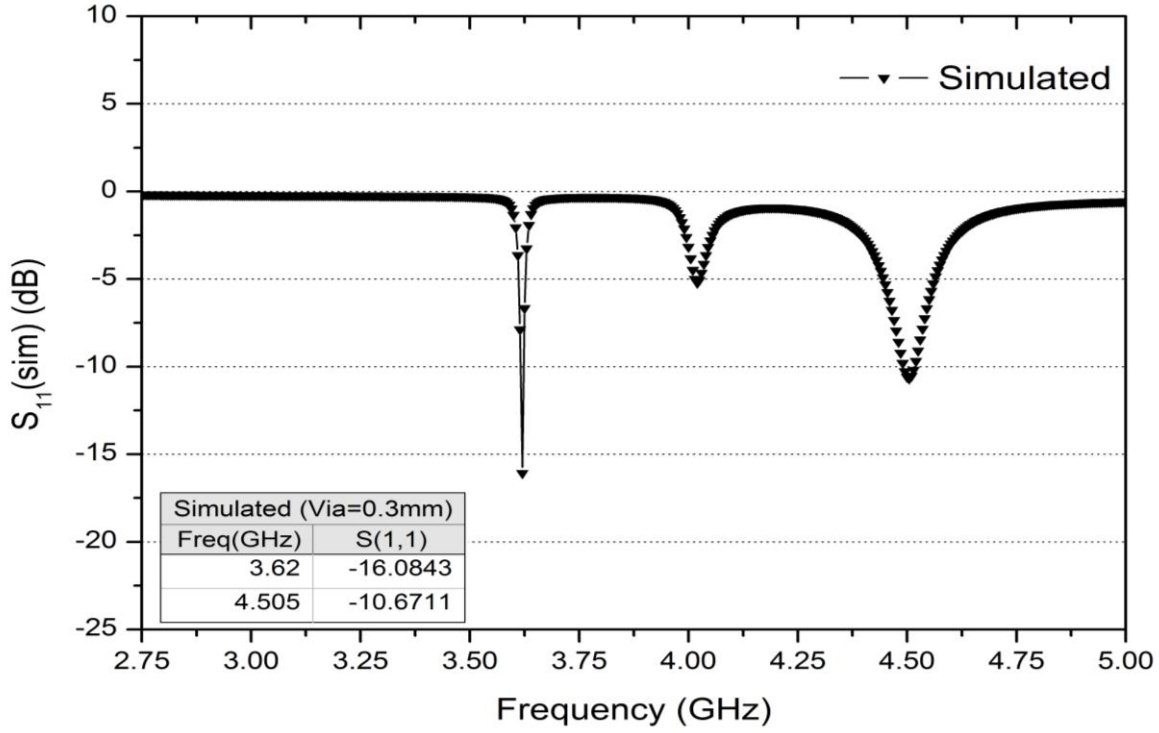

Figure 3.5 Reflection coefficient of the 3-unit cells ZOR antenna.

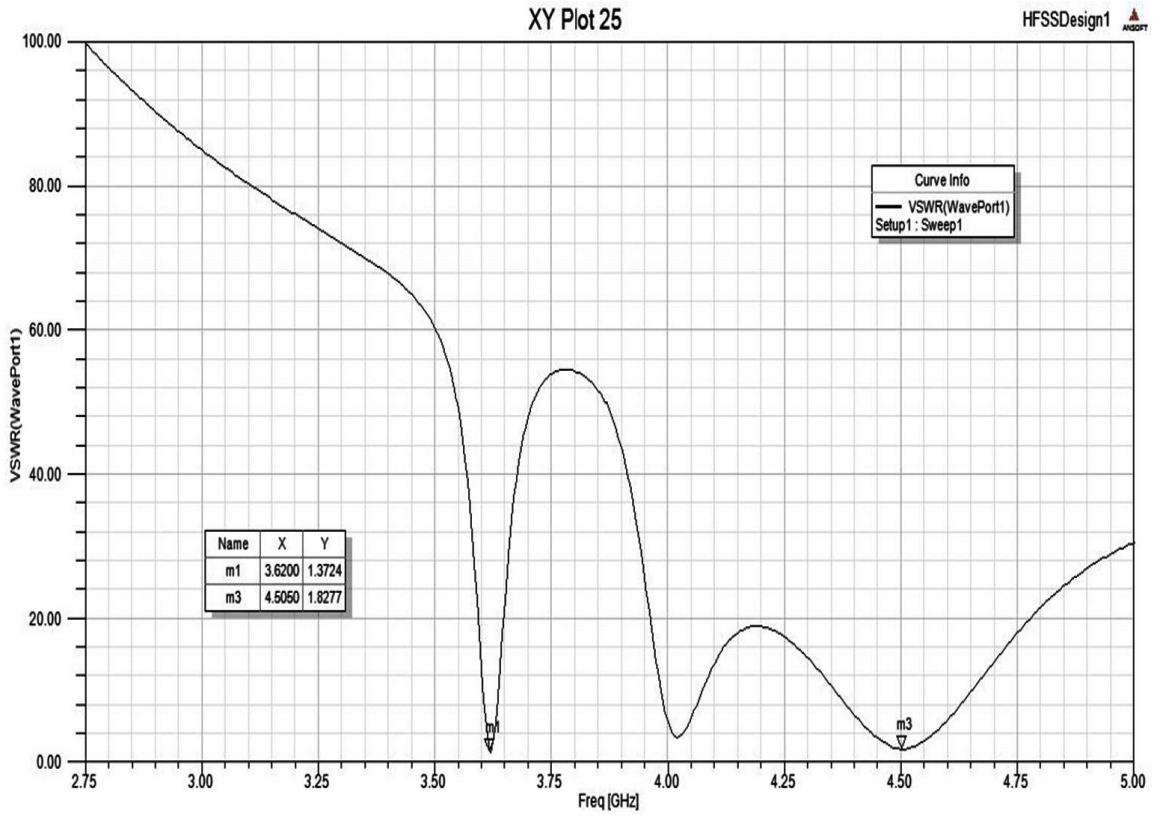

Figure 3.6 VSWR of the 3 unit cells ZOR antenna.

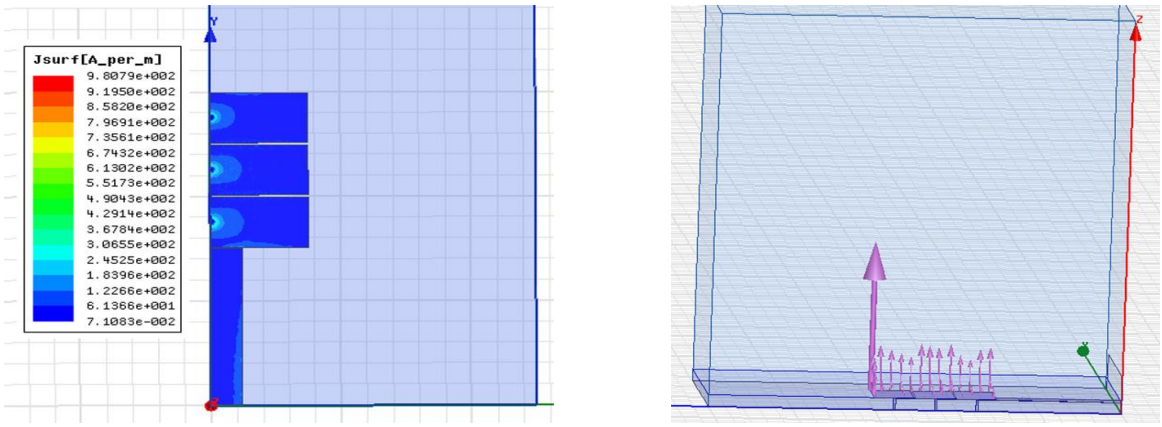

(a) (b)

Figure 3.7 (a) Surface current distributions and (b) E-field distributions at 4.505GHz.

From the surface current distribution, Figure 3.7 (a) it is realized that the inductive vias or stubs contribute significantly to antenna radiation. These inductive stubs can also be used as very suitable elements for tuning of the monopole ZOR antenna at the desired working frequency. This dependency of the resonant frequency on the inductive via radius is confirmed as a parametric study shown in Figure 3.13. At the zeroth order resonant frequency of 4.505 GHz, the electric field distribution shown in Figure 3.7 (b) are in phase and is shown to be uniformly vertical to the radiating patch. So an infinite wavelength is supported. Since, the magnetic field is locally circulating around the vias, to provide LH shunt inductance, so it is on an average perpendicular to the electric field. Hence, both the electric and magnetic fields essentially lie in a plane perpendicular to the direction of propagation.The uniform electric field vertically polarized along z-direction is a unique feature of ZOR antenna because its mode index is zero and it gives rise to a monopolar radiation pattern along E-planes (x-z plane and y-z plane) as shown in Figure 3.8 (a). Hence, magnetic current density forms a circulatory loop around the radiating patch which in turn gives rise to an omni-directional radiation pattern in H- plane (x-y plane) as shown in Figure 3.8 (b). Hence, a ZOR antenna supports an omni-directional radiation characteristic at the zeroth order mode.

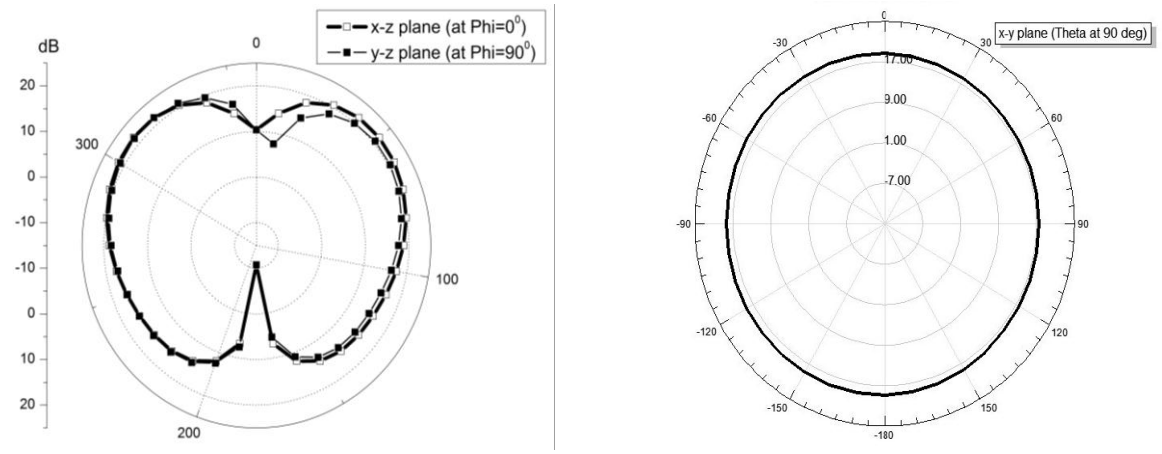

(a) E-Plane (b) H-Plane

Figure 3.8 Radiation patterns at 4.505 GHz.

The above facts are re-ascertained from the dispersion diagram for a single unit cell ZOR antenna shown in Figure 3.9. From the dispersion diagram it is confirmed that at 4.505 GHz, phase constant is 0 degrees. As it is well known that the composite right/left handed (CRLH) transmission line (TL) has unique property of an infinite-wavelength wave at specific non–zero frequency, a miniaturized antenna can be readily designed.

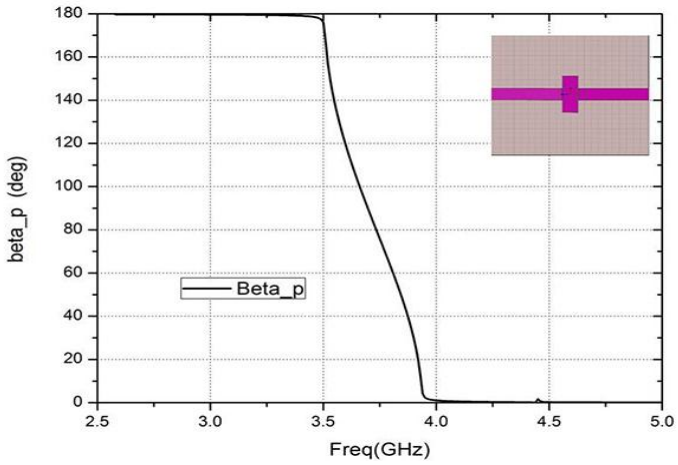

Figure 3.9 Simulated dispersion diagram for a single unit cell ZOR antenna.

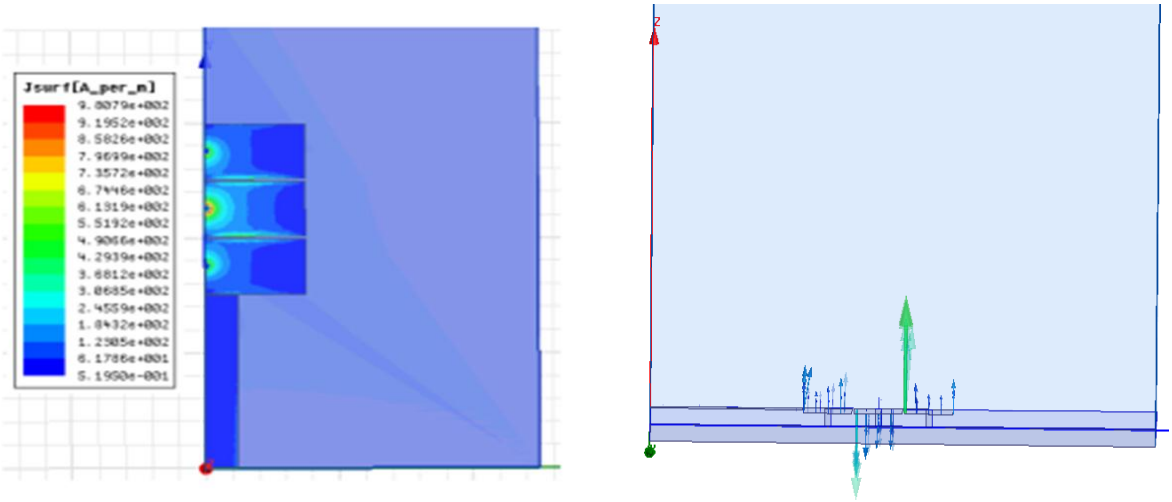

(a) (b)

Figure 3.10 (a) Surface current distributions and (b) E-field distributions at 3.62GHz.

From the surface current distribution shown in Figure 3.10 (a) it is observed that due to surface discontinuity most of the losses are incurred by the lossy inductive stubs which reduce antenna efficiency to 40%. At 3.62 GHz i.e.; -1st resonance mode, a 180 degree out of phase E-field pattern is obtained as shown in Figure 3.10 (b). As a result, the equivalent magnetic current densities along the perimeter of the antenna for the n= -1 mode form a half-wavelength distribution comparable to Figure 3.1 (a). So, a radiation pattern similar to a conventional patch antenna is expected as shown in Figure 3.11 (a), while, an omni-directional radiation pattern is obtained in H- plane (x-y plane) as shown in Figure 3.11 (b).

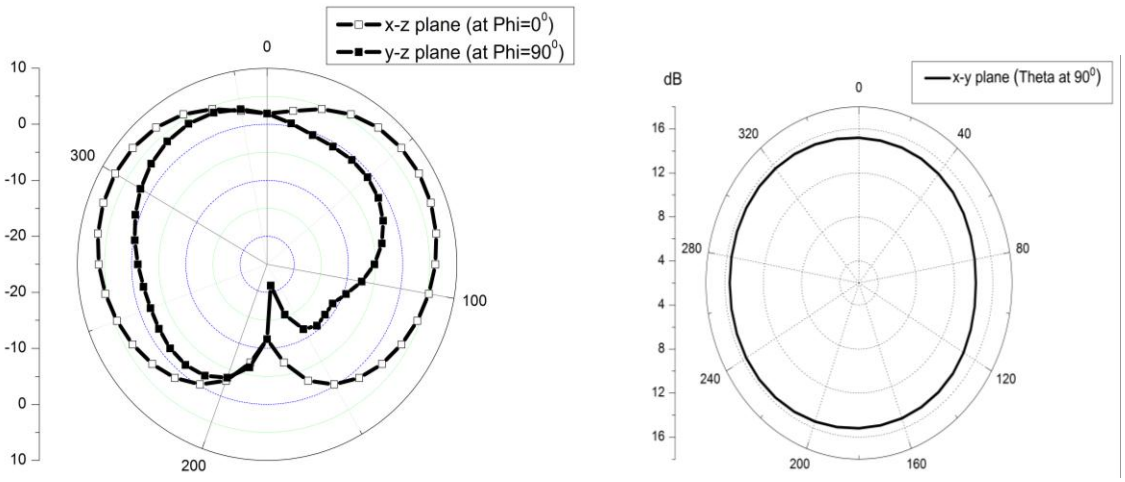

(a) E-Plane (b) H-Plane

Figure 3.11 Radiation patterns at 3.62GHz.

Figure 3.12 shows the 3D-Gain patterns of the proposed antenna at the two operating frequencies of 4.505 GHz and 3.62 GHz. The gain of the antenna at 4.505 GHz is 1.5075 dB and at 3.62 GHz is -1.3075 dB which is acceptable.

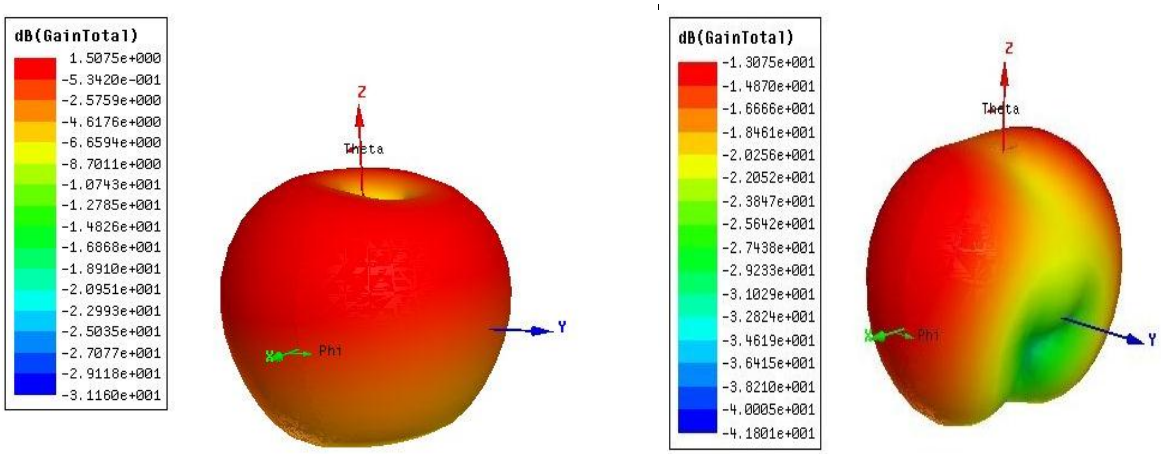

(a) 4.505GHz (b) 3.62GHz

Figure 3.12 3D-Gain of the resonant CRLH TL antenna.

3.4.3 Optimization and Parametric Analysis

Figure 3.13 shows the effect of changing via radius on the zeroth order resonant frequency. As shown in the figure it is ascertained that with increase in via radius, the zeroth order resonant frequency increases. Hence the inductive via can also be used as very suitable elements for tuning a given antenna to a desired working frequency. The simulated parametric analysis is defined to sweep the value of via radius from a minimum to a maximum range. The study presented here sweeps the variable with a limit of ±30% about the nominal value. The best parameterized result is obtained at via=0.12mm and via =0.3mm. Since, fabrication with via=0.12mm is very difficult so via radius with 0.3mm is chosen and

the corresponding experimental study is presented. Optimization analysis is done by using HFSS pattern search optimizer. As shown in Figure 3.14, optimization was done on the best parametric result to get the minimum reflection coefficient of -18.0736 dB at 4.28 GHz and -18.1915 dB at 3.255 GHz for via radius 0.225 mm. At 4.28 GHz a fractional bandwidth of 1.95% is achieved. Figure 3.15 shows the optimized output in which the cost function reduces to optimized minima for via radius 0.225 mm. Finally, Figure 3.16 shows the comparison of the optimised (optimal design) and simulated (nominal design using via radius=0.3 mm) reflection coefficients.

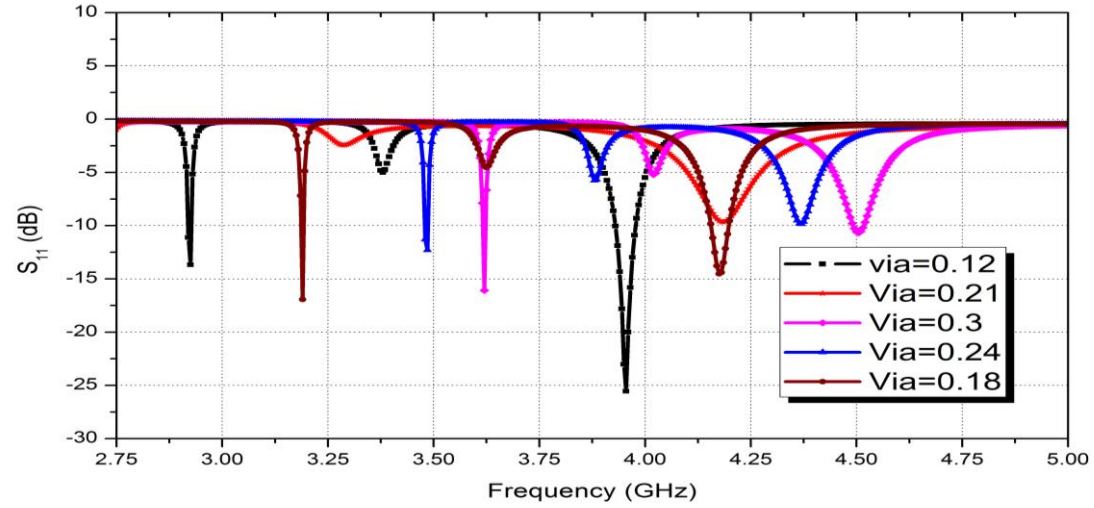

Via=0.12	
Freq(GHz)	S(1,1)
3.955	-25.551
2.925	-13.6752

Via=0.18	
Freq(GHz)	S(1,1)
3.19	-16.9355
4.175	-14.5283

Via=0.21	
Freq(GHz	S(1,1)
4.18	-9.6402

Via=0.3	
Freq(GHz)	S(1,1)
3.62	-16.0843
4.505	-10.6711

Via=0.24	
Freq(GHz)	S(1,1)
3.485	-12.3072
4.37	-9.8499

Figure 3.13 Parametric study on reflection coefficient (S_{11}) due to change of via radius.

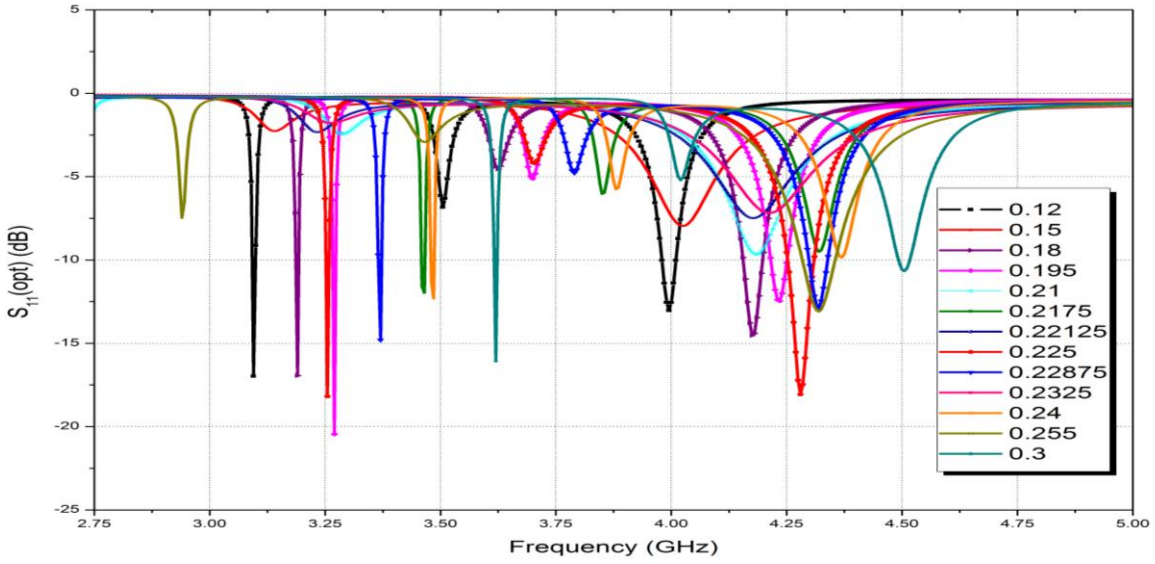

Figure 3.14 Optimized via radius for minimum reflection coefficient.

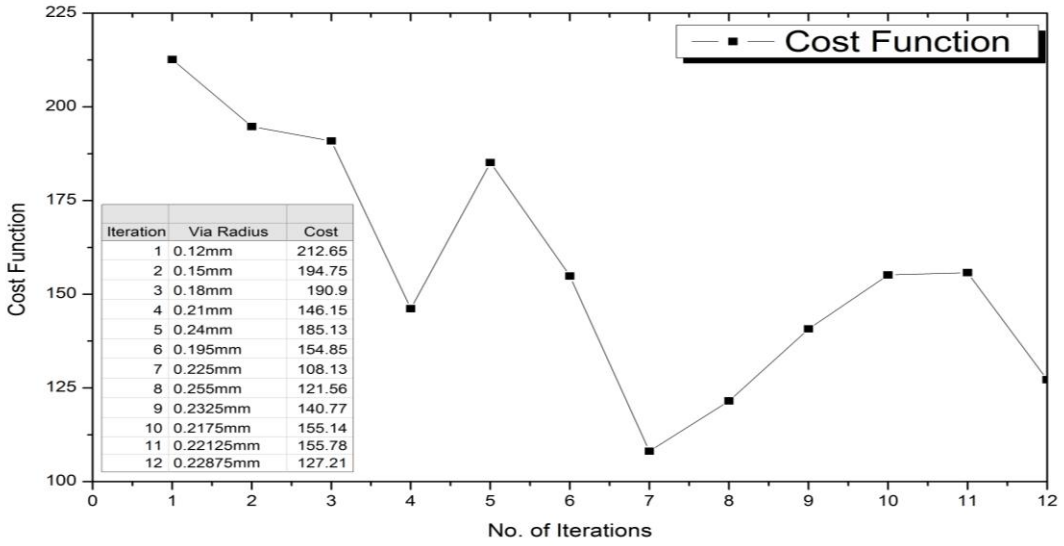

Figure 3.15 Plot for Cost function Vs no. of Iterations using Pattern Search Optimizer.

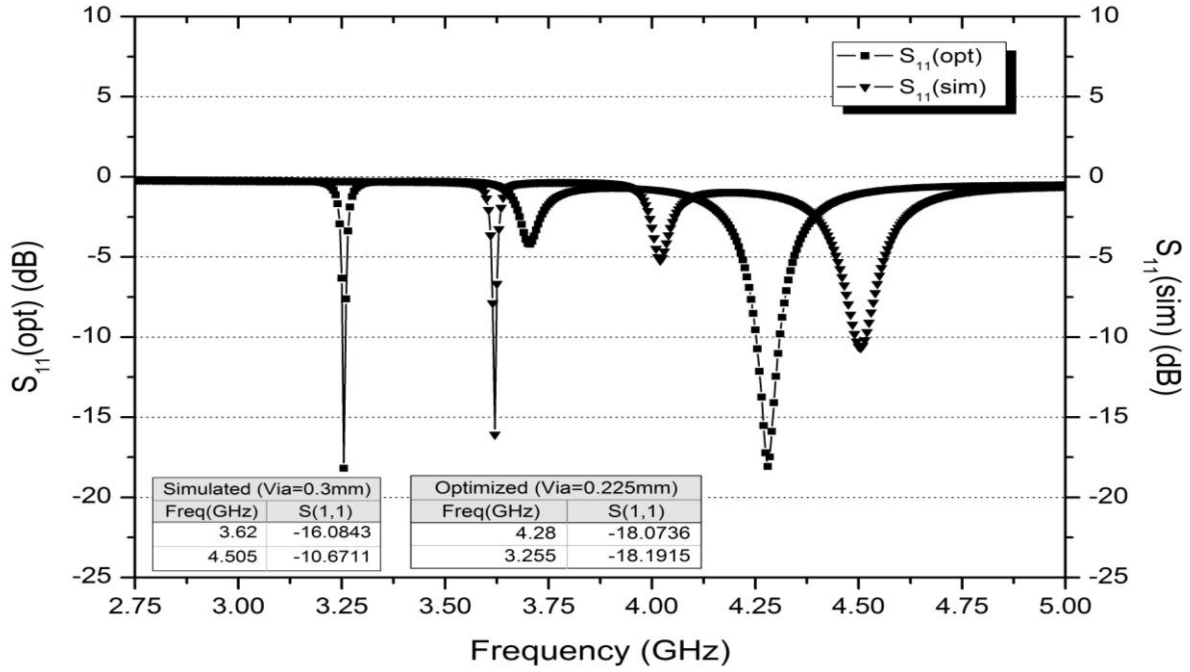

Figure 3.16 Comparison of optimized and simulated reflection coefficients.

3.5 Experimental Verification

Figure 3.17 shows the fabricated prototype of the designed antenna. Details of fabrication procedure are mentioned in Appendix A.2. Figure 3.18 shows the comparison of the simulated and measured reflection coefficients at -1st resonance of the antenna. A very good agreement between the measured and simulated results is obtained. The slight difference might be due to improper etching and the effect of SMA 50 Ω connectors. It is observed that the simulated resonant frequency at 3.62 GHz with a reflection coefficient of -16.0843 dB agrees well with the measured resonant frequency achieved at 3.58 GHz with a reflection

coefficient of -19.44 dB. Since with increase in the via radius the shunt inductance decreases; a narrow bandwidth of about 0.1% at f_{-1}=3.62 GHz is obtained. As these antennas are much less than quarter-wavelength antennas, it results in very high radiation resistance which can be impedance matched to a very narrow band of frequency.The operational bandwidth obtained at 3.62GHz is aptly suited for precise wireless communications which include the mobile and wireless local area network (WLAN) systems due to their large service area. The electrical size of the unit cell is $0.181\lambda_0$ x $0.058\lambda_0$ (15 mm x 4.8 mm) at 3.62 GHz.

Figure 3.19 shows the simulated and measured VSWR of the resonant CRLH TL. It is found that the VSWR is less than 2 in both the results. The antenna exhibits a very high efficiency of about 92.91% at the zeroth order mode of 4.505 GHz but suffers from a drawback of low radiation efficiency of about 40% at 3.62 GHz which can be improved by adding an additional air layer between the ground plane and the dielectric substrate carrying the antenna motif. In fact the gain of a microstrip based ZOR antenna is mostly negative. Scattering parameter measurements are carried out using Agilent E8363B Network Analyzer at Space Applications Center (SAC), ISRO, Ahmedabad, India.

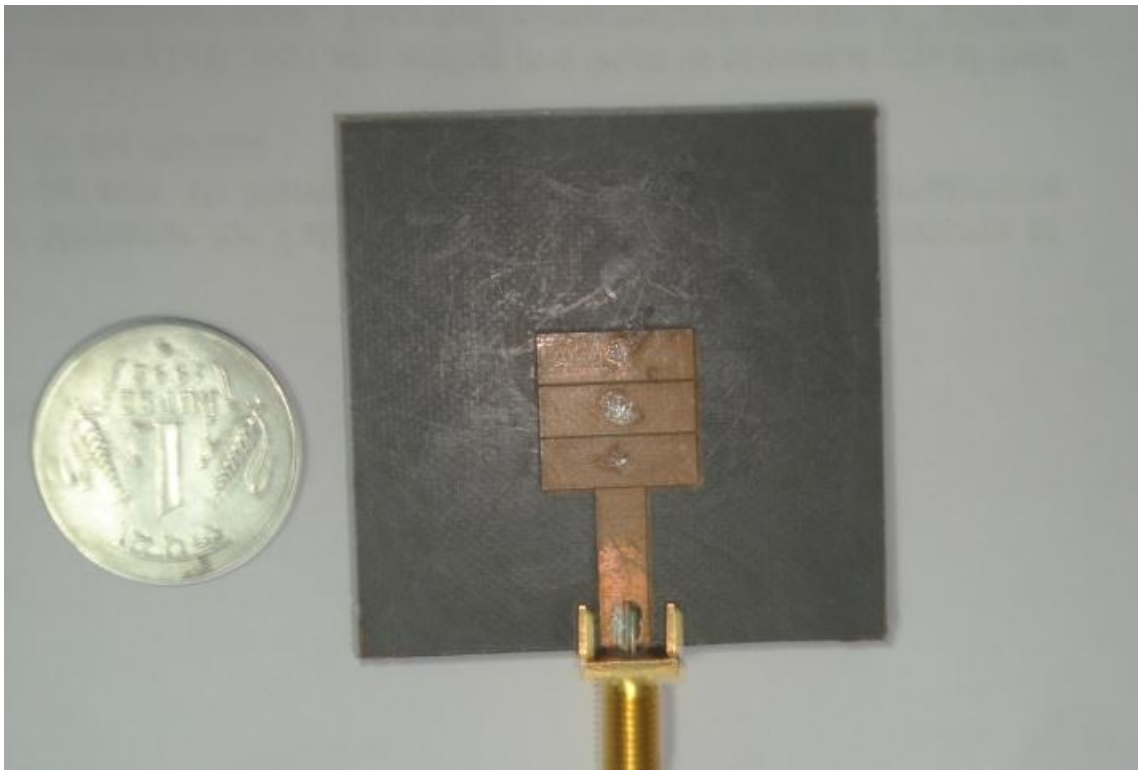

Figure 3.17 Fabricated prototype of the proposed antenna.

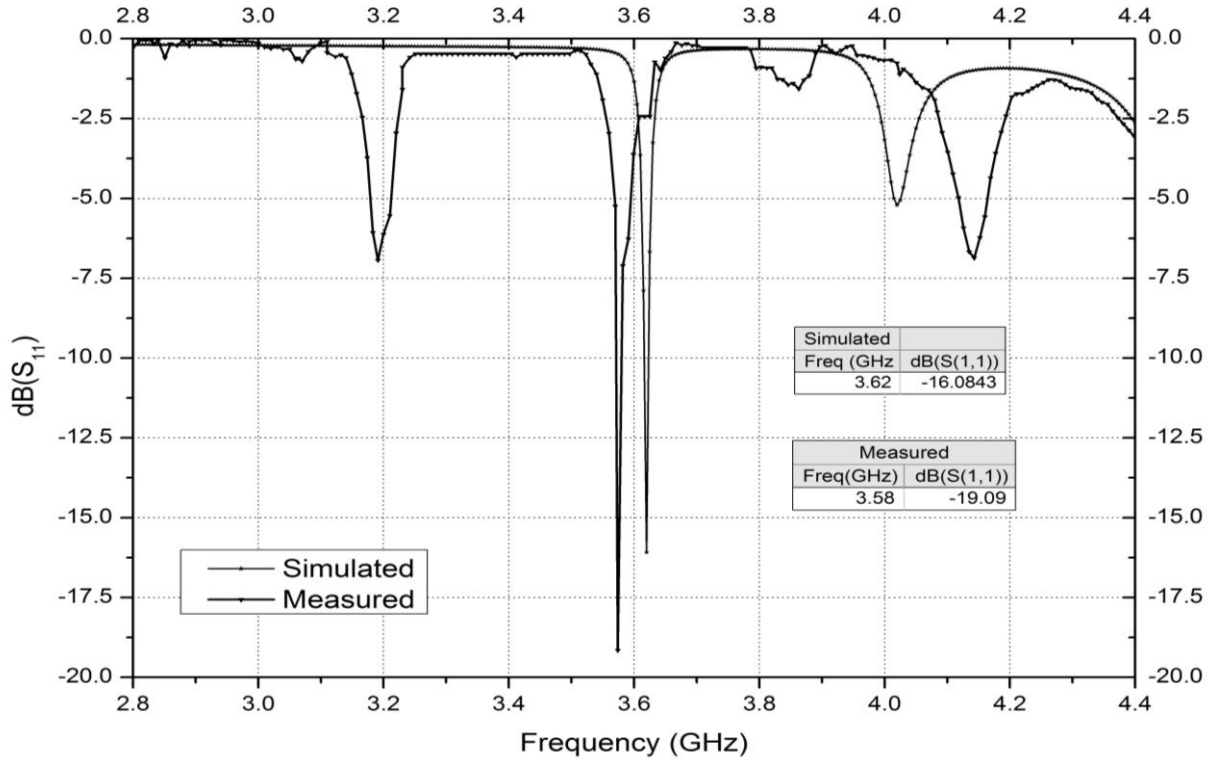

Figure 3.18 Comparison of simulated and measured reflection coefficients of the proposed antenna.

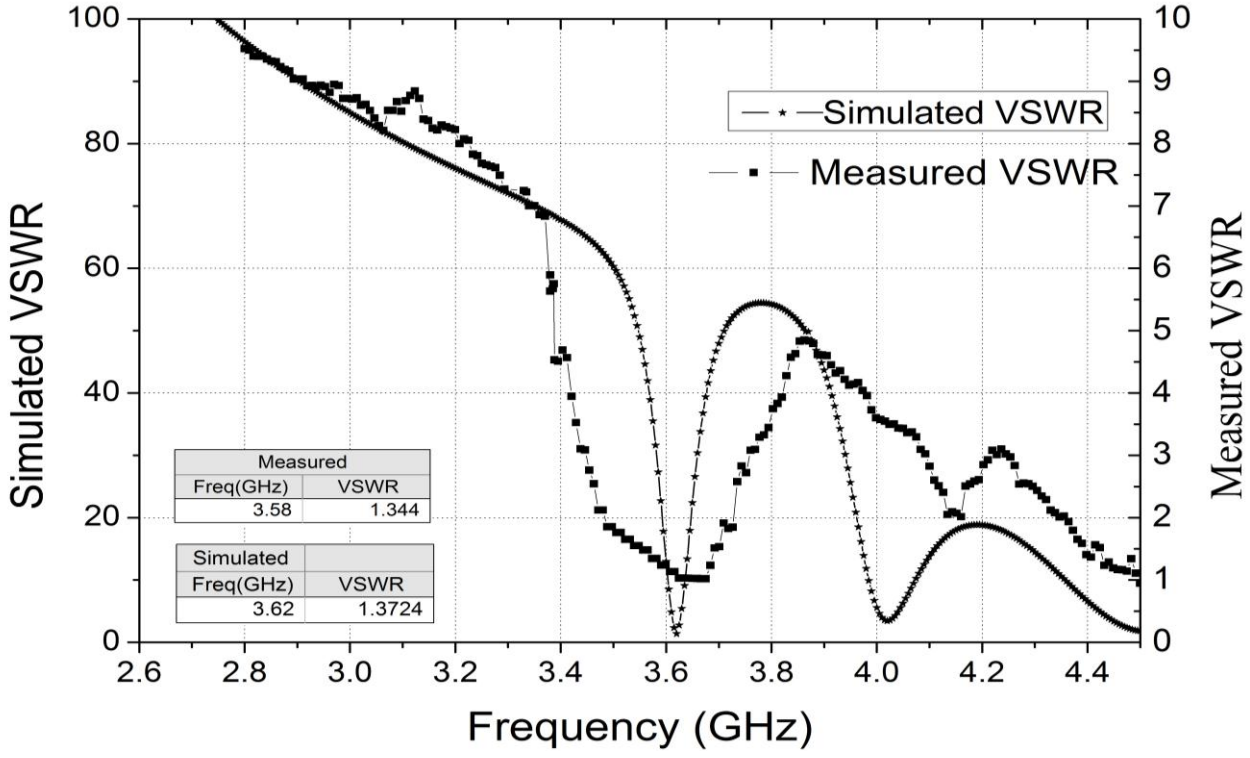

Figure 3.19 VSWR of the resonant CRLH TL antenna.

3.5.1 Antenna Radiation Pattern Measurements

Radiation pattern measurements are carried out in an Anechoic Chamber having size of 13m x 8m x 8m (L x W x H) respectively at Antenna Measurement Facility (AMF) at Space Application Centre, ISRO, Ahmedabad. Details of Anechoic Chamber and radiation pattern measurement set up is given in Appendix A.3.3.

Radiation patterns is measured at 3.58GHz. Figure 3.20 and Figure 3.21 shows the E-plane and H-plane radiation patterns at 3.58 GHz, respectively. Real time flight model testing is carried out with the test antenna mounted on to an aluminium plate fixture with an offset of 8cm and then aligned to a reference wideband horn antenna. Measurements outside the azimuth range $\pm 150^0$ could not be carried out since the positioner mounting interface shown in Figure 3.21 blocks the (relatively smaller) antenna assembly.

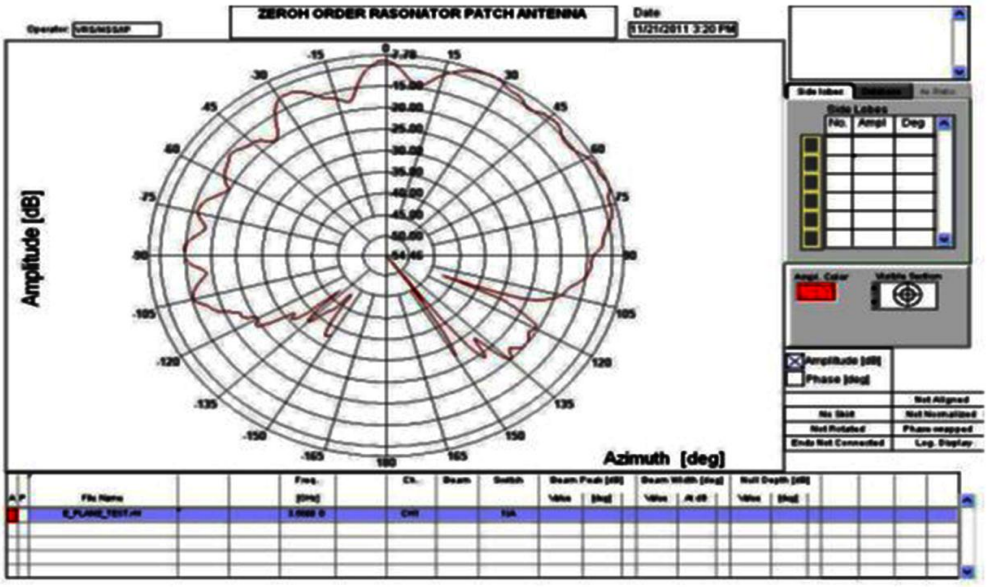

Measured at 3.58GHz.

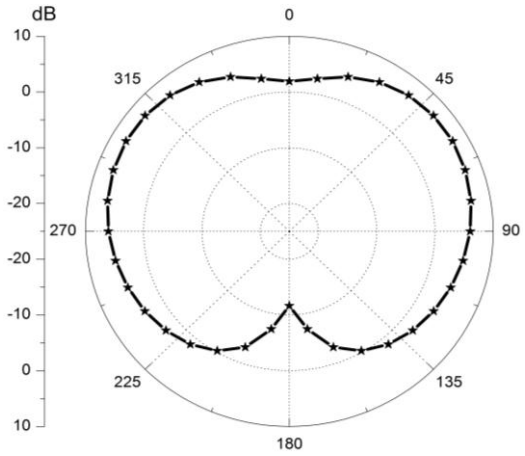

Simulated at 3.62 GHz.

Figure 3.20 (a) E-plane radiation patterns.

In Figure 3.20 (a), signal fluctuations in the main lobe of the measured radiation pattern is observed. This may be on account of the low coupled power from the single element. Leakage or reflections from RF absorbers are responsible for the characteristic maxima and minima. In Figure 3.20 (b) lesser amount of back-radiation can be seen which can be neglected. Nevertheless, the simulated and measured results agree well within experimental errors and uncertainties.

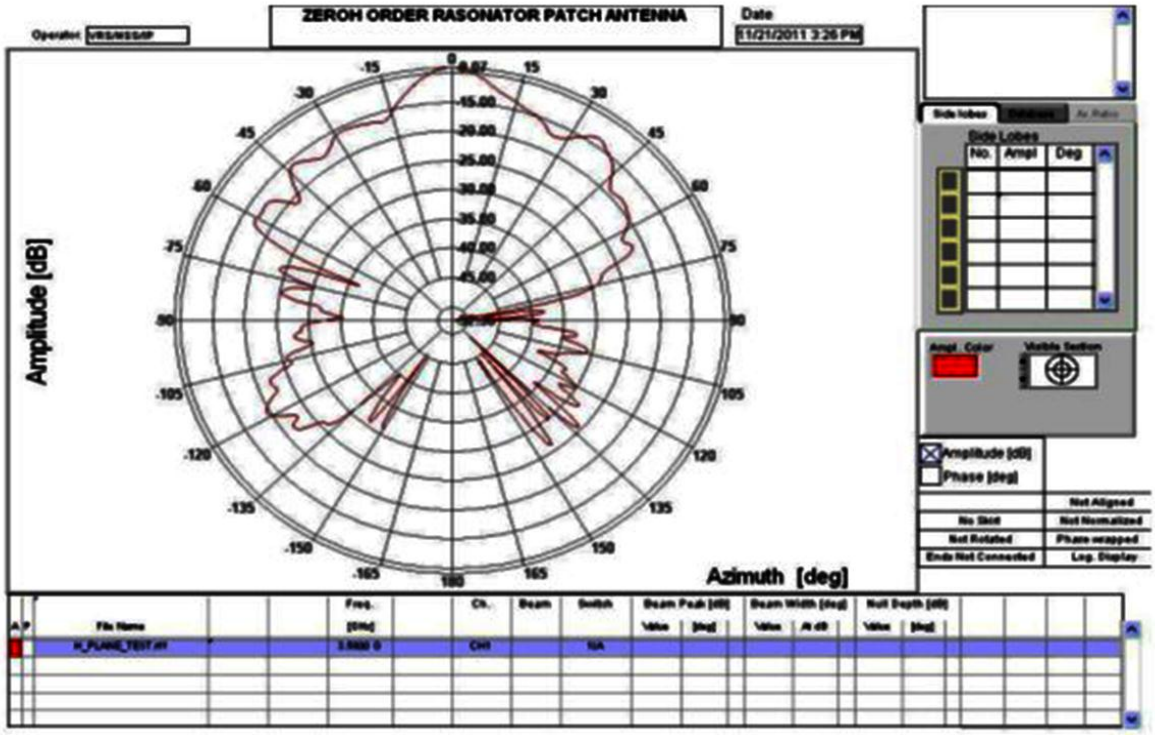

Measured at 3.58GHz.

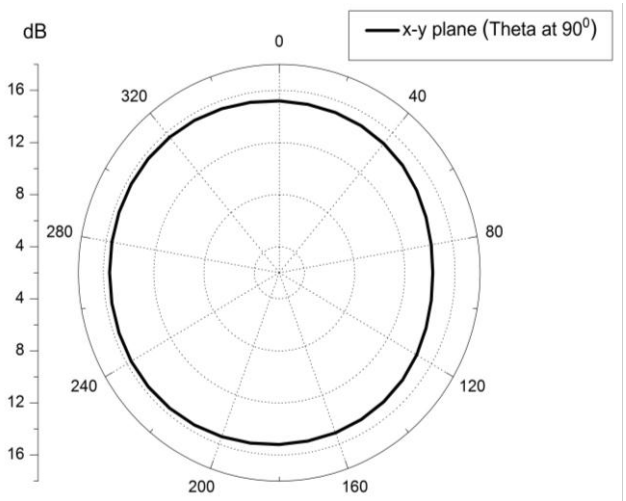

Simulated at 3.62 GHz.

Figure 3.20 (b) H-plane radiation patterns.

3.6 Summary

A compact microstrip based ZOR antenna with optimization and experimental verification is presented. Parametric analysis is used to study the effect of different via radius on the resonant frequency of the frequency independent antenna. The study shows that with increase in via radius, the zeroth order resonant frequency also increases. Through parametric study it is concluded that an inductive via can also be used as very suitable elements for tuning a given antenna to a desired working frequency. Optimization analysis is then performed on the best parametric result obtained for minimum reflection coefficient and enhanced bandwidth. The open ended antenna presented here is excited by the shunt mode of resonance. The operational frequency is independent of the physical size of the antenna structure but is determined by the shunt elements of the unit cell. In this case, the antenna exhibits monopolar radiation at its fundamental zeroth mode of resonant frequency 4.505 GHz. It is found from the simulated and measured reflection coefficients of the proposed antenna that the measured results varied from the simulated ones at the zeroth order mode by about 0.12% approximately. The ZOR phenomenon enables a small antenna to be realized. Due to the narrow bandwidth obtained at the zeroth order mode the realized antenna is aptly suitable for precise multiband wireless communication systems. Summarizing, the advantage of the microstrip based ZOR antenna is that miniaturisation of the antenna along with multi frequency operation is achieved and has the potential for frequency and pattern reconfigurability.

Chapter 4

Coplanar Waveguide fed Zeroth Order Resonant Antennas

4.1 Introduction

In the previous chapter, it is seen that a zeroth order mode supports omni-directional radiation pattern which is an essential feature for WLAN and WiMax applications but severely suffers from narrow bandwidth of just about 0.75%. This drawback impedes ZOR antennas to be used for wireless LAN applications. In this chapter, CPW fed multiband ZOR antennas with extended bandwidth for WLAN and WiMax applications are designed.

Emerging wireless technologies increase the need for multiband, light weight and easily fabricated antennas. Presently, the technologies of wireless communication systems have been rapidly growing for greater capacity broadband service and to shore up transmission speeds so as to support multimedia, image, speech and data communication. In order to meet the rapidly growing demands, an antenna should be capable of performing in many frequency bands. Accordingly, a multiband antenna with good radiation characteristic is desired in many systems. In order to achieve multi-band operation, several traditional approaches are used. Generally, multi-branched strips and parasitic elements are added to a single resonating device to stimulate multiple resonant bands, which generally leads to a large volume or requires a large ground plane. Slots are cut into radiator or ground plane to excite multiple resonant modes.

Indeed, the improvement of antenna performance by means of metamaterials has been a subject of intensive research in recent years. Metamaterials have been exhibiting their potentiality in the implementation of resonant antennas, which also provide a conceptual route for multi-band operations. Although metamaterial antennas provided a good multiband solution, it also produced multiple narrow matched bandwidths, as was shown in the previous chapter. Generally speaking, metamaterial antennas suffer from narrow band or structural complexity due to via or other extra line connected to ground in order to get shunt inductance that is necessary for practical realization of transmission-line metamaterials. There have been several concepts in improving bandwidth in the recent years. So it will be an added advantage if a zeroth order resonant antenna exhibits multiband functionality with extended bandwidth.

This chapter focuses on improving the bandwidth and gain of transmission line metamaterial antennas without compromising antenna efficiency. To serve our purpose, two new coplanar waveguide fed ZOR antennas is proposed and its performance analysed for multiband WLAN and Wi-Max applications. To achieve extended bandwidth two new methodologies are adopted and implemented as discussed in the succeeding sections. This chapter is organized as follows. Next section demonstrates the principle of the CPW-based ZOR antenna and the bandwidth extension through the design parameters rather than the material properties. In this paper, two antenna configurations are presented employing the

proposed idea to achieve maximum bandwidth for the proposed antenna configuration. Finally, comparison of their performance characteristic is tabulated and conclusions are drawn.

4.2 Bandwidth Extension Technique and Design Methodology

According to Equation (2.31), in case of open-ended CRLH TL, the fractional bandwidth is given by,

$$BW = G \times \sqrt{\frac{L_L}{C_R}} \cdot \tag{4.1}$$

Where, G is the shunt conductance of a lossy transmission line,

C_R is the shunt LH capacitance,

and L_L is the shunt inductance.

Although this equation does not consider impedance matching at the input terminals, it provides an intuitive concept by means of which the bandwidth can be efficiently increased. As discussed in Chapter 2 and 3, ZOR antennas are known to suffer from a narrow bandwidth problem compared to conventional resonant antennas. This is because the Q-factor of a ZOR antenna is only related to C_R and L_L . For example, in a microstrip structure, L_L and C_R are realized by the shorting pin (via) and parallel plate between the top patch and bottom ground. Since the LH inductance L_L in a microstripline (MSL) is directly proportional to the via height, which, in turn depends on the substrate height, greater flexibility in the variation of the parameter L_L is not possible to achieve enhanced bandwidth. The microstrip structure hence limits the value of L_L . In addition, since the thickness and size of the substrate determine the capacitance of the parallel plate, the MSL has a large C_R . According to Equation (2.33), the narrow bandwidth originates from the small L_L and large C_R . Therefore, the ZOR antenna in microstrip technology has a narrow bandwidth due to the structural problem. In order to extend the bandwidth of the microstrip structure, a thick substrate with low permittivity is generally utilized. However, this leads to excitation and surface wave losses.

In this chapter as well as in subsequent chapters, focus is laid on antennas with a large L_L and small C_R , which result in improved bandwidth without degrading the efficiency, due to the shunt conductance. Moreover, a structure which can be easily fabricated and offers more design freedom, is being suggested here.The CRLH TL based ZOR antennas proposed in this chapter is implemented using CPW technique. Coplanar waveguides are uniplanar transmission line structures where the ground plane and the signal trace are placed on the same side of the substrate. The advantage of having both conductors in the same plane lies in

the fact that it is easier to mount lumped components between the two planes and it is easier to realize large shunt and series configurations. Hence, a CPW structure provides more flexibility to change the shunt parameters (C_R, L_L) of a CRLH TL to achieve extended bandwidth. It provides smaller shunt parasitic RH capacitance C_R if the distance between the CPW grounds from the radiating patch is increased and larger shunt LH inductance L_L if the lengths of the short ended spiral inductors are increased. But in case of microstrip technique as the signal trace is separated from the ground plane by a dielectric layer (i.e.; by a substrate material), C_R tends to be large. This is because it depends on the capacitance of the host microstrip line to the ground plane. Also here the shunt inductance L_L is small because the LH inductance provided by the vias is directly proportional to its height, which in turn is restricted by the substrate's height. The compact vialess ZOR antenna proposed by Jang et al is simple and easy to fabricate but operated over a single band. In this section the proposed metamaterial antenna is designed to operate over multiband suitable for wireless LAN applications.

Two antenna designs based upon the described technique are presented. They are chosen to operate in the 1 GHz - 5 GHz band. All the designs are built on a Rogers RT/ Duroid 5880 (ε_r = 2.2, tan δ = 0.0009) substrate of thickness 1.6 mm and a thickness of 0.017 mm of copper cladding.The substrate is chosen in order to achieve high efficiency and low loss.

4.2.1 Generalized Equations for Unit Cell Block Design

Consider the unit cell block of Figure 4.2. Typical guidelines for the design of CRLH TL structure may be the following:

1. Appropriate transition frequency is selected as defined by the relation:

$$\omega_0 = \frac{1}{\sqrt[4]{L_R C_R L_L C_L}} = \sqrt{\omega_R \omega_L} = \sqrt{\omega_{se}\omega_{sh}} \tag{4.2}$$

where

$$\omega_R = \frac{1}{\sqrt{L_R C_R}}, \omega_L = \frac{1}{\sqrt{L_L C_L}}, \omega_{se} = \frac{1}{\sqrt{L_R C_L}}, \omega_{sh} = \frac{1}{\sqrt{L_L C_R}} \tag{4.3}$$

2. Applying the matching condition of Equation (2.14) to ports of impedance calculate Z_c using the following equations:

$$Z_R = \sqrt{\frac{L_R}{C_R}} = Z_c \tag{4.4(a))}$$

$$Z_L = \sqrt{\frac{L_L}{C_L}} = Z_c \qquad (4.4\ (b))$$

3. Equations (4.2) and (4.4) consists of four unknowns $L_R, C_R, L_L and C_L$ can be calculated using eigen frequency method detailed in Section 2.3.4.

4. Number of unit cells is set to two.

Once the constitutive lumped element values of the CRLH TL are known, depending on whether RH or LH, it is then multiplied or divided by the length of unit-cell (cell size), to obtain the associated per-unit-length and times unit-length component values:

$$L_R^{'} = \frac{L_R}{p}, C_R^{'} = \frac{C_R}{p}, L_L^{'} = L_L.p, C_L^{'} = C_L.p \qquad (4.5)$$

The constitutive parameters extracted for the unit cell in accordance with the procedure given in Section 2.3.4 and Section 4.3 (a) consists of L_L (due to shunt square spiral inductors) =9.592 nH while L_L (due to the via plated through inductor) =0.032 nH. L_R=2.262 nH, C_R (between the top patch and the CPW ground) =0.118 pF whereas C_R (between the top patch and the bottom conducting strip) =0.569 pF at f_0 = 2.46 GHz.

4.3 Extended Bandwidth Multiband ZOR Antenna

In this section a coplanar waveguide fed compact metamaterial antenna is proposed to achieve extended bandwidth in comparison to microstrip based ZOR antenna described in the previous chapter. Spirals as shunt inductors are incorporated in the proposed structure to achieve our purpose. Here two cases pertaining to the proposed antenna structure is considered. In the first case the antenna structure had a single unit cell while in the second case the proposed antenna consisted of two unit cells. For both cases, the antennas are simulated and experimentally verified to ascertain the fact that as the number of unit cells increases there is only a slight variation in the zeroth order mode. It also confirms that with increase in the number of cells, the multiband functionality of the antenna also increases but resonant frequencies decreases. Figure 4.1 (a) shows pictorially how to physically realize a CPW fed CRLH TL based spiral resonant antenna consisting of two unit cells. The proposed ZOR antenna consists of a single layer substrate material made of Rogers RT/ Duroid 5880 having dielectric constant $\varepsilon_r = 2.2$ and a thickness of 1.6 mm. Each unit cell (6 mm x 7.8 mm) consists of symmetrically placed spiral inductors on both sides of the unit cell. Each unit cell is shorted to ground through inductive via stubs of height 1.6 mm and radius 0.3 mm. Impedance matching is an important factor to increase the bandwidth. So on the bottom, a narrow partial conducting strip is placed beneath the radiating patch to achieve good impedance matching of about 42 ohms. Vias are connected to this strip. As a result the dominantly radiating part of the antenna comes from the shunt spiral stub and vertical vias. Each spiral stub consists of five turns each having a width and spacing of 0.4 mm. These spiral inductors introduce the shunt LH inductance L_L. Some of the main features of

these spiral inductors being that, firstly the length of these spiral inductors is directly proportional to the shunt inductance thereby it increases the shunt LH inductance $L_{L,}$ which in turn leads to bandwidth enhancement; and, secondly it has an inherent property to provide multi frequency multi band resonances. The unit cells or the radiating patch is separated by a small gap of 0.2 mm. This gap provides the series LH capacitance C_L, while, the magnetic flux produced by the current flow along the radiating patch provides the parasitic series RH inductance L_R. A short stub provided on top of the substrate also helps to achieve good impedance matching. The gap between the stub and the unit cell provides coupling capacitance (C_C) which impedance matches the antenna to 42 ohms. A CPW feed line and proximity coupling are used as the feed network to excite the whole CRLH TL structure by open circuiting. Shunt resonance ω_{sh} initiates, with energy being stored in the shunt elements. The proposed design exhibits triband, pentamode characteristics that can be used for precise multiband wireless LAN applications.

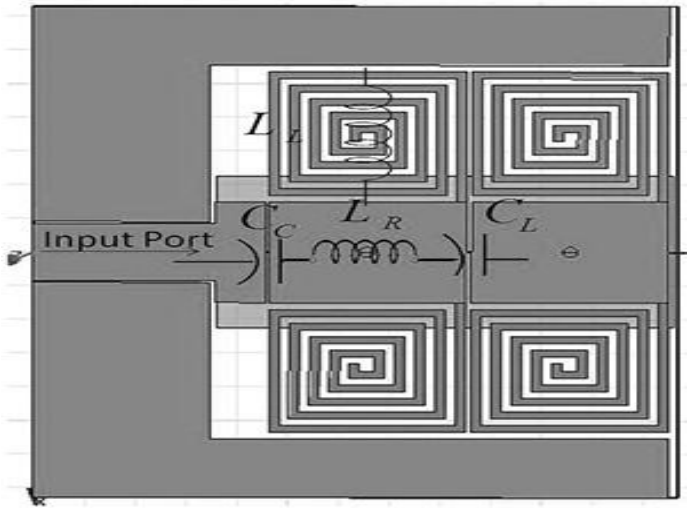

Figure 4.1 (a) Realization of CPW fed CRLH Transmission Line resonant antenna.

4.3 (a) Effect of mutual inductance and mutual capacitance of CRLH TL topology using square spiral inductors (SSI)

CRLH transmission line topology consists of series parameters (RH inductance L_R and LH capacitance C_L) and shunt parameters (LH inductance L_L and RH capacitance C_R). The open-ended CRLH TL antennas proposed in this thesis is excited by shunt mode of resonance, so we here adhere to the extraction of only shunt parameters L_L and C_R. The methodology adopted to extract the RH shunt capacitance will be same as that applicable for any conventional microstrip antennas as specified by Equation 4.12 whereas design Equations (4.6 – 4.11) can be adopted for the extraction of LH shunt inductors.

4.3 (b) Extraction of shunt lumped inductance L_L

The left handed inductance L_L is produced by the shunt shorted stub (via plated through hole) or square spiral inductors as they constitute the main building blocks of the CRLH TL unit cell implemented in this thesis. In [100, 101] calculation methods for inductances of single line segments as well as square spiral inductors is being addressed. It is observed that in a shunt stub or via the LH shunt inductance is mainly controlled by the stub length and determined by its self-inductance. Similarly in case of square spiral inductors, the LH inductance is influenced by both self and mutual inductances (i.e.; magnetic flux linkages from segment to segment) of the line segments. These equation are based on the configurations shown in Figure 4.1.1.

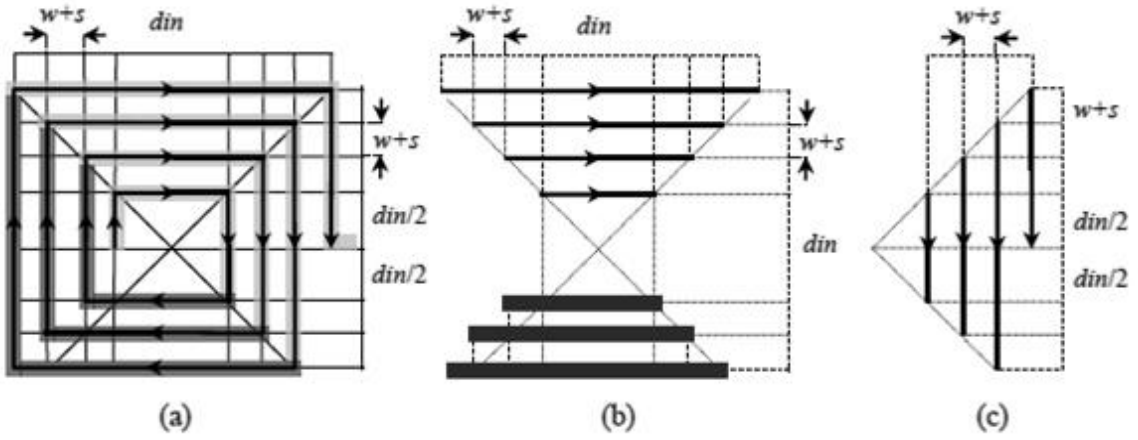

Figure 4.1.1. (a) Square spiral inductor with n=3.5 turns, inner diameter d_{in}, segment width w and spacing between segments s, (b) segments on the opposite sides of the square inductor contributing to the negative mutual inductance and (c) segments on the same side of the square inductor contributing to the positive mutual inductance [100, 101].

Case 1: LH inductance L_L due to square spiral inductors:

In case of symmetrical structure shown in Figure 4.1.1. (a), there is a linear relation between the total length l and the inner diameter d_{in}:

$$l = (4n+1)d_{in} + (4N_i + 1)N_i(w+s) \tag{4.6}$$

Where n the number of is turns, N_i is the integer part of n, w is the metal width and s is the spacing between segments. Therefore, four parameters of n, w, s and either l or d_{in} can fully determine the lateral structure of the spiral inductor. Thickness of the metal t is to be considered in case of 3D structures. So, a straight segment of the length l_{seg} has the self-inductance $L_{self-seg}$ [100]:

$$L_{self-seg} = \frac{\mu_0}{2\pi} l_{seg}\left(\ln \frac{2l_{seg}}{w+t} + 0.5 \right) \tag{4.7}$$

Where μ_0 is the permeability of free space given as $4\pi \times 10^{-7}\, Hm^{-1}$.

The total inductance of a square spiral inductor consists of the inductor self-inductance (L_{self}) and the remaining part, arises from the total negative (due to anti-parallel segments) and total positive mutual inductances; this includes all positive and all negative interactions between all segments [100]. Thus the total LH shunt inductance L_L of a square spiral inductor is:

$$L_L = \frac{\mu_0}{2\pi} l\left(\ln \frac{l}{n(w+t)} - 0.2 - 0.47.n + (n-1).\left(\ln\left(\sqrt{1+\left(\frac{l}{4nd^+} \right)^2} + \frac{l}{4nd^+} \right) - \sqrt{1+\left(\frac{4nd^+}{l} \right)} + \frac{4nd^+}{l} \right) \right) \tag{4.8}$$

Where d^+ is the average distance for the constituting factor of positive mutual inductance, calculated as

$$d^+ = (w+s)\frac{(3n-2N_i-1)(N_i+1)}{3(2n-N_i-1)} \tag{4.9}$$

It is therefore concluded that with increase in l and a decrease in w and s of a square spiral inductor, the shunt inductance is increased due to increase in mutual coupling between the turns. The magnetic field and current distributions in the segment will change because of current constriction (skin-effect) and proximity effects of neighboring metal segments. At low frequency, the substrate acts like a good ground plane and partially shields the metal segments from each other so the effect of mutual capacitance can be neglected but at high frequency due to finite conductivity of the substrate as well as the non-zero impedance that grounds the substrate externally, the substrate will begin to float electrically. In this situation the substrate will not be able to shield the metal segments effectively and the effect of mutual capacitance will increase.

Case 2: LH inductance L_L due to via inductors:

Generally, there are two types of via holes implemented by different techniques. In one method, the via hole is completely filled with metal while in the other the via hole is plated through hole. This latter procedure is implemented in this thesis. Inductance for both methods can be obtained from the following relations:

$$L_{via-platedthrough} = 5.08.h.\left[\ln \frac{4h}{r} + 1 \right] \tag{4.10}$$

and,

$$L_{via-filled} = \frac{\mu_0}{2\pi}\left[h.\ln\left(\frac{h+\sqrt{r^2+h^2}}{r} \right) + \frac{3}{2}\left(r - \sqrt{r^2+h^2} \right) \right] \quad (4.11)$$

where h is the via conductor height and r is the via radius, both in meters.

4.3 (c) Extraction of shunt parasitic capacitance C_R

The RH shunt capacitance C_R is the parasitic capacitance that exists between the top conductor plate and the ground plane and can be calculated using:

$$C_R = \varepsilon_r.\varepsilon_0.\frac{A}{d} \quad (4.12)$$

Equation (4.12) implies that the capacitance of a parallel-plate-capacitor is directly proportional to the overlap cross sectional area, A, of the two plates and inversely proportional to the distance, d, between them. Therefore, according to the equation, C_R is mainly controlled by A and d.

4.3.1 *Case-I: Antenna Geometry and Simulation Results with 1-unit cell*

Figures 4.2 shows the geometry of the CPW fed triband, triple mode CRLH TL antenna. A substrate of size 29.2mm x 17.2mm x 1.6mm is used. The proposed antenna is designed to have its zeroth order mode at 2.46 GHz using Ansoft HFSSv12. Antenna parameters are adjusted according to the general design guideline that the electrical size of the unit cell is approximately less than $\lambda_g/4$ where λ_g is the guided wavelength at zeroth order resonance. The electrical size of the unit cell of the antenna is $0.0492\lambda_0$ x $0.064\lambda_0$ (6 mm x 7.8 mm) at 2.46 GHz. The overall area of the antenna aperture is approximately $0.239\lambda_0$ x $0.141\lambda_0$ x $0.013\lambda_0$ (29.2 mm x 17.2 mm x 1.6 mm) at 2.46 GHz. The parameters of the bottom patch is adjusted to achieve a good impedance matching of 42 ohms.

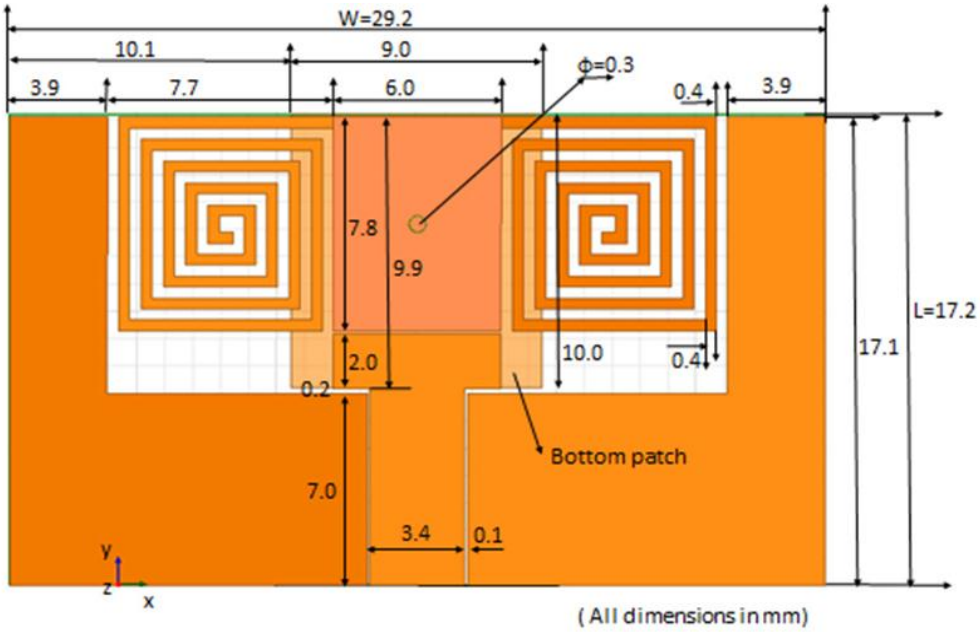

Figure 4.2 Geometry of the proposed 1-unit cell CRLH based spiral resonant antenna.

From the electric field vector distribution shown in Figure 4.3 (a), a constant phase electric field distribution uniformly vertical to the radiating patch is achieved at 2.46 GHz. From the surface current distribution, Figure 4.3 (b) it is realized that the spiral inductive stubs contribute significantly to antenna radiation as the current is mostly concentrated in the shunt spiral inductive line region. These inductive stubs can also be used as very suitable elements for tuning of the planar ZOR antenna at the desired working frequency.

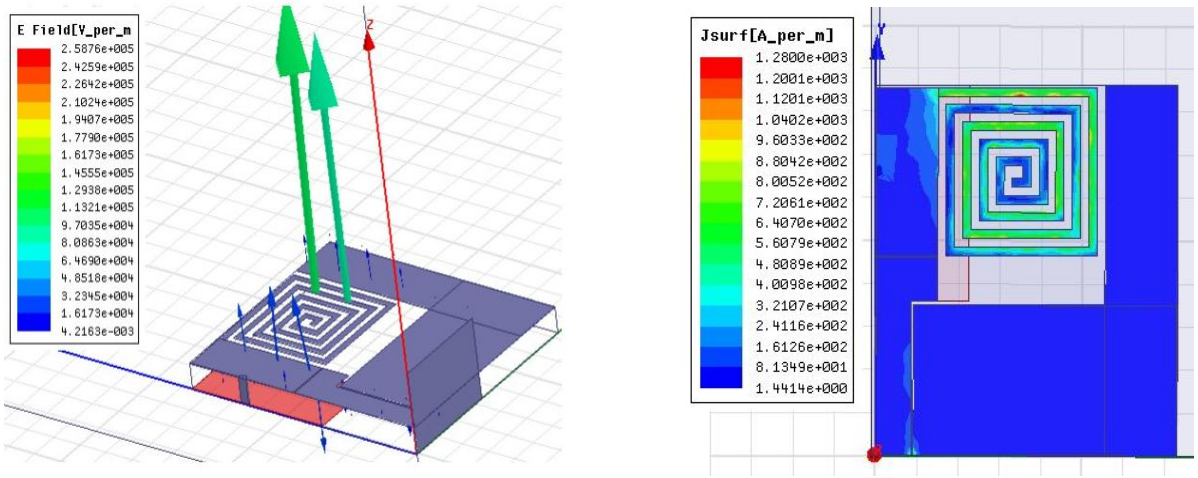

(a) (b)

Figure 4.3 (a) E-field vector distributions and (b) Surface current distributions at 2.46 GHz.

Figure 4.4 shows the simulated reflection coefficients of the proposed ZOR antenna. It is observed that with a single unit cell the zeroth order resonant frequency shifts downwards to 2.46 GHz. The reflection coefficient obtained at resonant frequencies 2.46 GHz and 3.68 GHz are -18.6581 dB and -11.1389 dB respectively. In this case with a single unit cell a

bandwidth enhancement of 0.01% and efficiency of 59.03% is achieved with a gain of about -1.1807 dB at the zeroth order frequency of 2.46 GHz. Figure 4.5 shows the simulated VSWR of the resonant CRLH TL. It is found that the VSWR is less than 2 in each of the resonant frequencies.

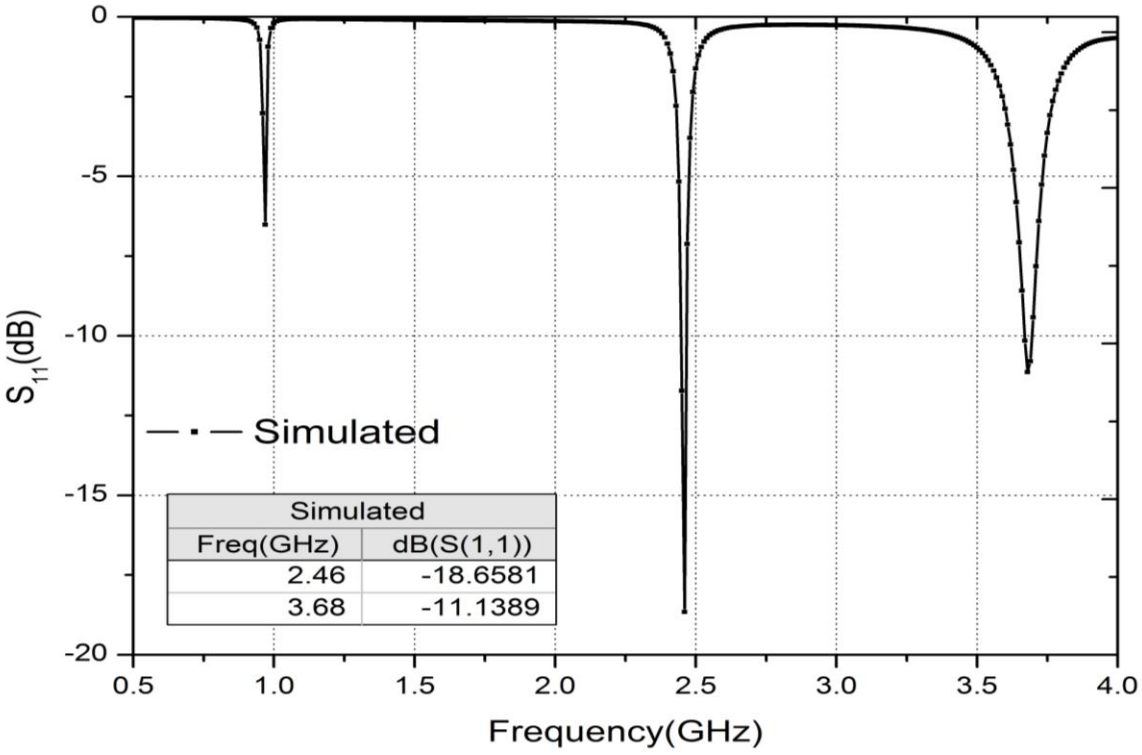

Figure 4.4 Simulated reflection coefficient of the 1-unit cell CRLH based resonant antenna.

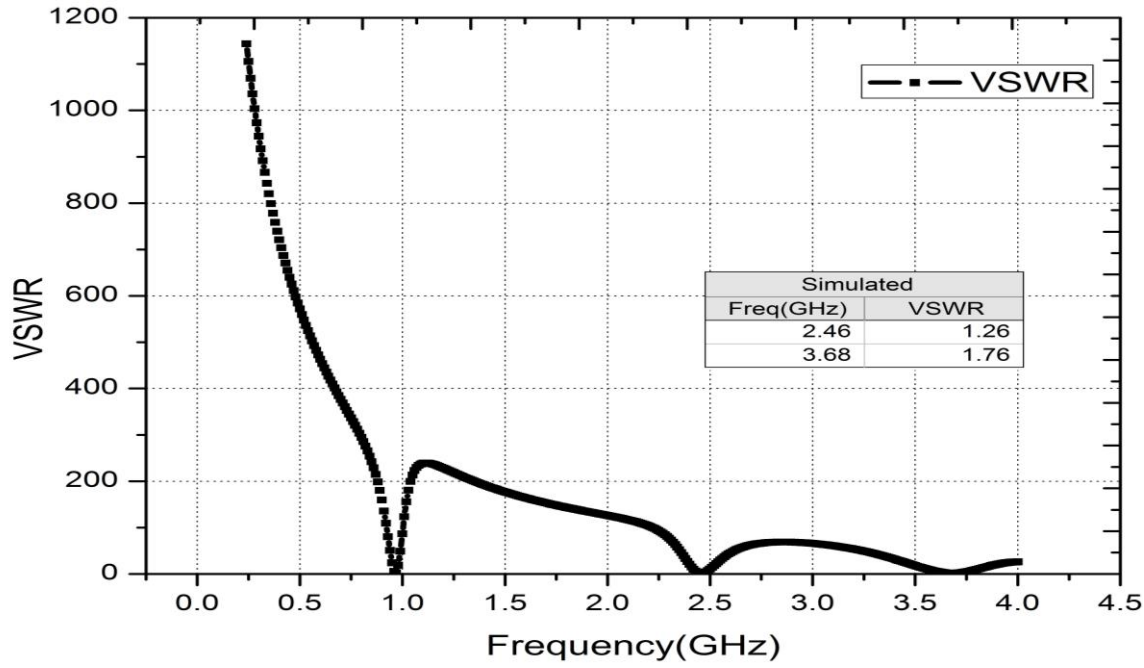

Figure 4.5 VSWR for the proposed structure.

Figures 4.6 and 4.7, show the 2D radiation patterns and 3D gain patterns at 3.68 GHz and 2.46 GHz respectively. A dumb-bell shaped E-radiation pattern (y-z plane) and an omni-directional H-radiation pattern (x-z plane) is obtained. Since the magnetic field is locally circulating around the spiral lines to provide LH shunt inductance, thereby it leads to an omni-directional radiation pattern in H-plane. The proposed antenna is suitable for multiband WiMax applications at 3.68 GHz ((3.666 - 3.692) GHz) and for WLAN applications at 2.46 GHz ((2.45 - 2.47) GHz). The proposed multiband antenna with a single unit cell is most suitable to meet the demands for portable devices. Being small in size it provides additional features such as multi frequency and multi functionality bands with omni-directional characteristics suitable for wireless applications. The performance characteristic of the antenna is tabulated in Table 4.1.

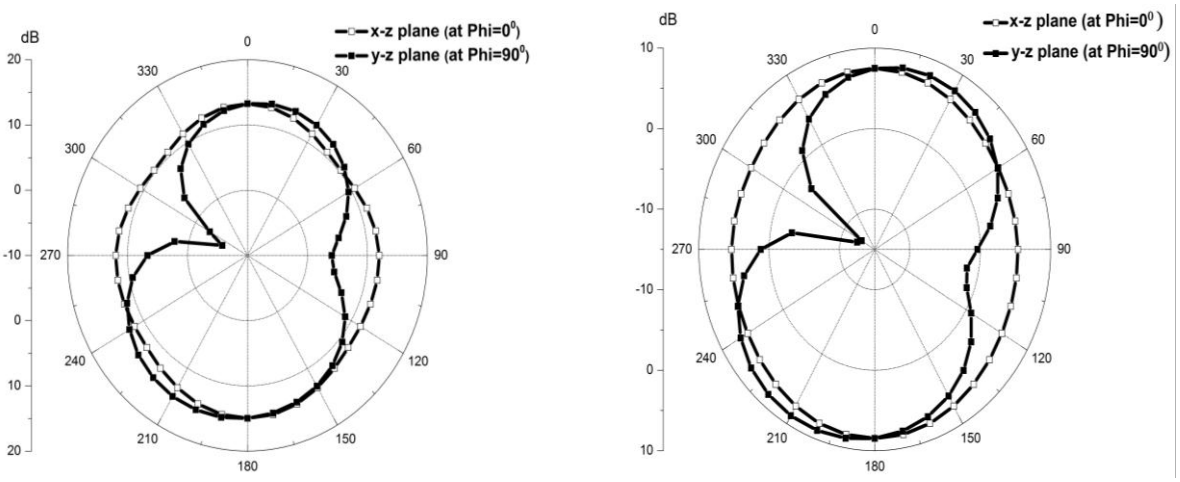

(a) 3.68 GHz **(b) 2.46 GHz**

Figure 4.6 Simulated 2D Radiation patterns for the proposed1-unit cell CRLH based spiral antenna.

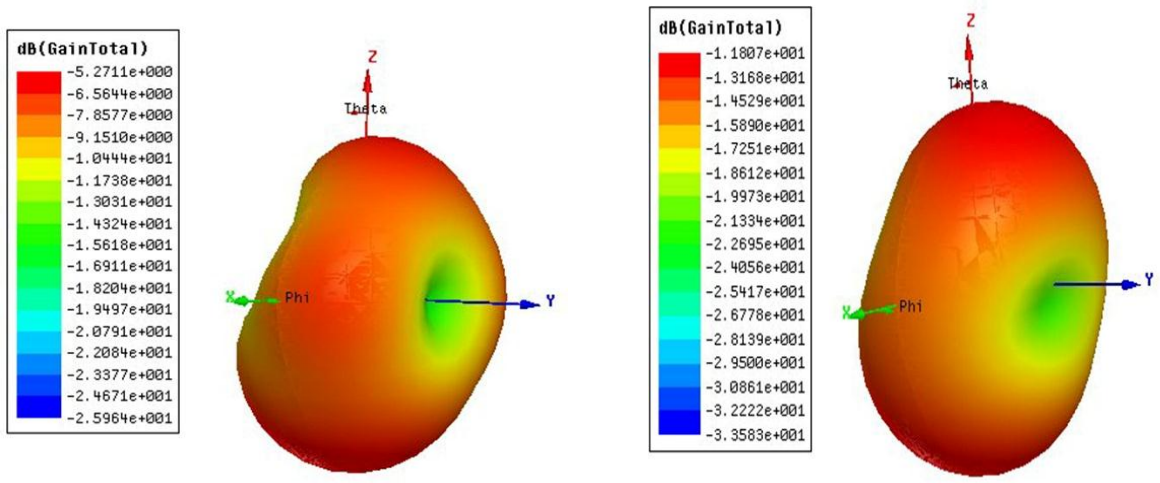

(a) 3.68GHz **(b) 2.46 GHz**

Figure 4.7 Simulated 3D Gain Patterns for the proposed 1-unit cell CRLH based spiral antenna.

Table 4.1 Performance Characteristics of the proposed CRLH based spiral antenna with a single unit cell.

Resonant Freq (GHz)	**Reflection Coefficient (dB)**	**Gain (dB)**	**Bandwidth (%)**	**Radiation Efficiency**
f_{+1}=3.68 (WiMax)	-11.1389	-5.2711	0.0071	0.51028
f_0=2.46 (WLAN)	-18.6581	-1.1807	0.0079	0.5903

4.3.2 Experimental Verification

Figure 4.8 shows the fabricated prototype of the designed CRLH based spiral resonant antenna. Details of fabrication procedure are mentioned in Appendix A.2.

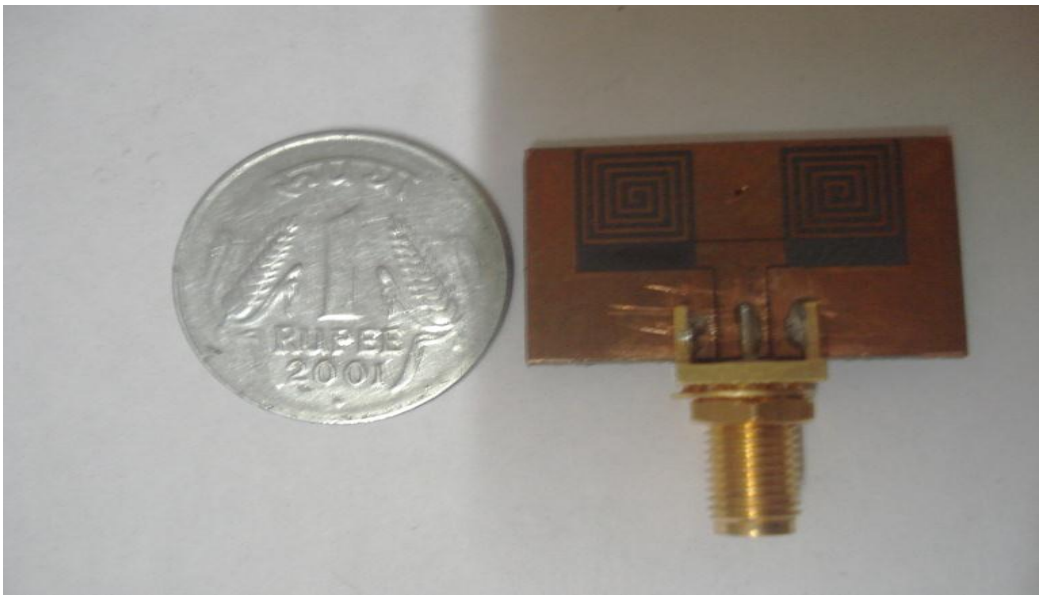

Figure 4.8 Fabricated prototype of the proposed 1-unit cell CRLH based spiral resonant antenna.

Figure 4.9 shows the comparison of the simulated and measured reflection coefficients of the antenna at 3.68 GHz and 2.46 GHz respectively. A very good agreement between the measured and simulated results are obtained. The slight difference might be due to improper etching and the effect of SMA 50 Ω connectors. Also manufacturing tolerance in antenna realization especially related to physical dimensions of small gaps and shunt stub (spiral inductors and vias) contribute to Δf =0.31GHz at zeroth mode. So as a result the values of lumped capacitor and inductor elements needs to be adjusted by modifying either the length or width of the square spiral inductors and the space between successive inductors so that the resonant frequency would be approximately nearer to that obtained through simulations. All measurements are carried out with Agilent E8363B Network Analyser.

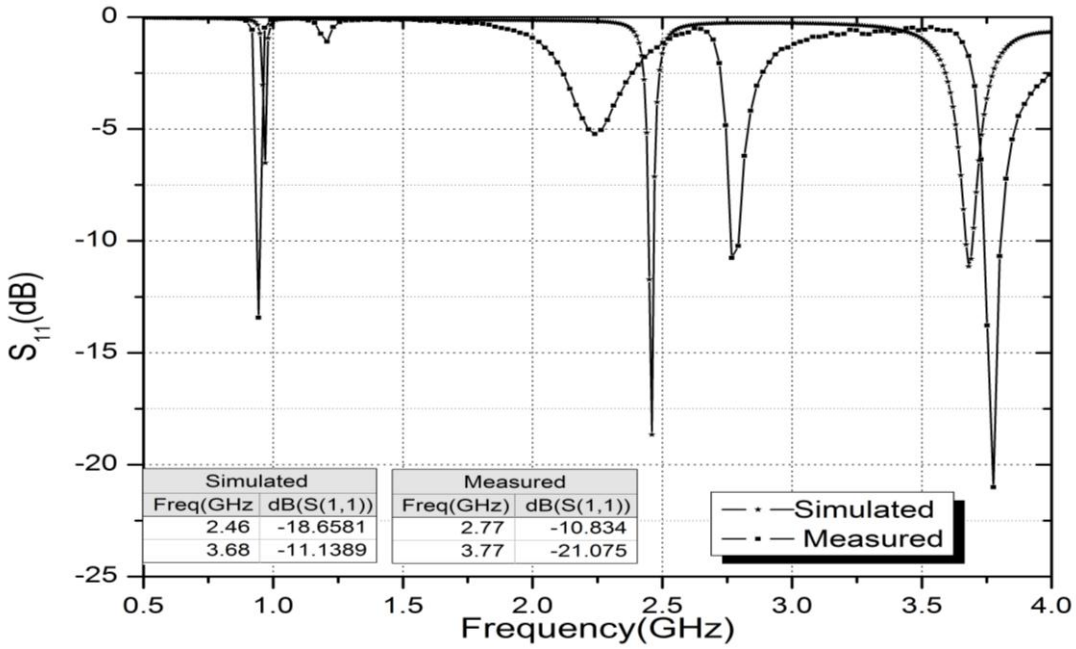

Figure 4.9 Comparison of simulated and measured reflection coefficients of the proposed 1-unit cell CRLH based resonant antenna.

4.3.3 Antenna Radiation Pattern and Gain Measurements

Figures 4.10 and 4.11 show the measured H-plane and E-plane radiation pattern cuts at 2.772 GHz and 3.776 GHz respectively. The antenna is tested at Antenna Measurement Facility (AMF), Space Application Centre, ISRO, Ahmedabad. Details of anechoic chamber and measurements of Gain and radiation pattern is given in Appendix A.3.3. Since, radiation pattern measurements are undertaken with the test antenna mounted on to an aluminium plate fixture which is aligned to a reference wideband horn antenna so there is a slight variation in the simulated and measured radiation patterns. Measurements outside the azimuth range $\pm 150^0$ could not be carried out since the positioner mounting interface shown in Figure 3.21 blocks the (relatively smaller) antenna assembly. Also signal fluctuations in the main lobe of the measured radiation pattern is observed which may be either due to low coupled power from the single element or due to leakage and reflections from RF absorbers thereby leading to the characteristic maxima and minima. Nevertheless, the simulated and measured results agree within experimental uncertainties. The measured peak gain of the fabricated antenna at 2.772 GHz is -2.74 dBi and at 3.776 GHz is -5.92 dBi. The Gain of the antennas has been measured using Gain comparison method, details of which are given in Appendix A.3.4.

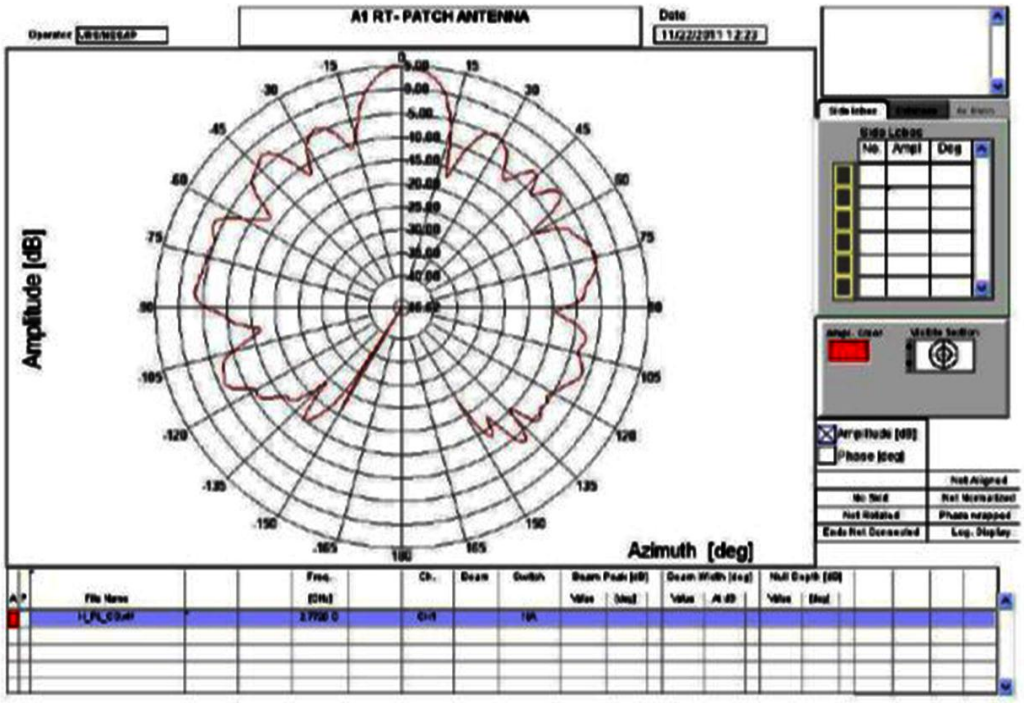

Measured at 2.772 GHz.

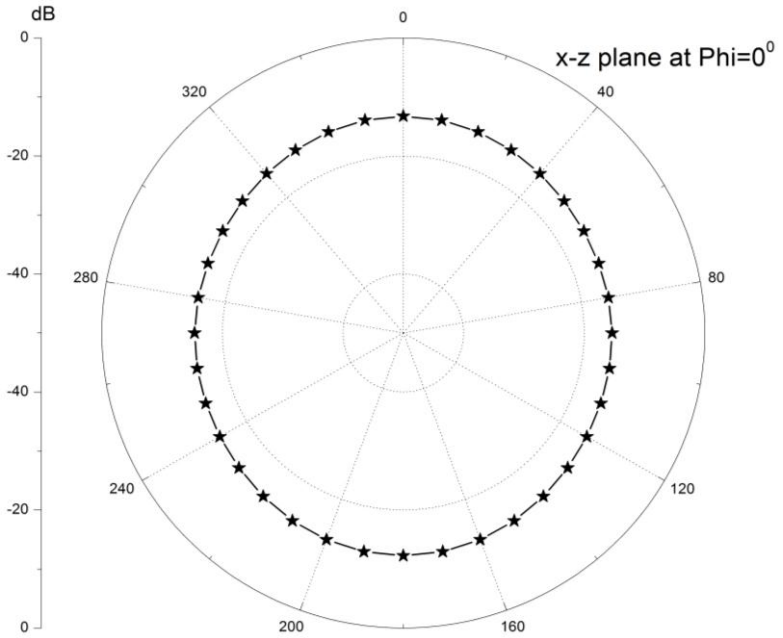

Simulated at 2.46 GHz.

Figure 4.10 (a) H-plane radiation patterns.

In Figure 4.10 (a), the measured and simulated results are found to be good agreement with each other. An omni- directional H-plane radiation pattern is achieved with slight signal fluctuations due to errors in fabrication of vias and square spiral stub inductors.

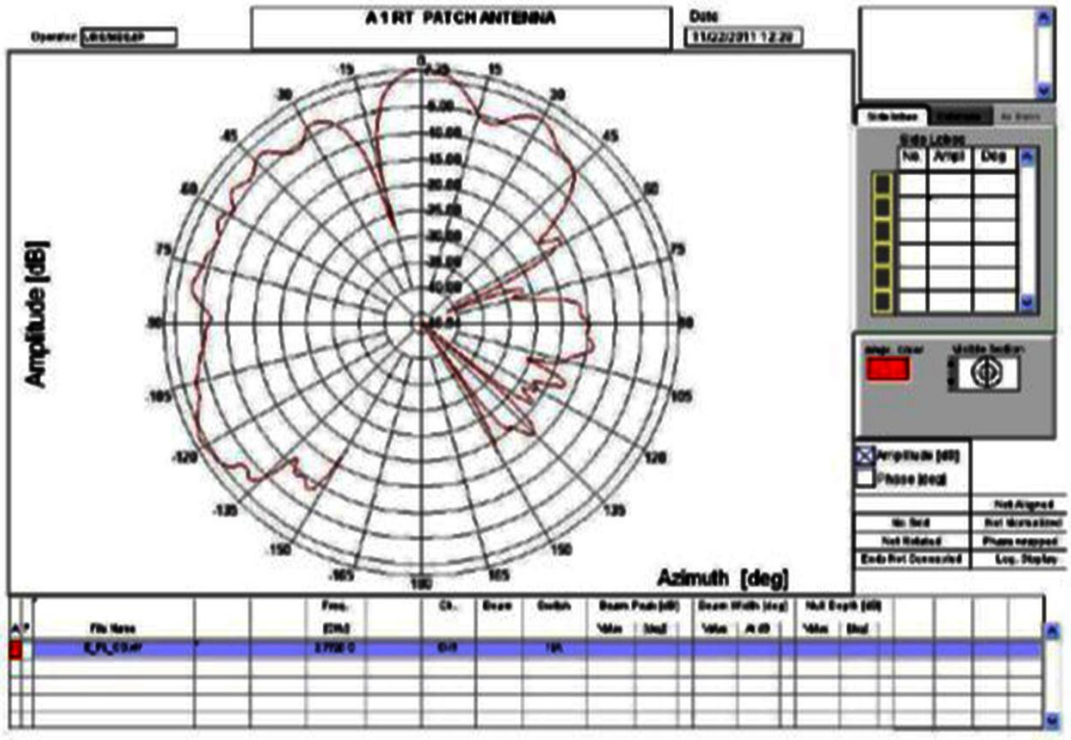

Measured at 2.772 GHz.

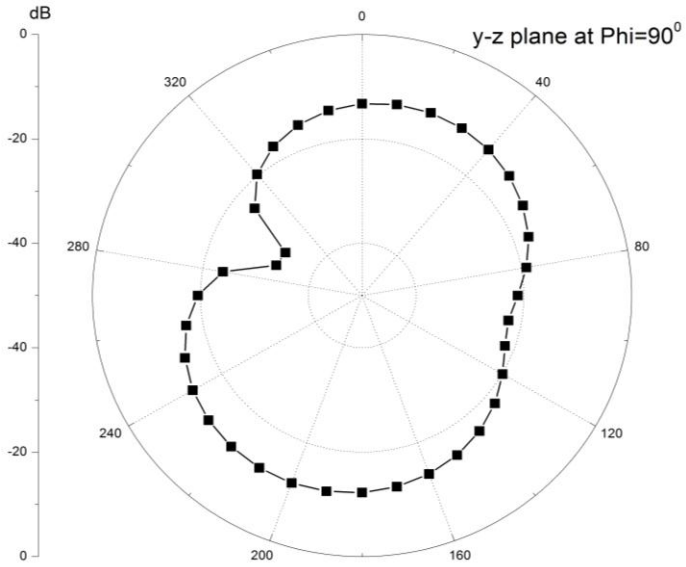

Simulated at 2.46 GHz.

Figure 4.10 (b) E-plane radiation patterns.

In Figure 4.10 (b) a monopolar E-plane radiation pattern is observed. The measured and simulated radiation patterns are found to be in good agreement with each other exhibiting broadside radiation in lower half. At low frequency, less signal fluctuations in the main lobe of the measured radiation pattern is observed.

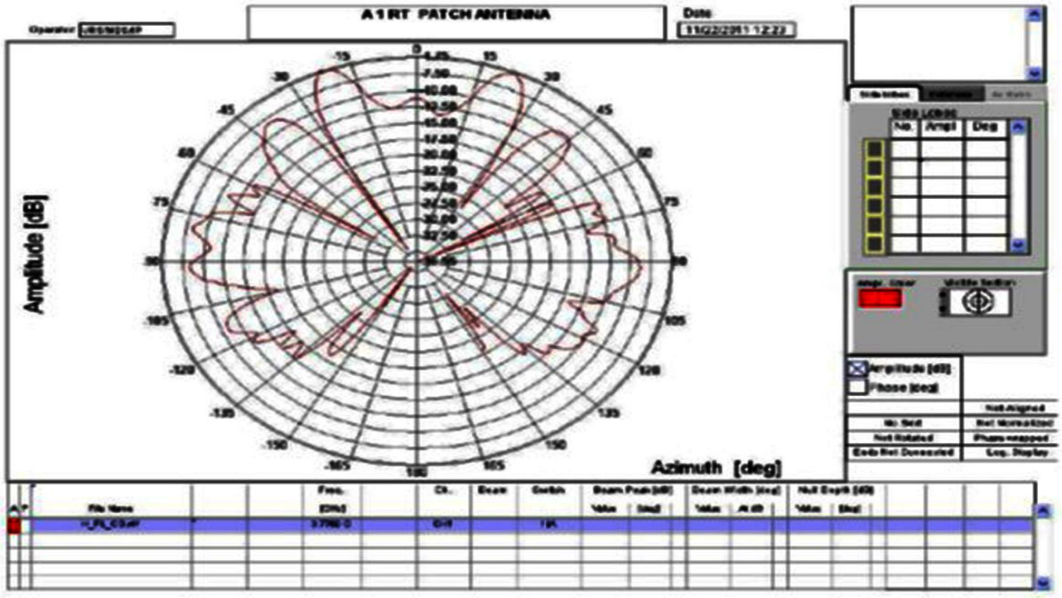

Measured at 3.776 GHz.

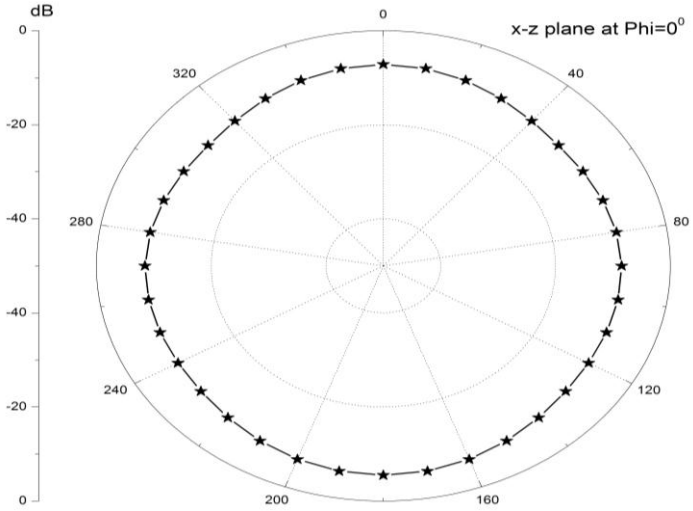

Simulated at 3.68 GHz.

Figure 4.11 (a) H-plane radiation patterns.

In Figure 4.11 (a), simulated H-plane radiation pattern resembles an omni-directional radiation pattern while the measured pattern consists of large signal fluctuations. It is observed that as frequency increases, there is an increase in signal fluctuations which may be either due to low coupled power from the single element or due to leakage and reflections from RF absorbers thereby leading to the characteristic maxima and minima.

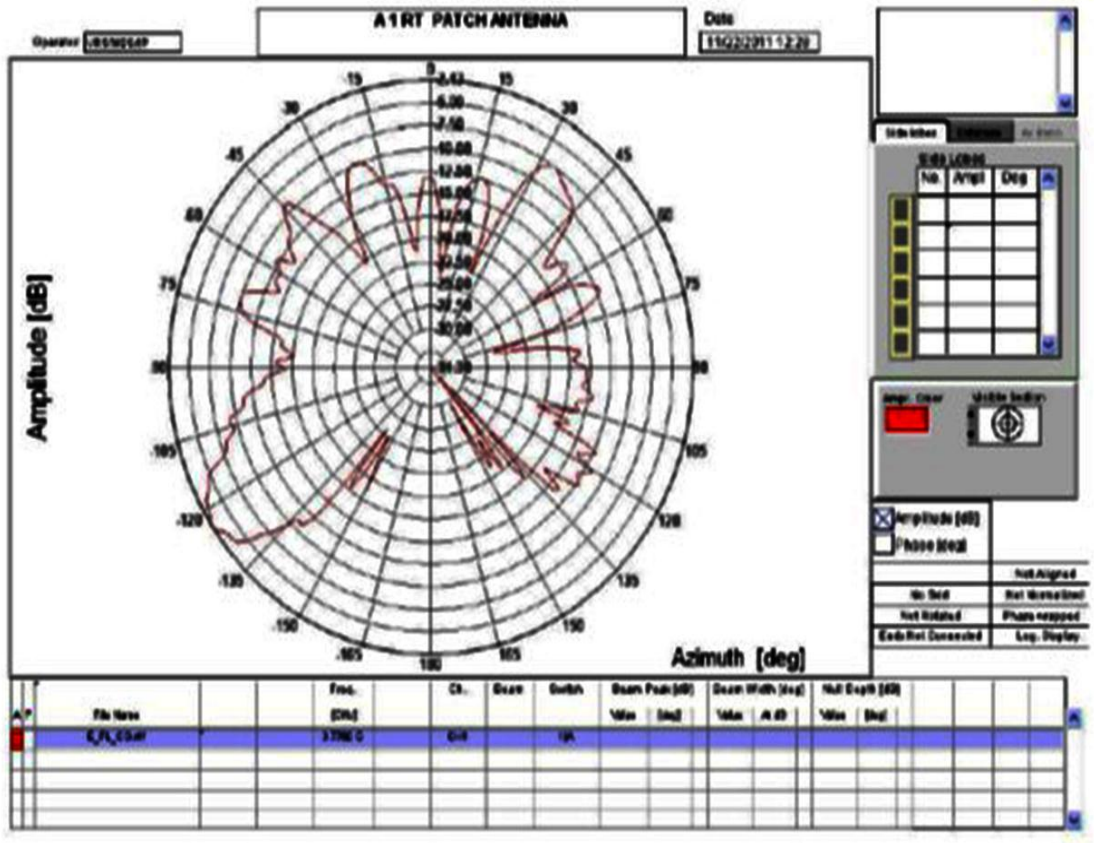

Measured at 3.776 GHz.

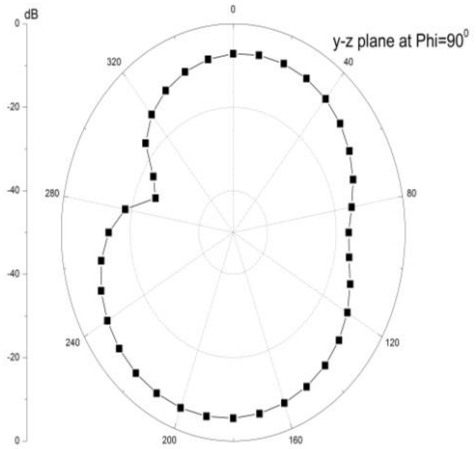

Simulated at 3.68 GHz.

Figure 4.11 (b) E-plane radiation patterns.

In Figure 4.11 (b), monopolar E-plane radiation pattern is obtained while the measured E-radiation pattern undergoes large fluctuations due to leakage and reflections from RF absorbers thereby leading to large characteristic maxima and minima.

4.3.4 *Case-II: Antenna Geometry and Simulation Results with 2-unit cells*

Figure 4.12 shows the geometrical model of the CPW fed triband, pentamode CRLH TL antenna consisting of two unit cells. Here a substrate of size 29.2 mm x 25.4 mm x 1.6 mm made up of Rogers RT/ Duroid 5880 having dielectric constant $\varepsilon_r = 2.2$ and a thickness of 1.6 mm. Each unit cell (6 mm x 7.8 mm) is shorted to ground through a via of radius 0.3 mm. Vias are connected to the bottom patch placed beneath the radiating top patch. Parameters of antenna radiating patch and the bottom patch is adjusted to achieve an impedance matching of 42 ohms. The proposed antenna have its zeroth order mode at 2.48 GHz which approximately corresponds to the case discussed above. The electrical size of the unit cell of the antenna is $0.0496\lambda_0$ x $0.064\lambda_0$ (6 mm x 7.8 mm) at 2.48 GHz. The overall area of the antenna aperture is approximately $0.241\lambda_0$ x $0.210\lambda_0$ x $0.013\lambda_0$ (29.2 mm x 25.4 mm x 1.6 mm) at 2.48 GHz.

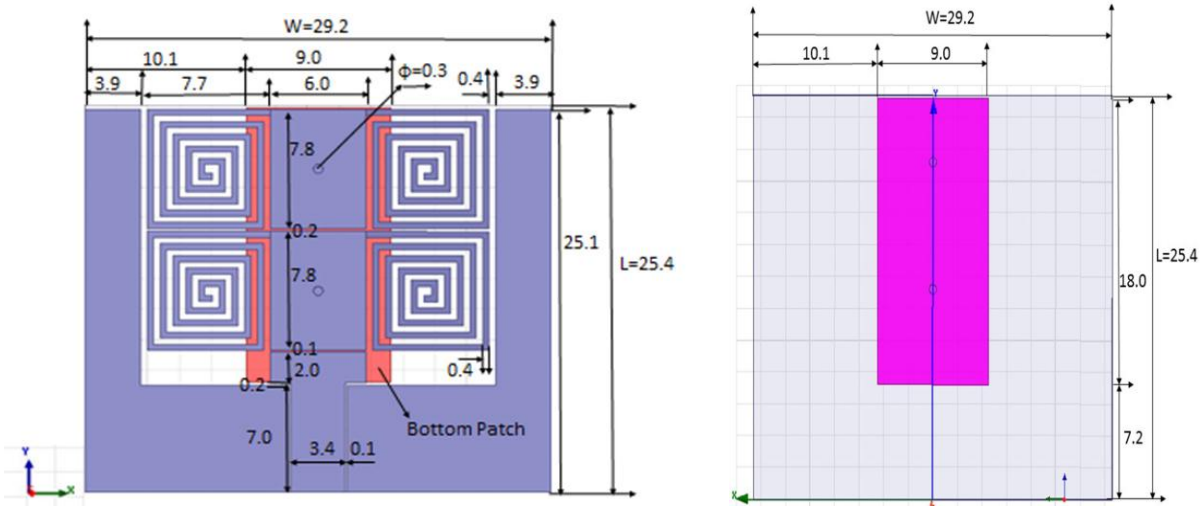

(a) Top Patch (b) Bottom Patch

Figure 4.12 Geometry of the proposed 2-unit cells CRLH based spiral resonant antenna. (All dimensions in mm)

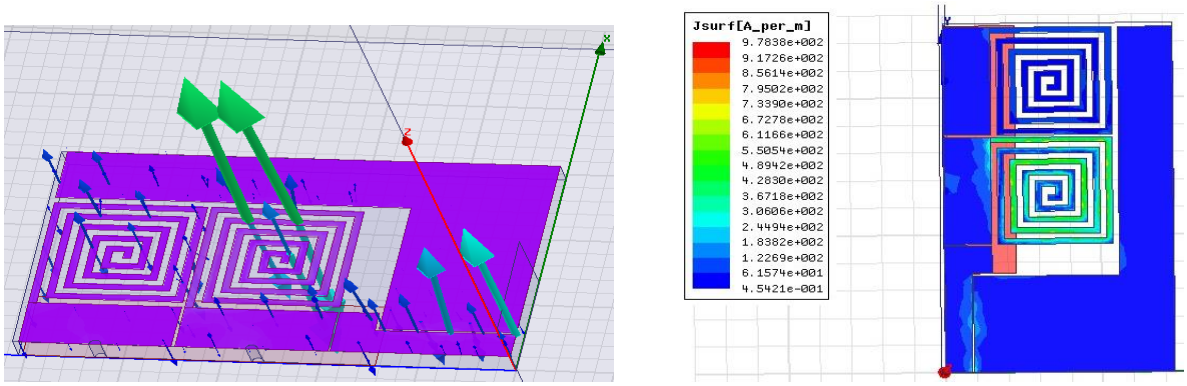

(a) **(b)**

Figure 4.13 (a) E-field vector distributions and (b) Surface current distributions at 2.48 GHz.

From the electric field vector distribution shown in Figure 4.13 (a) a constant phase electric field distribution, uniformly vertical to the radiating patch is achieved at 2.48 GHz which is similar to the distribution obtained in Figure 4.3 with only a slight shifting in the zeroth order resonant frequency as the number of unit cells increases. This implies that the zeroth order resonant frequency, at which a constant phase electric field distribution is realised, does not depend on the physical length of the resonator, but, only on the amount of reactance provided by its unit cells. This fact can be exploited to achieve miniaturised zeroth order resonant antennas. From the surface current distribution, Figure 4.13 (b) it is reaffirmed that the spiral inductive stubs contribute significantly to antenna radiation as the current is mostly concentrated in the shunt spiral inductive line region thus making it most effective as tuning elements.

Figure 4.14 shows the simulated reflection coefficients of the proposed ZOR antenna. . All simulations are carried out using Ansoft HFSS using Driven set up. No. of passes used is 6 and convergence ratio (ΔS): 0.02 is the maximum change in the magnitude of the S-parameters between two consecutive adaptive passes. The antenna is excited with wave port excitations. It is observed that a reflection coefficient of -20.2014 dB at the zeroth mode of 2.48 GHz is obtained. A bandwidth of 2.964% and 1.36% respectively at 3.54 GHz and 2.48 GHz is obtained.

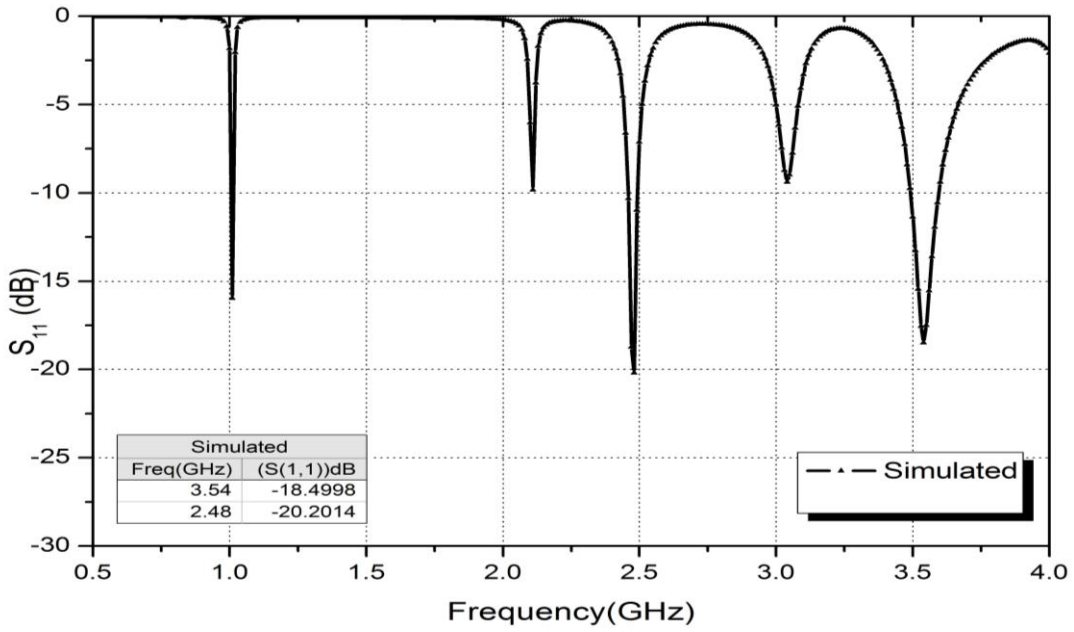

Figure 4.14 Simulated reflection coefficients of the proposed 2-unit cells CRLH based spiral resonant antenna.

Figure 4.15 shows the simulated VSWR of the proposed antenna. It is found that VSWR is less than 2 at 2.48 GHz and 3.54 GHz which is quite acceptable. The lower negative resonance shows very low antenna gain and efficiency.

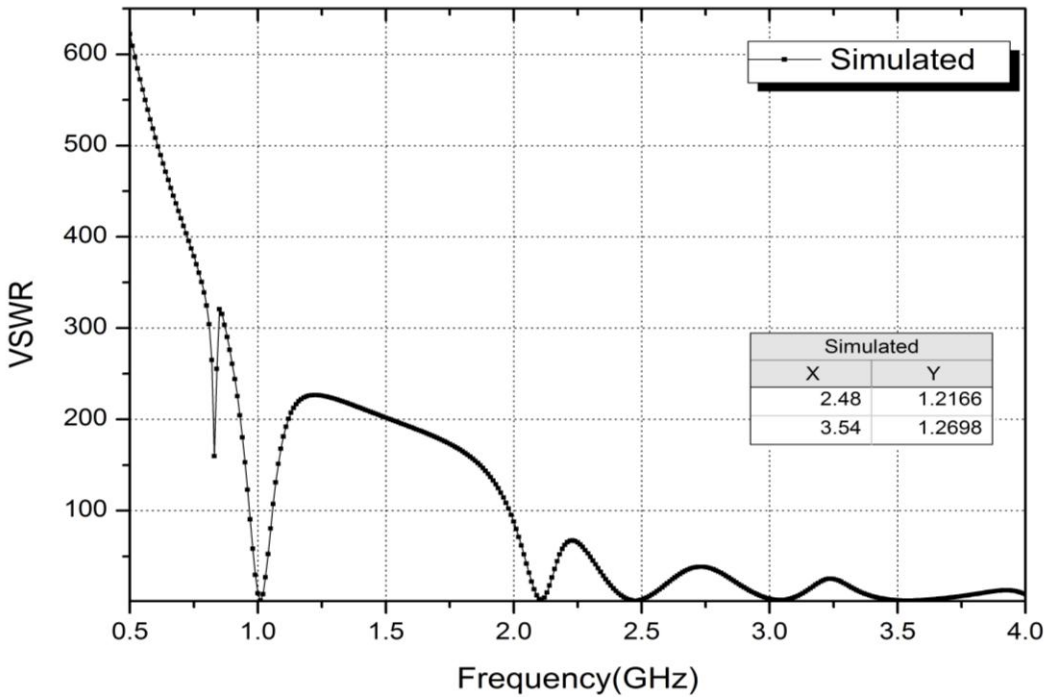

Figure 4.15 VSWR for the proposed CRLH based spiral antenna.

The simulated radiation efficiency (%) and gain (dB) according to the operating band are presented in Figure 4.16. In this proposed antenna, a bandwidth of 1.36% and radiation efficiency of 55.31% are achieved at zeroth order resonance of 2.48 GHz with a gain of -5.1607 dB.

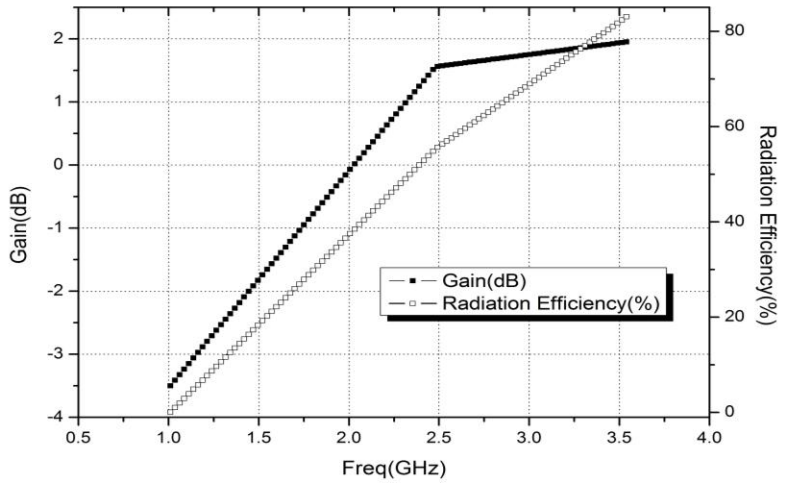

Figure 4.16 Simulated radiation efficiency and gain for the proposed structure.

Figures 4.17 and 4.18 show the 2D radiation patterns and 3D Gain patterns at 3.54 GHz, 2.48 GHz and 1.01 GHz. At each resonant frequency a dumb-bell shaped E- radiation pattern (y-z plane) and an omni-directional H-radiation pattern (x-z plane) are obtained. Radiation efficiency of 55.31% is achieved at zeroth order resonance of 2.48GHz with a gain of -5.1607dB.

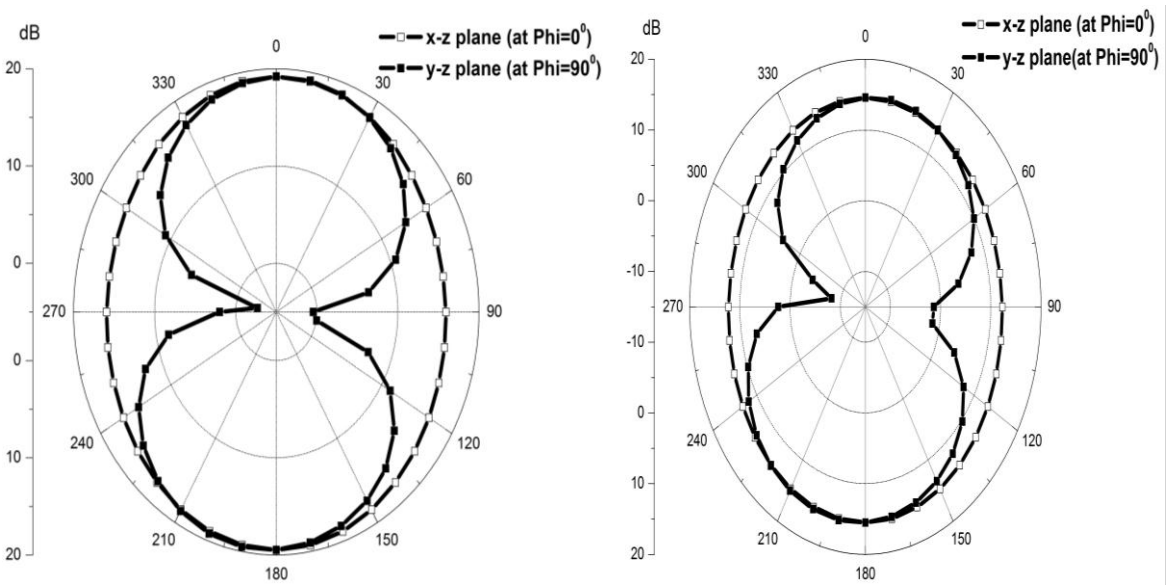

(a) 3.54 GHz **(b) 2.48 GHz**

Figure 4.17 Simulated Radiation patterns for the proposed 2-unit cells CRLH based spiral resonant antenna.

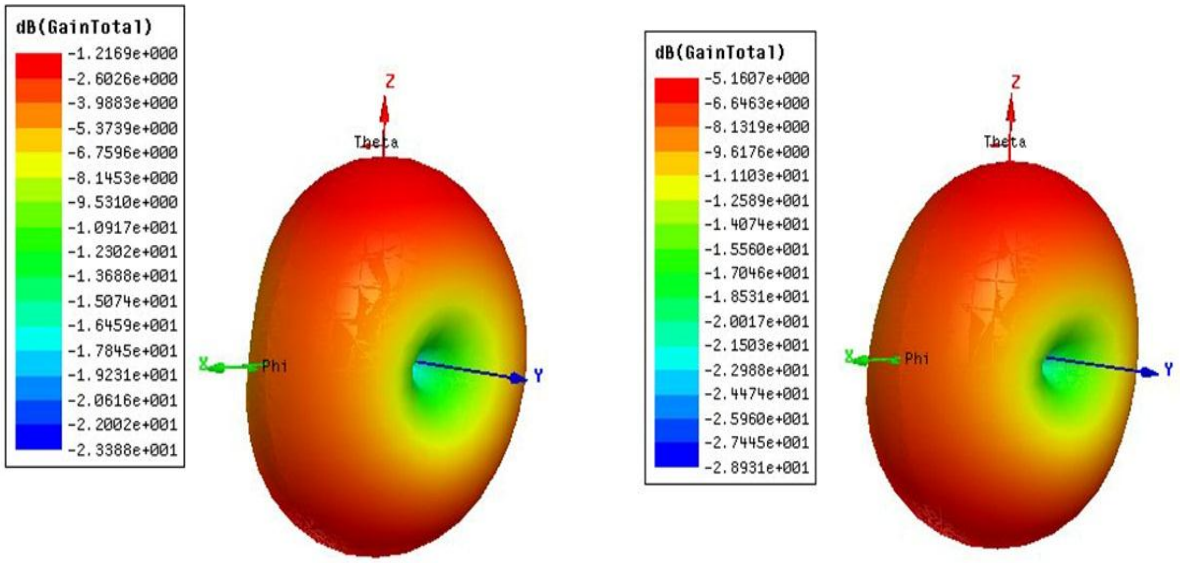

(a) 3.54 GHz **(b) 2.48 GHz**

Figure 4.18 Simulated 3D Gain Patterns for the proposed CRLH resonant antenna.

Table 4.2 shows the performance characteristics of the proposed antenna consisting of two unit cells.

Table 4.2 Performance Characteristics of the proposed metamaterial antenna with two unit cells.

Resonant Freq (GHz)	Reflection Coefficient (dB)	Gain (dB)	Bandwidth (%)	Radiation Efficiency (%)
f_{+2}=3.54 (WiMax)	-18.4998	-1.2169	2.964	82.52
f_0=2.48 (ISM)	-20.2014	-5.1607	1.36	55.31

4.3.5 Experimental Verification

Figure 4.19 shows the fabricated prototype of the designed antenna. Details of fabrication procedure are mentioned in Appendix A.2. Figure 4.20 shows the comparison of the simulated and measured reflection coefficients of the antenna. A very good agreement between the measured and simulated results is obtained. The measured reflection coefficient is slightly shifted from that of the simulated one which can be attributed to minor errors in the fabrication of vias or due to improper etching and the effect of 50 ohm SMA connectors. All measurements are carried out with Agilent E8363B Network Analyser

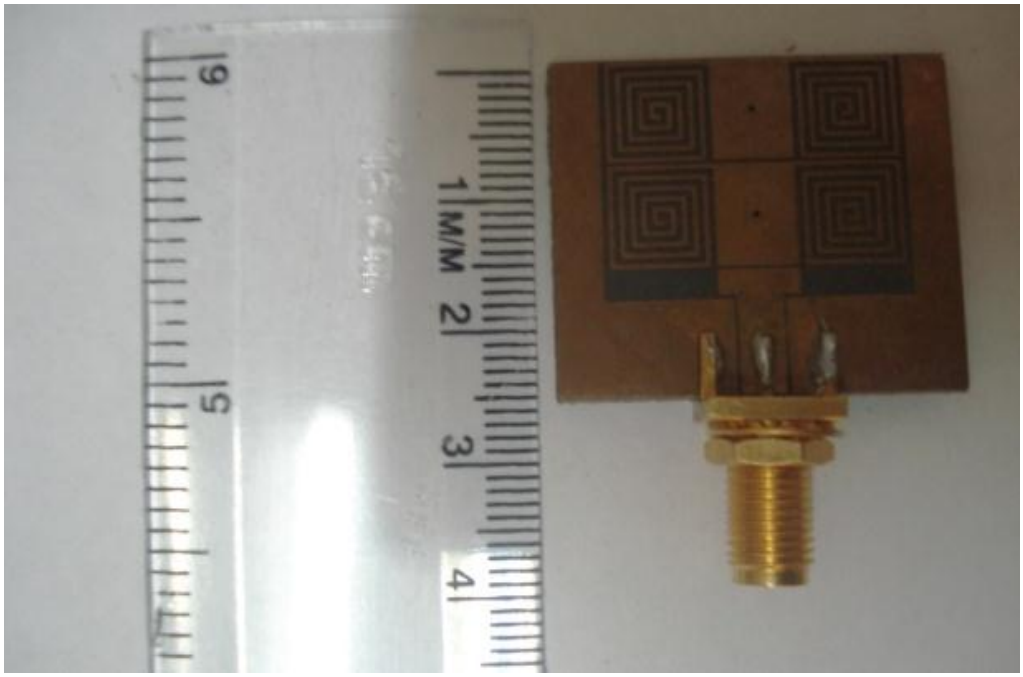

Figure 4.19 Fabricated prototype of the proposed 2-unit cells CRLH based spiral resonant antenna.

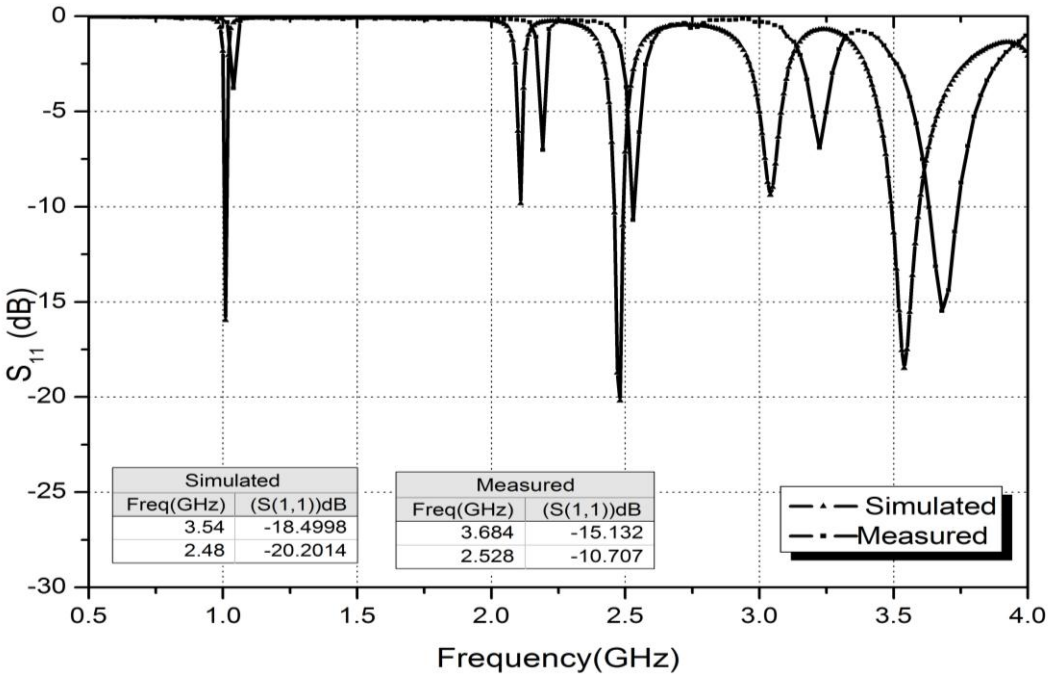

Figure 4.20 Comparison of simulated and measured reflection coefficients of the proposed CRLH based spiral resonant antenna.

4.3.6 Antenna Radiation Pattern and Gain Measurements

Figures 4.21 show the measured E-plane and H-plane radiation pattern cuts at 2.528 GHz and 3.684 GHz respectively. The antenna is tested at Antenna Measurement Facility (AMF), Space Application Centre, ISRO, Ahmedabad. Details of Anechoic Chamber and measurement set up is given in Appendix A.3.3. Radiation pattern measurements are undertaken with utmost precision with the test antenna mounted on to an aluminium plate fixture and then it is aligned to a reference wideband horn antenna. Measurements outside the azimuth range $\pm 150^0$ could not be carried out since the positioner mounting interface shown in Figure 3.21 blocks the (relatively smaller) antenna assembly. Scattering effects can be observed in the measured results. This may be attributed to leakage / reflections from the walls, floor and ceiling of the anechoic chamber lined with RF absorbers. Simulated radiation patterns agree well with the measured patterns within experimental errors. The measured peak gain of the fabricated antenna at 2.528 GHz is -3.61dBi and at 3.684 GHz is -1.26 dBi. The Gain of the antennas has been measured using Gain comparison method, details of which are given in Appendix A.3.4.

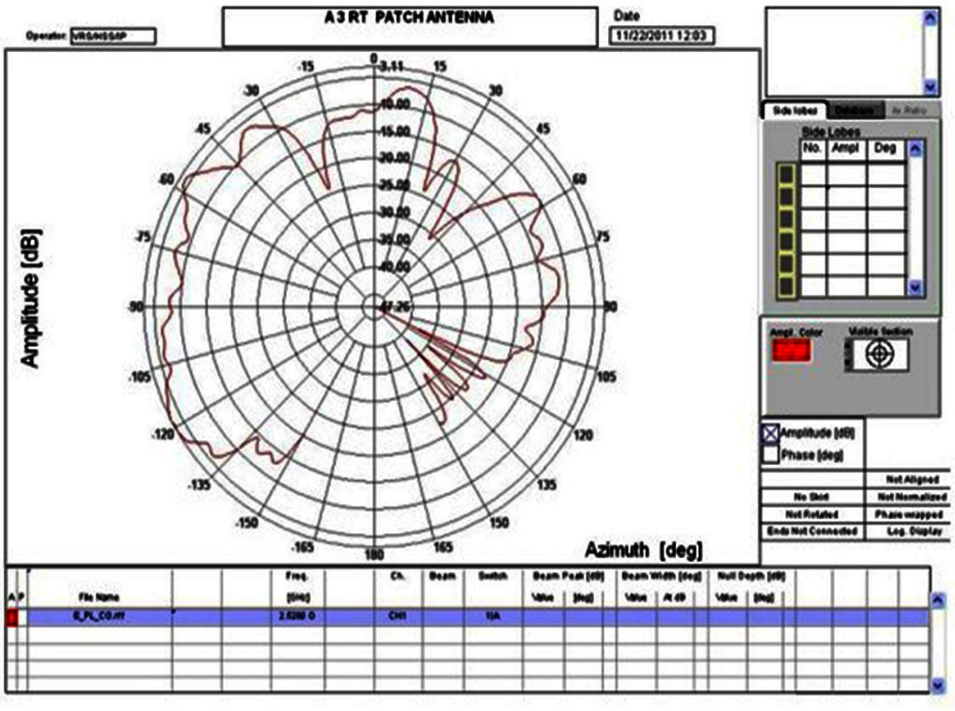

Measured at 2.528 GHz.

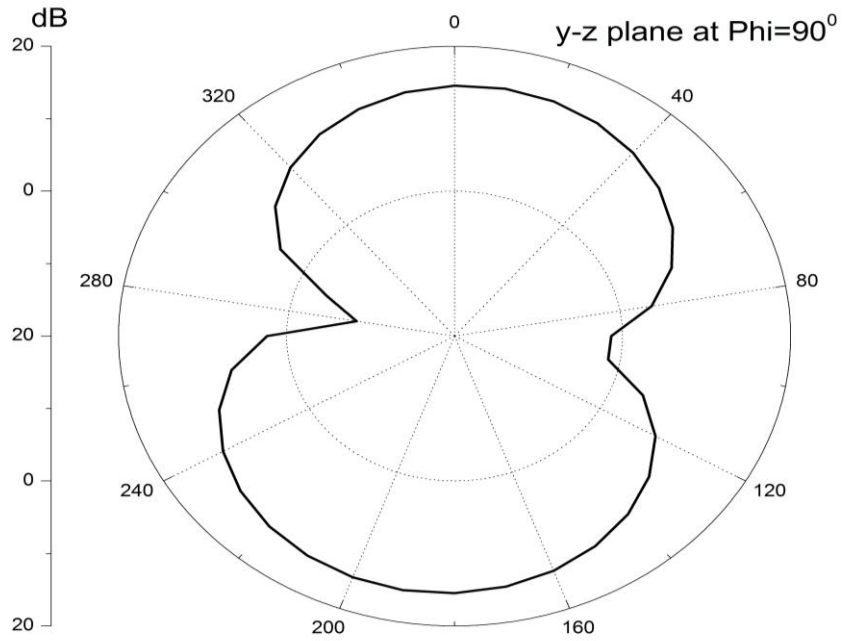

Simulated at 2.48 GHz.

Figure 4.21 (a) E-plane radiation patterns.

In Figure 4.21 (a), a dumb-bell shaped simulated E-radiation pattern is observed. It is found to be in good agreement with the measured result. Scattering effects are seen in the measured result. It may be due to leakage / reflections from the walls, floor and ceiling of the anechoic chamber lined with RF absorbers.

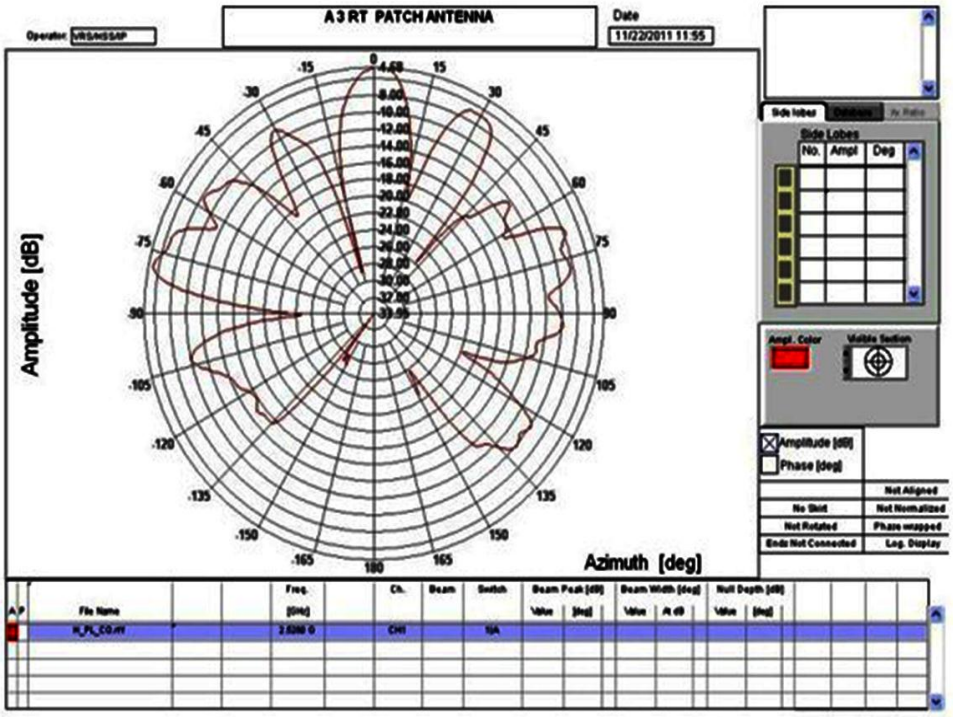

Measured at 2.528 GHz.

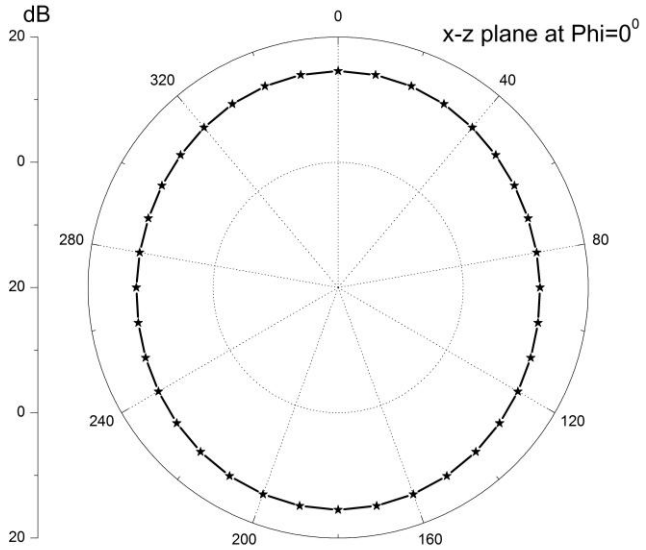

Simulated at 2.48 GHz.

Figure 4.21 (b) H-plane radiation patterns.

In Figure 4.21 (b), simulated omni-directional radiation pattern is observed but in the measured result scattering is more pronounced at low frequency. This may be attributed to

reflections from the walls, floor and ceiling of the anechoic chamber lined with RF absorbers. Simulated radiation patterns agree well with the measured patterns within experimental errors.

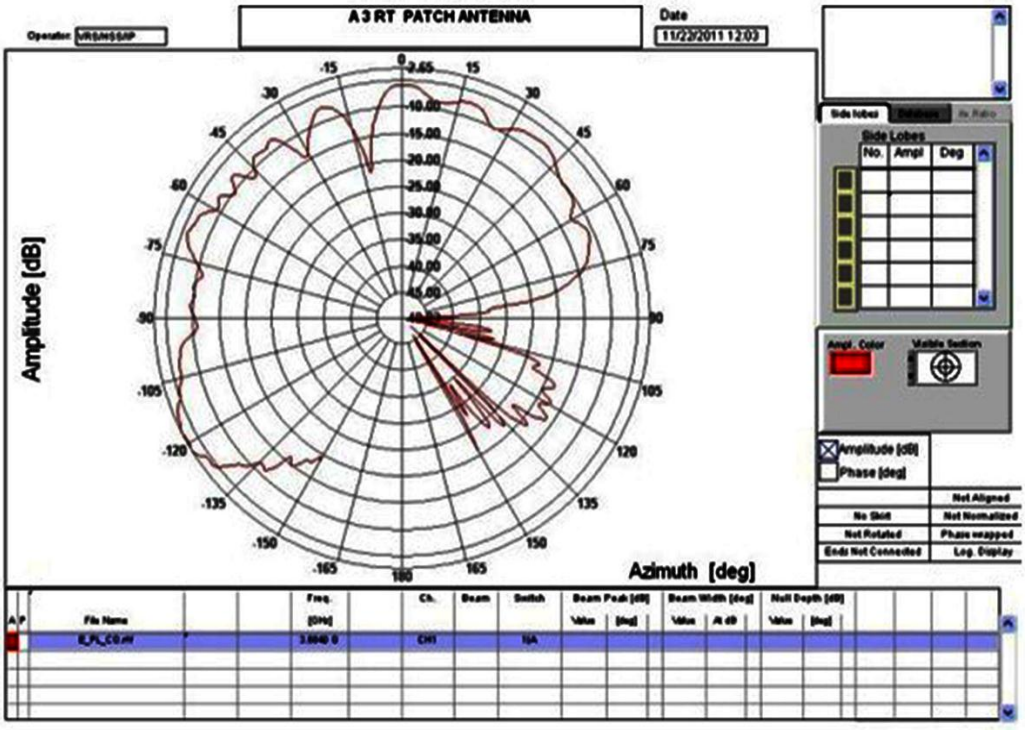

Measured at 3.684 GHz.

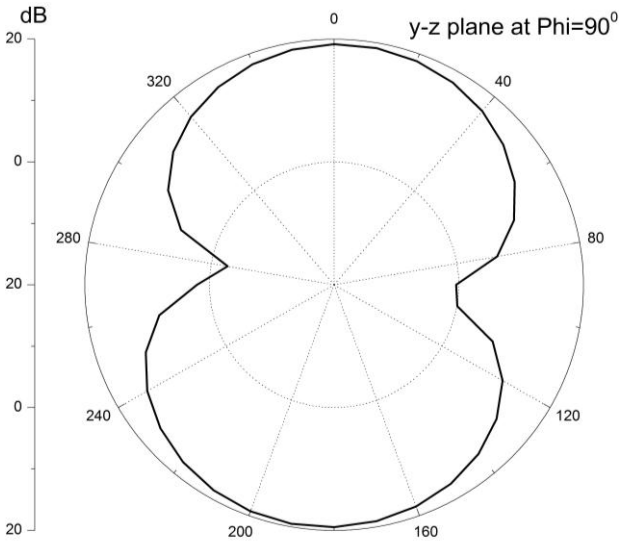

Simulated at 3.54 GHz.

Figure 4.22 (a) E-plane radiation patterns.

In Figure 4.22 (a), a dumb-bell shaped simulated E- plane radiation pattern is observed. Measured results agrees well with the simulated result within experimental errors. Scattering

effects can be observed in the measured results but is less pronounced as frequency increases. This may be attributed to low coupled power from the single element.

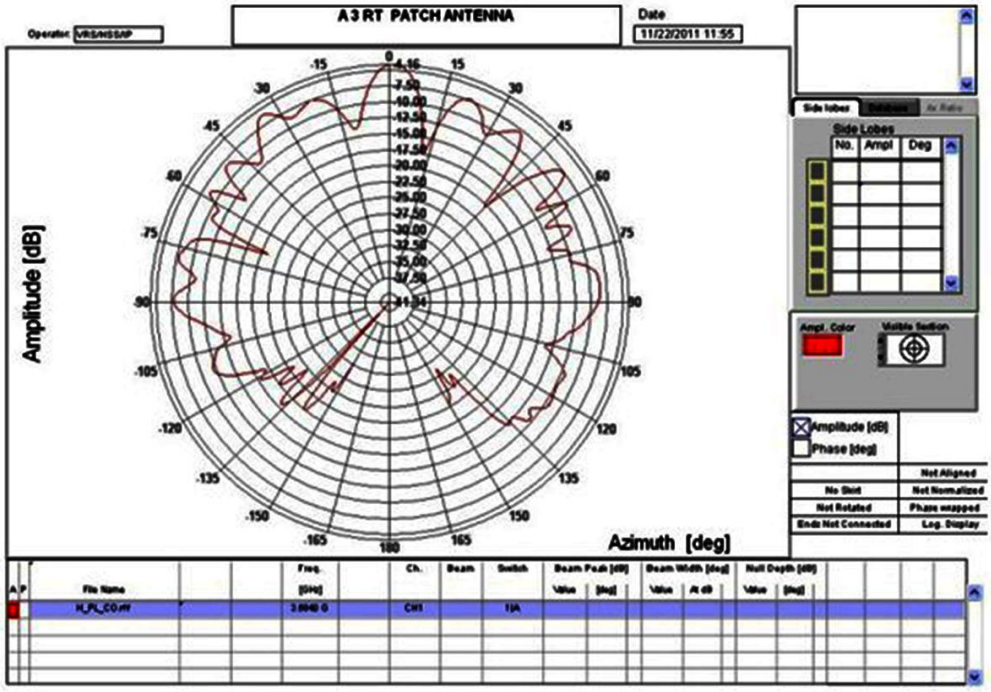

Measured at 3.684 GHz.

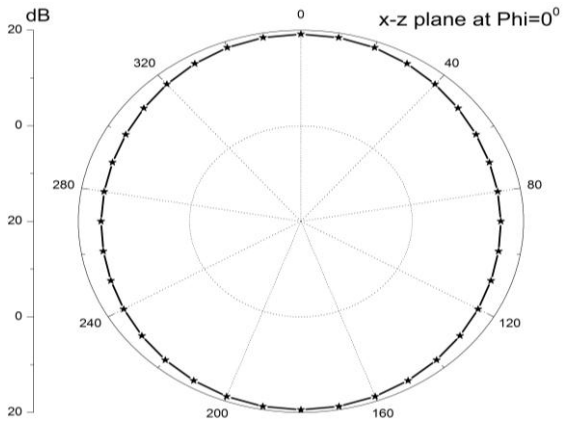

Simulated at 3.54 GHz.

Figure 4.22 (b) H-plane radiation patterns.

In Figure 4.22 (b), simulated H-plane radiation pattern agrees well with measured radiation pattern within experimental uncertainties. Slight signal fluctuations in the main lobe of the measured radiation pattern is observed which may be either due to low coupled power from the single element or due to leakage and reflections from RF absorbers thereby leading to the characteristic maxima and minima.

4.3.7 Comparison of performance characteristic of the proposed ZOR antennas

From Figures 4.4 and 4.14 it is found that when varying the number of unit cells, the zeroth order resonant frequency slightly shifts downwards to 2.46 GHz from 2.48 GHz. Also the frequencies at n=±1 modes in case of a single unit cell antenna structure closely approximates the frequencies obtained at n= ±2 modes in case of the proposed triband antenna structure with two unit cells. This shows that in the proposed structure the first unit cell contributes to the n= ±2 modes while the second unit cell contributes to the n=±1 modes. In case of 2-unit cell CRLH based spiral antenna, the LH shunt inductance contributed by the spiral inductors leads to bandwidth enhancement of about 1.36% and efficiency of about 55% at the zeroth order mode of 2.48 GHz while at other higher mode of 3.54 GHz a high bandwidth of 3% with an efficiency of 83% is achieved; whereas, in the case of a single unit cell based CRLH antenna, a narrow bandwidth with low efficiency is obtained. Table 4.3 summarizes the performance characteristics of the proposed ZOR antennas discussed in the above two cases.

Table 4.3 Comparison of the performance characteristics of the proposed ZOR antennas.

Substrate	No. of Unit cells	No. of resonating modes/ bands	Resonant Frequency (GHz)	Reflection Coefficient(dB)	Gain (dB)	Bandwidth (%)	Radiation Efficiency (%)
RT Duroid	2	3	$f_{+2} = 3.54$ (WiMax)	-18.4998	-1.2169	2.964	82.52
			$f_0 = 2.48$ (ISM)	-20.2014	-5.1607	1.36	55.31
RT Duroid	1	2	$f_{+1} = 3.68$ (WiMax)	-11.1389	-5.2711	0.0071	51.028
			$f_0 =$ 2.46 (WLAN)	-18.6581	-1.1807	0.0079	59.03

4.3.8 Conclusion

In section 4.3, a compact, multiband CRLH based spiral resonant antenna with 1- and 2-unit cells are proposed. In both cases, the antennas exhibit omni-directional radiation pattern with triband characteristic making it most suitable for modern IEEE 802.11 a/ b/ g wireless LAN applications. Single unit cell triband CRLH antenna, is suitable for WiMax applications at 3.68 GHz (3.666 GHz - 3.692 GHz) and WLAN applications at 2.46 GHz (2.450 GHz - 2.47 GHz); whereas 2-unit cell CRLH based resonant antenna finds applications in areas such

as the Wireless Local Area Network (WLAN) in the 2.48 GHz band ((2.459 - 2.4924) GHz) of IEEE 802.11b/g ISM band and worldwide interoperability for microwave access (WiMax) standards in the 3.54 GHz band ((3.491 - 3.596) GHz) of IEEE 802.11a. Hence, the proposed antenna serves the criteria for modern multiband wireless LAN application systems which include the mobile and wireless local area network (WLAN) communication systems due to their large service area. In the next section, focus is on increasing the bandwidth at the zeroth mode by incorporating spiral and anti-spiral lines to CPW fed antenna structure.

4.4 Maximized Bandwidth Multiband ZOR Antenna

In this section a coplanar waveguide fed compact pentaband metamaterial antenna is proposed to achieve maximum bandwidth in comparison to CPW fed ZOR antenna described in the previous section. In the previous section, vias are used to short the spirals to ground. This led to fabrication errors and entailed a maximum bandwidth of about 3%. In this section, spirals and anti-spirals as shunt inductors are incorporated in the proposed structure to achieve our purpose of maximising the bandwidth up to about 9%. In addition, because of a single layer and no grounded via, the antenna is easier to be fabricated. In this methodology, one end of the spiral and anti-spiral stubs are connected to the unit cell while the other end is shorted through CPW ground. In this way the shorted shunt LH inductance is successfully realised. The antenna consisting of two unit cells is simulated and experimentally verified. Figure 4.26 shows the pictorial representation of the proposed CPW fed CRLH TL antenna structure consisting of two unit cells. The proposed ZOR antenna consists of a single layer substrate material made of Rogers RT/ Duroid 5880 having dielectric constant $\varepsilon_r = 2.2$ and a thickness of 1.6 mm. Each unit cell (6 mm x 7.8 mm) consists of symmetrically placed spiral and anti-spiral inductors on both sides of the unit cell. As a result the dominantly radiating part of the antenna comes from the shunt spiral and anti-spiral stubs. Each spiral and anti-spiral stub consists of six turns each having a width and spacing of 0.2 mm. The unit cells or the radiating patch is separated by a small gap of 0.2 mm. This gap provides the series LH capacitance C_L, while the magnetic flux produced by the current flow along the radiating patch provides the parasitic series RH inductance L_R. Each unit cell is connected in parallel to the two open ended spiral and anti-spiral inductors having 6 turns. Figure 4.23 shows pictorial representation of the proposed CPW fed CRLH TL antenna structure. A CPW feed line and proximity coupling are used as the feed network to excite the open ended CRLH TL structure to initiate shunt mode of resonance ω_{sh}, with energy being stored in the shunt elements. The proposed design exhibits pentaband with omni-directional characteristics. This is of great advantage in modern multiband WLAN and WiMax applications. For these applications, multiband and high-performance antennas with good radiation characteristics are needed.

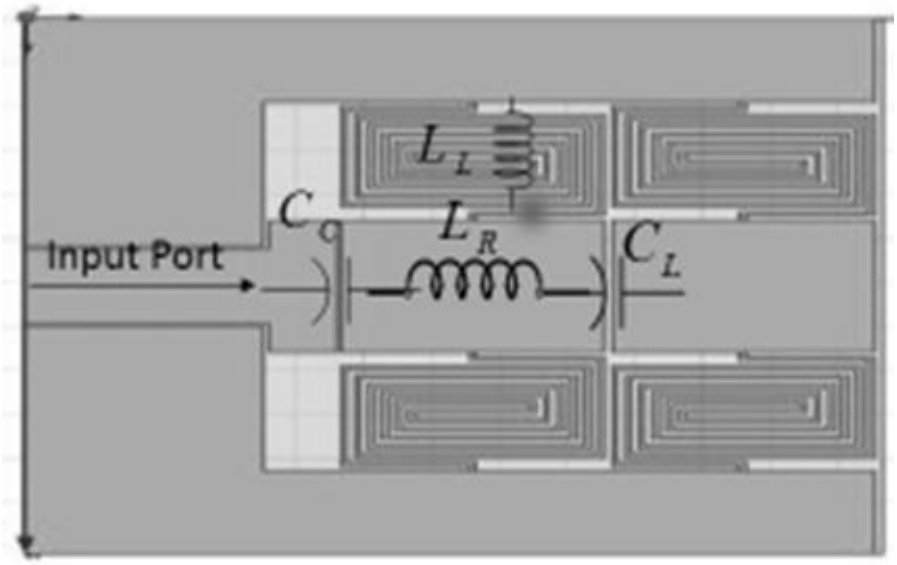

Figure 4.23 Realization of CPW fed CRLH based spiral and anti-spiral resonant antenna.

4.4.1 Generalized Equations for Unit Cell Block Design

Consider the unit cell block of Figure 4.23. Typical guidelines for the design of CRLH TL structure may be the following:

1. Appropriate transition frequency is selected as defined by the relation:

$$\omega_0 = \frac{1}{\sqrt[4]{L_R C_R L_L C_L}} = \sqrt{\omega_R \omega_L} = \sqrt{\omega_{se} \omega_{sh}} \tag{4.13}$$

   where

$$\omega_R = \frac{1}{\sqrt{L_R C_R}}, \omega_L = \frac{1}{\sqrt{L_L C_L}}, \omega_{se} = \frac{1}{\sqrt{L_R C_L}}, \omega_{sh} = \frac{1}{\sqrt{L_L C_R}} \tag{4.14}$$

2. Applying the matching condition of Equation (2.14) to ports of impedance calculate Z_c using the following equations: 2.15(a) and 2.15(b).

$$Z_R = \sqrt{\frac{L_R}{C_R}} = Z_c \tag{4.15 (a))}$$

$$Z_L = \sqrt{\frac{L_L}{C_L}} = Z_c \tag{4.15 (b))}$$

3. Equations (4.13) and (4.15) consists of four unknowns $L_R, C_R, L_L and C_L$ can be calculated using eigen frequency method detailed in Section 2.3.4.

4. Number of unit cells is set to two.

Once the constitutive lumped element values of the CRLH TL are known, depending on whether RH or LH, it is then multiplied or divided by the length of unit-cell (cell size), to obtain the associated per-unit-length and times unit-length component values:

$$L_R^{'} = \frac{L_R}{p}, C_R^{'} = \frac{C_R}{p}, L_L^{'} = L_L.p, C_L^{'} = C_L.p \tag{4.16}$$

The constitutive parameters extracted for the unit cell in accordance with the procedure given in Section 2.3.4 and Section 4.3 (a) consists of L_L (due to shunt square spiral inductors) =13.69 nH, L_R=2.262 nH while C_R (between the top patch and the CPW ground) =0.118 pF at f_0=3.97 GHz.

4.4.2 Antenna Geometry and Simulation Results

Figure 4.24 shows the geometry of the CPW fed pentaband CRLH TL antenna. It is designed on a substrate of size 24.4 mm x 25.4 mm x 1.6 mm is used. The proposed antenna is designed to have its zeroth order mode at 3.97 GHz by using EM simulator Ansoft HFSSv12. Antenna parameters are adjusted according to the general design guideline that the electrical size of the unit cell is approximately less than $\lambda_g/4$ where λ_g is the guided wavelength at zeroth order resonance. The electrical size of the unit cell of the antenna is $0.0794\lambda_0$ x $0.1032\lambda_0$ (6 mm x 7.8 mm) at 3.97 GHz. The overall area of the radiating patch is approximately $0.323\lambda_0$ x $0.336\lambda_0$ x $0.021\lambda_0$ (24.4 mm x 25.4 mm x 1.6 mm) at 3.97 GHz. Parameters of the short stub provided on top of the substrate is adjusted to achieve good impedance matching. The gap between the stub and the unit cell provides coupling capacitance (C_C) which impedance matches the antenna to 42 ohms. From the electric field vector distribution shown in Figure 4.25 (a) a constant phase electric field distribution evenly symmetric to the radiating patch is achieved at 3.97 GHz. From the surface current distribution shown in Figure 4.25 (b) it is realized that the spiral inductive stubs contribute significantly to antenna radiation as the current is mostly concentrated in the shunt spiral and anti-spiral inductive line region. By varying the length and width of these inductive stubs, it can be used as suitable elements for tuning of the planar ZOR antenna at the desired working frequency.

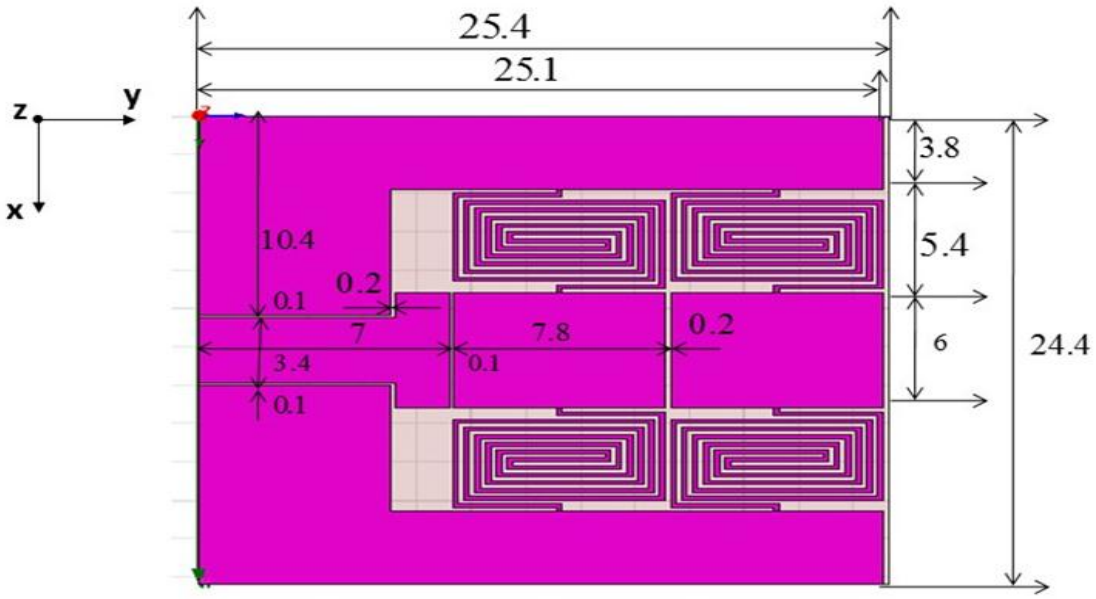

Figure 4.24 Geometry of the proposed CRLH based spiral and anti-spiral resonant antenna. (All dimensions in mm)

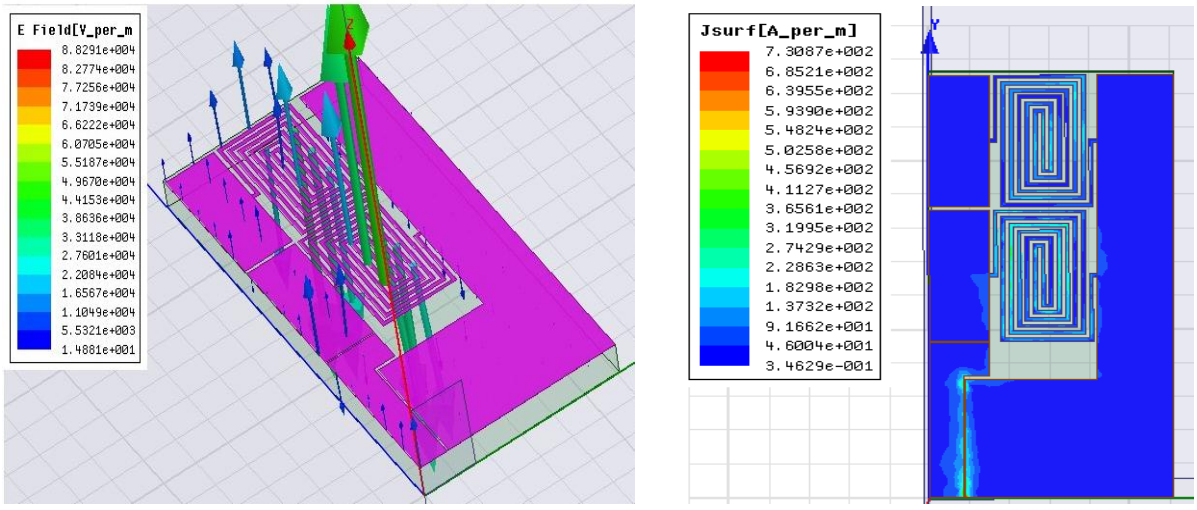

(a) **(b)**

Figure 4.25 (a) E-field vector distributions and (b) Surface current distributions at 2.46 GHz.

Figure 4.26 shows the simulated reflection coefficients of the proposed ZOR antenna. It is observed that the zeroth-order mode is achieved at 3.97 GHz with a reflection coefficient of -31.278 dB. Pentaband is obtained here with n = +2 mode at 4.48 GHz with -22.74 dB, n = +1 mode at 4.19 GHz with -13.19 dB, n = 0 mode at 3.97 GHz with -31.278 dB, n = -1 mode at 3.11 GHz with -11.92 dB, and n = -2 mode at 2.73 GHz with -23.68 dB. At the zeroth order mode of 3.97 GHz, bandwidth improvement and radiation efficiency of 3.28% and 73.42% is achieved, whereas, at other modes a high bandwidth and radiation efficiency of 9% and 83.88% at 4.48 GHz and 3.53% and 81.61% at 3.11 GHz are achieved. Figure 4.27

shows the simulated VSWR of the resonant CRLH TL. It is found that the VSWR is less than 2 in each of the resonant frequencies.

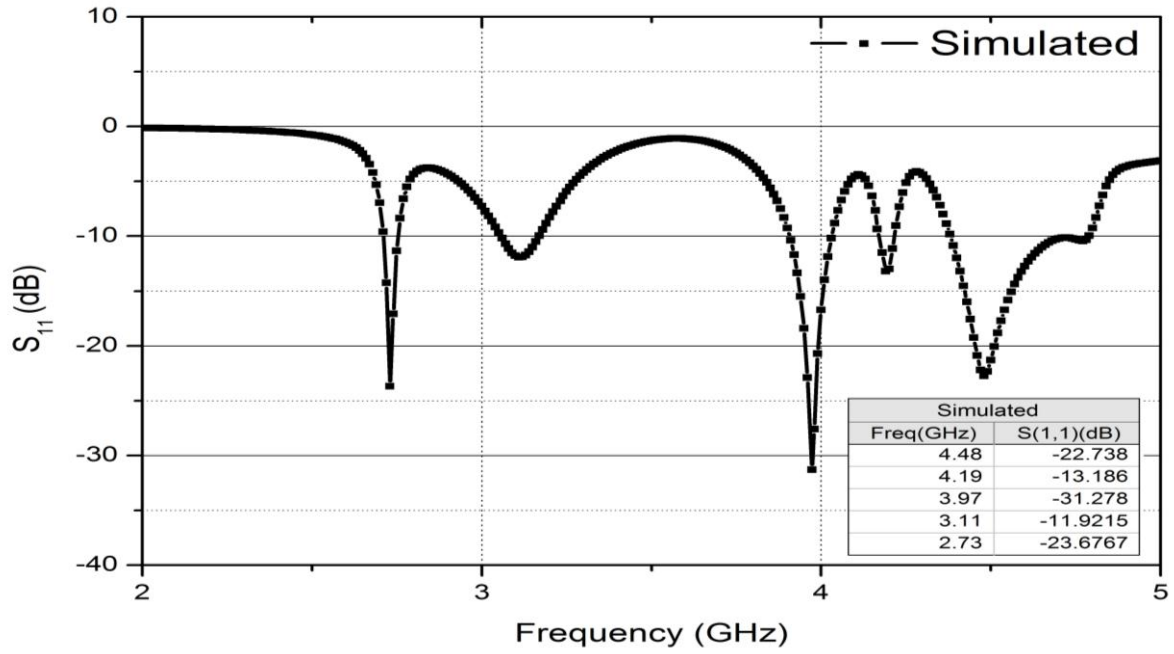

Figure 4.26 Simulated reflection coefficient of the CRLH based pentaband antenna.

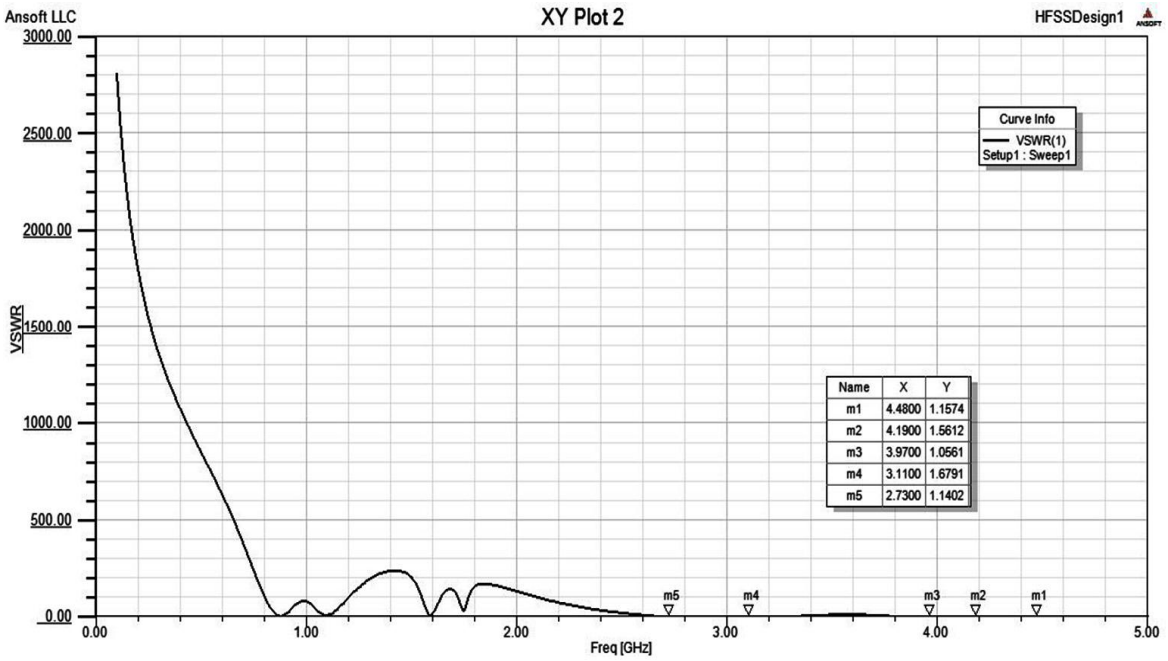

Figure 4.27 VSWR for the proposed structure.

Figures 4.28 and 4.29 show the simulated 2D radiation patterns and 3D gain patterns at 4.48 GHz, 4.19 GHz, 3.97 GHz, 3.11 GHz and 2.73 GHz respectively. Dumb-bell shaped E-radiation pattern (y-z plane) is attained along with an omni-directional H-radiation pattern (x-z plane). Since the magnetic field is locally circulating around the spiral and anti-spiral

lines to provide LH shunt inductance which leads to an omni-directional radiation pattern in H-plane. Highest gain of 4.58 dB is obtained at 2.73 GHz. The performance characteristic of the antenna is tabulated in Table 4.4.

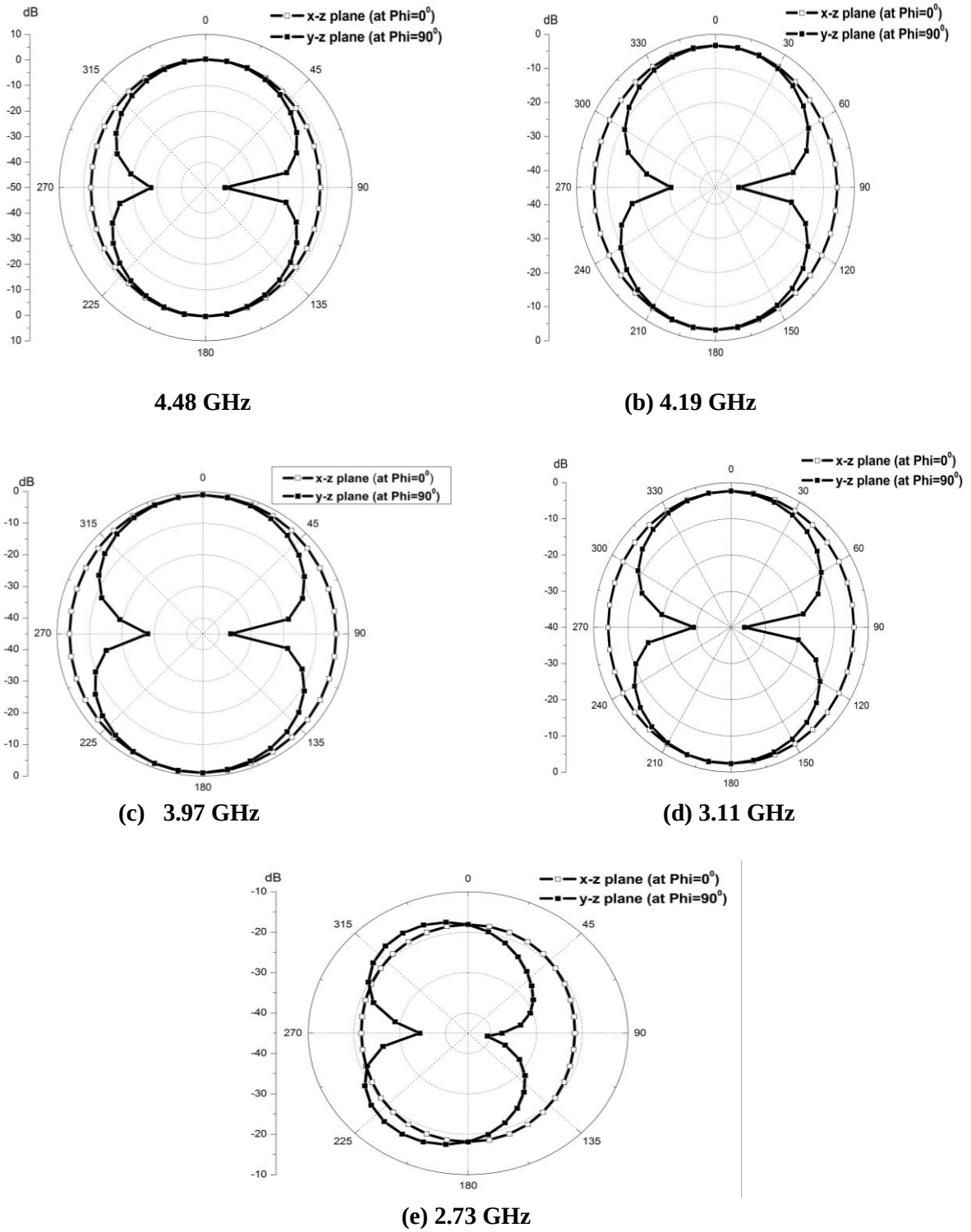

4.48 GHz **(b) 4.19 GHz**

(c) 3.97 GHz **(d) 3.11 GHz**

(e) 2.73 GHz

Figure 4.28 Simulated Radiation Patterns for the proposed CRLH based pentaband resonant antenna.

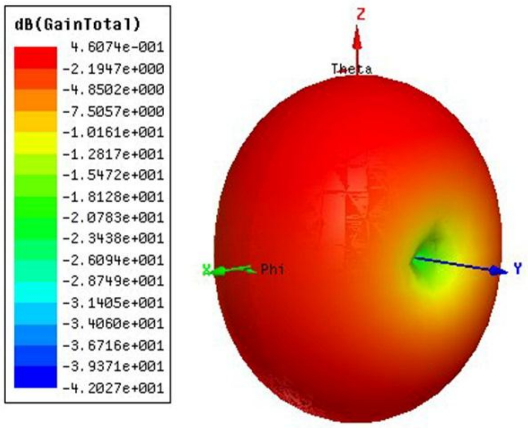

(a) 4.48 GHz

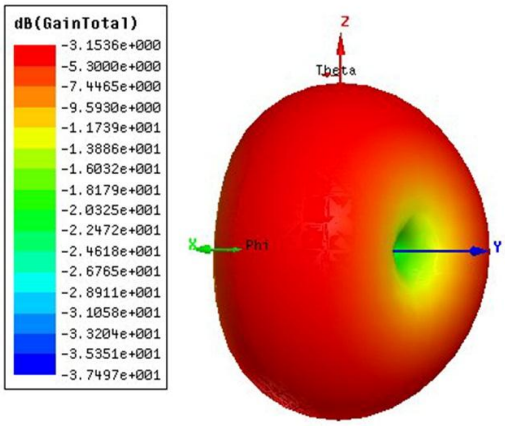

(b) 4.19 GHz

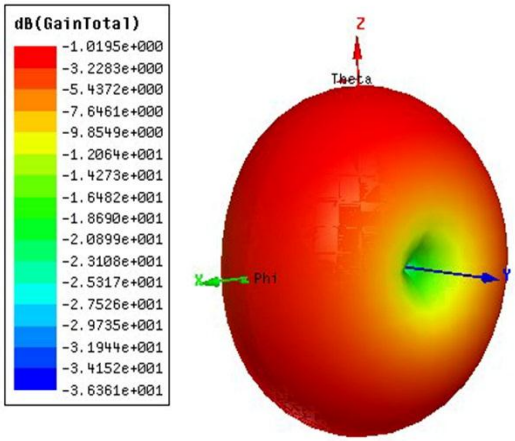

(c) 3.97 GHz

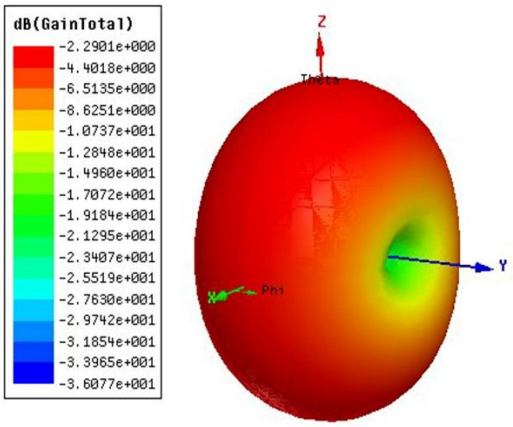

(d) 3.11 GHz

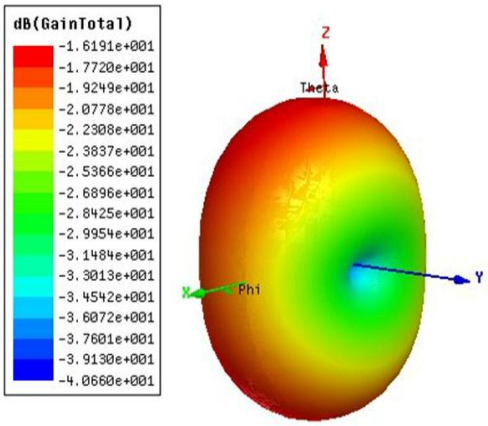

(e) 2.73 GHz

Figure 4.29 Simulated 3D Gain Patterns for the proposed CRLH based pentaband resonant antenna.

The simulated radiation efficiency (%) and directivity (dB) according to the operating band are presented in Fig. 4.30.

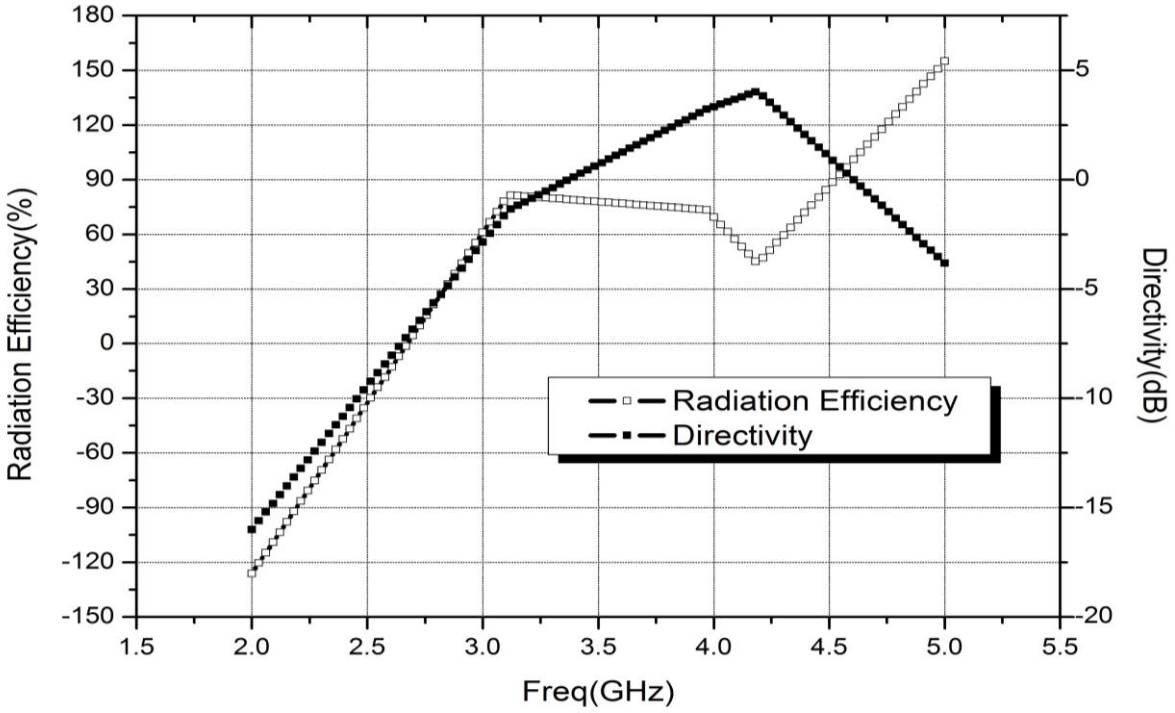

Figure 4.30 Simulated radiation efficiency and directivity for the proposed CRLH antenna.

Table 4.4 Performance Characteristics of the proposed pentaband metamaterial antenna at 4.48GHz, 4.19GHz, 3.97GHz, 3.11GHz and 2.73 GHz.

Substrate	**No. of Unit cells**	**No. of resonating modes/ bands**	**Resonant Freq (GHz)**	**Reflection Coefficient (dB)**	**Gain (dB)**	**Bandwidth (%)**	**Radiation Efficiency (%)**
RT Duroid	2	5	$f_{+2} = 4.48$	-22.7383	4.6074	9%	83.877
			$f_{+1} = 4.19$	-13.1860	-3.1536	1%	44.081
			$f_0 = 3.97$	-31.278	-1.0195	3.28%	73.42
			$f_{-1} = 3.11$	-11.9215	-2.2901	3.53%	81.614
			$f_{-2} = 2.73$	-23.6767	-1.619	1.58%	50.503

4.4.3 Experimental Verification

Figure 4.31 shows the fabricated prototype of the designed antenna. Details of fabrication procedure are mentioned in Appendix A.2. Figure 4.32 shows the comparison of the simulated and measured reflection coefficients of the antenna at 4.48 GHz, 4.19 GHz, 3.97 GHz, 3.11 GHz and 2.73 GHz respectively. A very good agreement between the measured and simulated reflection coefficients is obtained and it is found that the measured results varied from the simulated ones at each mode by about 0.16% approximately. The slight difference might be due to improper etching and the effect of Sub-Miniature Type-A 50Ω connectors. All measurements are carried out by using Agilent E8363B Network Analyser.

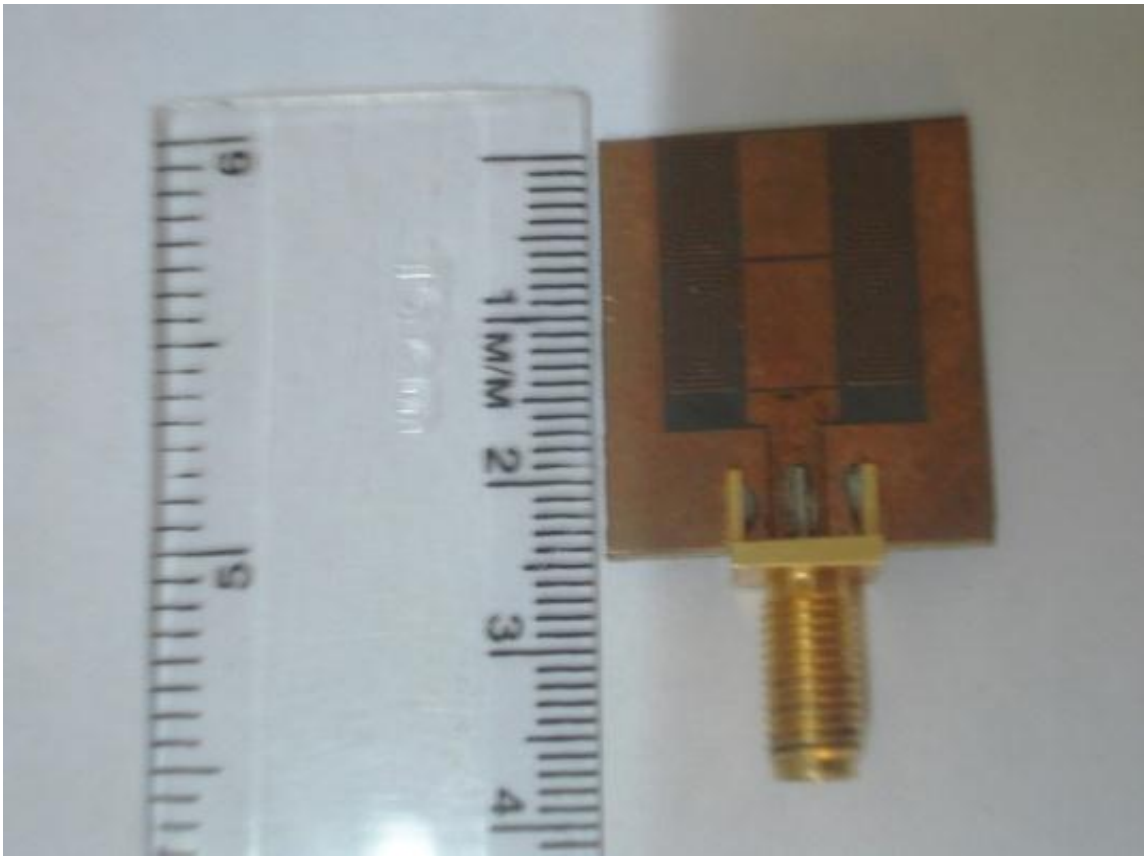

Figure 4.31 Fabricated prototype of the proposed CRLH based spiral anti-spiral pentaband antenna.

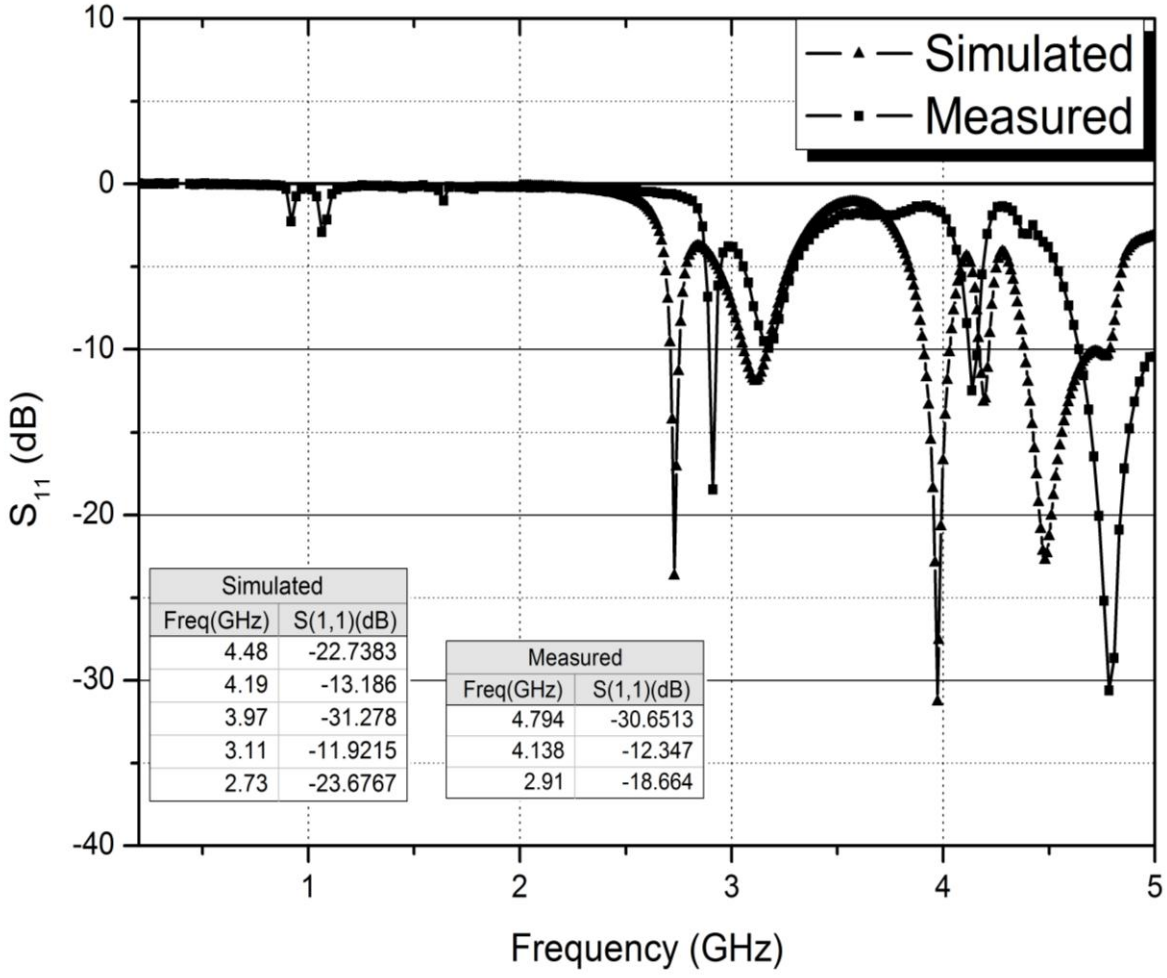

Simulated	
Freq(GHz)	S(1,1)(dB)
4.48	-22.7383
4.19	-13.186
3.97	-31.278
3.11	-11.9215
2.73	-23.6767

Measured	
Freq(GHz)	S(1,1)(dB)
4.794	-30.6513
4.138	-12.347
2.91	-18.664

Figure 4.32 Comparison of simulated and measured reflection coefficients of the proposed CRLH antenna.

4.4.4. Antenna Radiation Pattern and Gain Measurements

Figures (4.33 - 4.35) show the measured H-plane and E-plane radiation pattern cuts at 4.794 GHz, 4.138 GHz and 2.91 GHz respectively. The antenna is tested at Antenna Measurement Facility (AMF), Space Application Centre, ISRO, Ahmedabad. Details of Anechoic chamber and measurement set up is given in Appendix A.3.3. Radiation pattern measurements are undertaken with the test antenna mounted on to an aluminium plate fixture which is then aligned to a reference wideband horn antenna. Measurements outside the azimuth range $\pm 150^0$ could not be carried out since the positioner mounting interface shown in Figure 3.21 blocks the (relatively smaller) antenna assembly. A signal fluctuation in the main lobe of the measured radiation pattern is observed. This may be on account of the low coupled power from the single element. Scattering effects are observed in the measured radiation patterns which may be due to leakage or reflections from RF absorbers are responsible for the characteristic maxima and minima. Nevertheless, the simulated and measured results agree well within experimental errors and uncertainties. The measured peak gain of the fabricated antenna at 4.138 GHz is -8.1 dBi and at 2.91 GHz is -4.32 dBi. The Gain of the antennas has

been measured using Gain comparison method, details of which are given in Appendix A.3.4. Table 4.5 tabulates the comparative study between the simulated and measured performance characteristics of the proposed pentaband ZOR antenna.

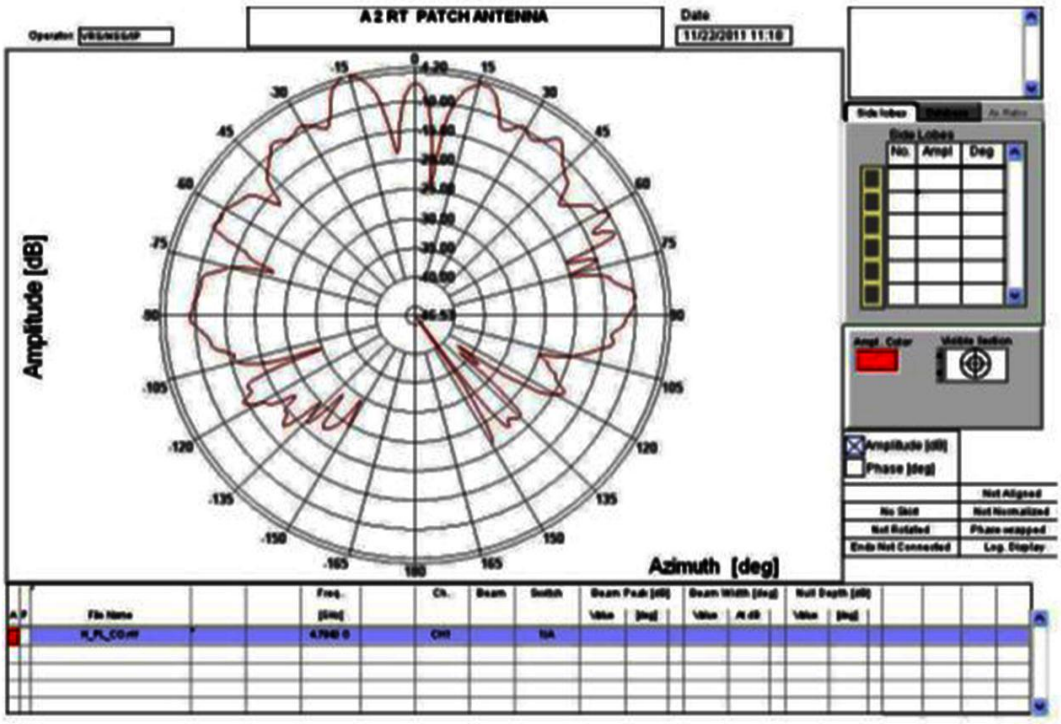

Measured at 4.794 GHz.

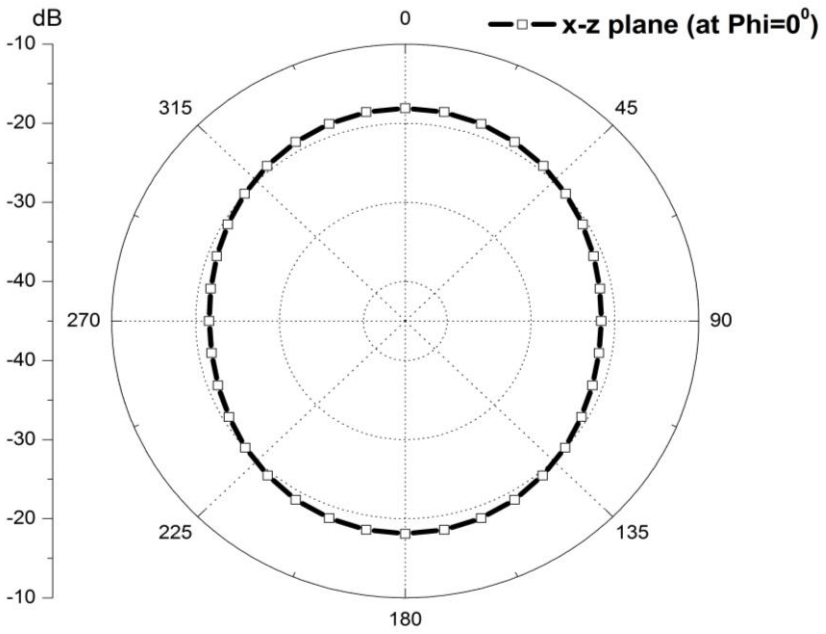

Simulated at 4.48 GHz.

Figure 4.33 (a) H-plane radiation patterns.

In Figure 4.33 (a) simulated H-plane radiation pattern agrees well with the measured radiation pattern. A slight signal fluctuation in the main lobe of the measured radiation pattern is observed. This may be on account of the errors in etching and fabrication of the square spiral stub inductors. Nevertheless, the simulated and measured results agree well within experimental errors and uncertainties.

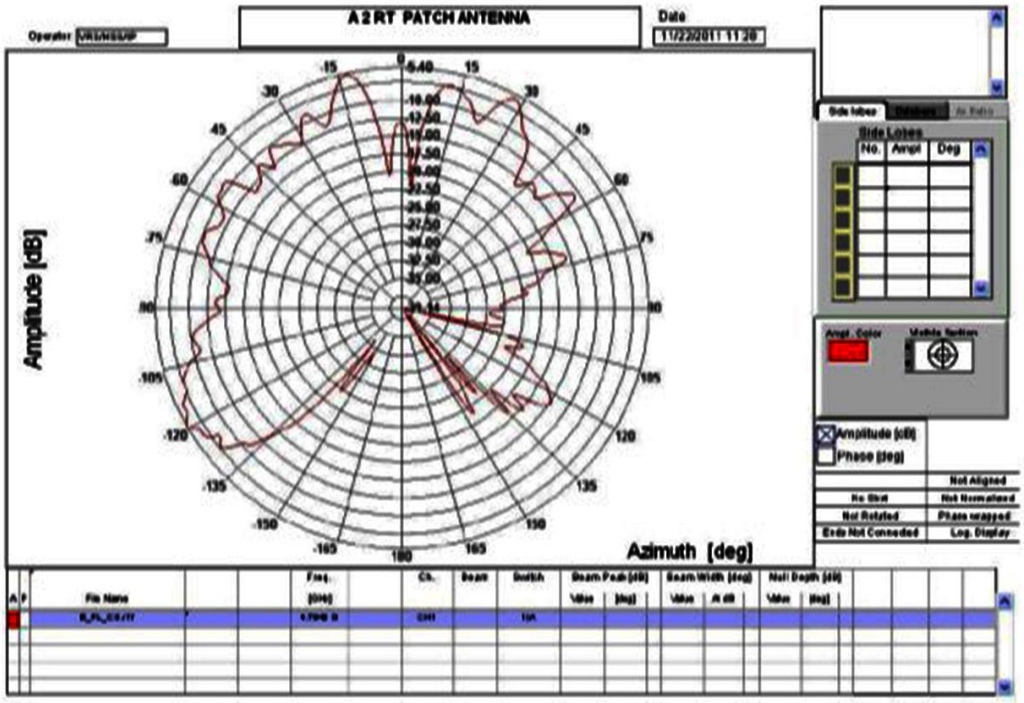

Measured at 4.794 GHz.

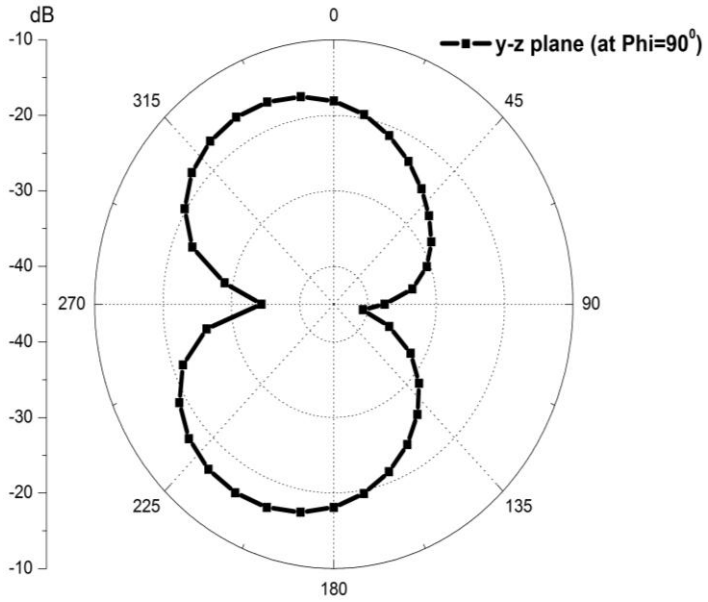

Simulated at 4.48 GHz.

Figure 4.33 (b) E-plane radiation patterns.

In Figure 4.33 (b), a dumb-bell shaped simulated E-radiation pattern is obtained and agrees well with the measured radiation pattern within limits of experimental errors. A slight signal fluctuation in the main lobe of the measured radiation pattern is observed. This may be accounted for scattering effects due to leakage or reflections from RF absorbers are responsible for the characteristic maxima and minima.

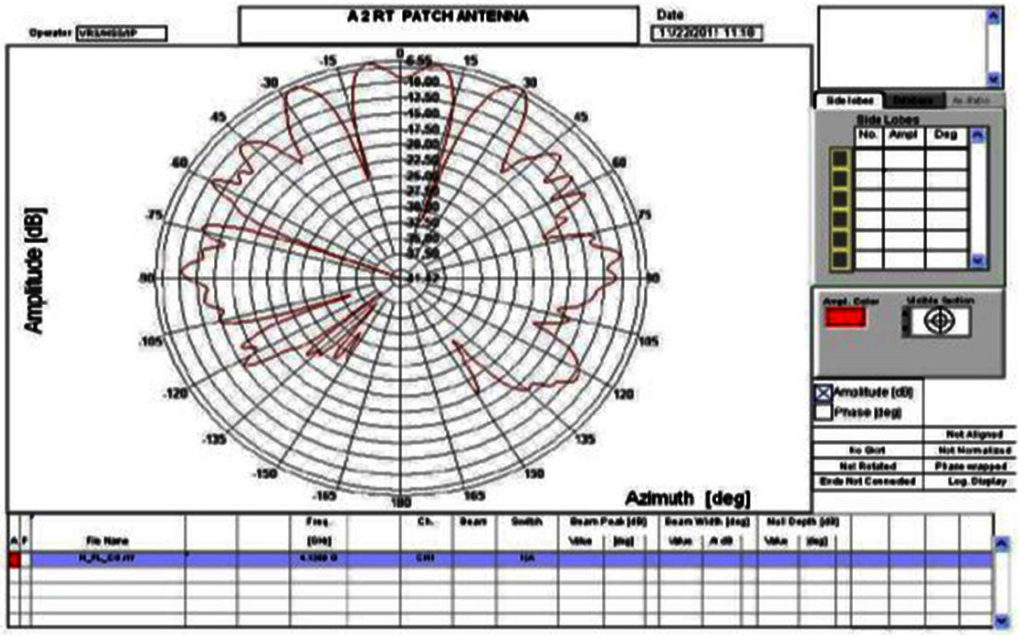

Measured at 4.138 GHz.

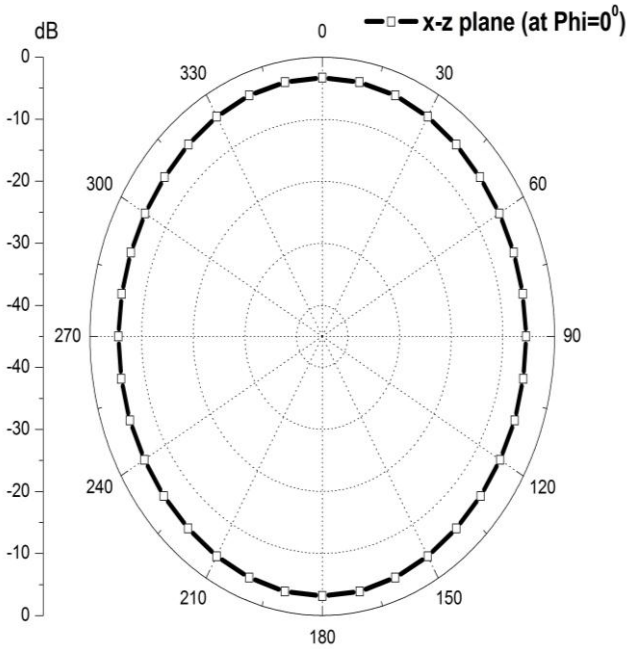

Simulated at 4.19 GHz.

Figure 4.34 (a) H-plane radiation patterns.

In Figure 4.34 (a), an omni-directional simulated H-plane radiation pattern is obtained and it agrees well with the simulated radiation pattern. Slight signal fluctuations in the main lobe of the measured radiation pattern are observed. This may be on account of the low coupled power from the single element. Scattering effects are observed in the measured radiation patterns which may be due to leakage or reflections from RF absorbers are responsible for the characteristic maxima and minima. Nevertheless, the simulated and measured results agree well within experimental errors and uncertainties.

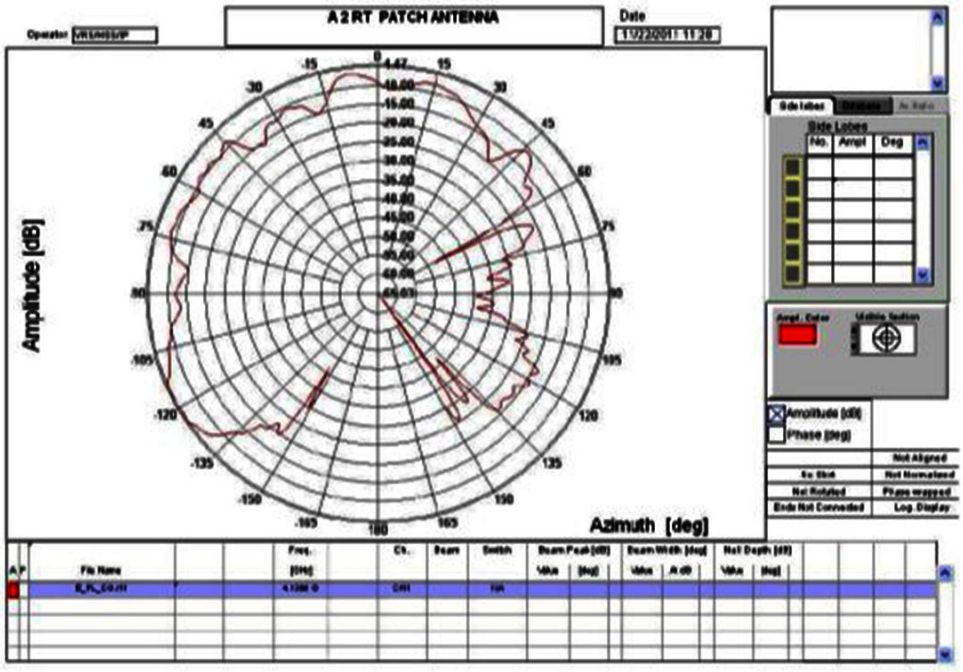

Measured at 4.138 GHz.

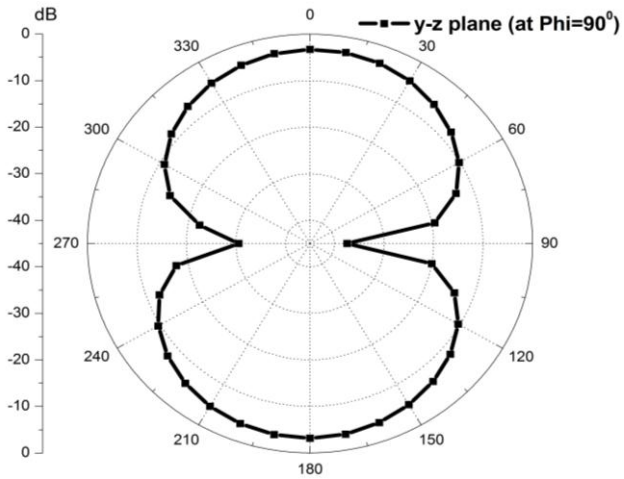

Simulated at 4.19 GHz.

Figure 4.34 (b) E-plane radiation patterns.

In Figure 4.34 (b), a dumb-bell shaped simulated E-plane radiation pattern is obtained. It agrees well with the measured E-plane radiation pattern within experimental errors and uncertainties. Signal fluctuations in the main lobe of the measured radiation pattern are less pronounced as frequency increases. Scattering effects are observed in the measured radiation patterns which may be due to leakage or reflections from RF absorbers are responsible for the characteristic maxima and minima.

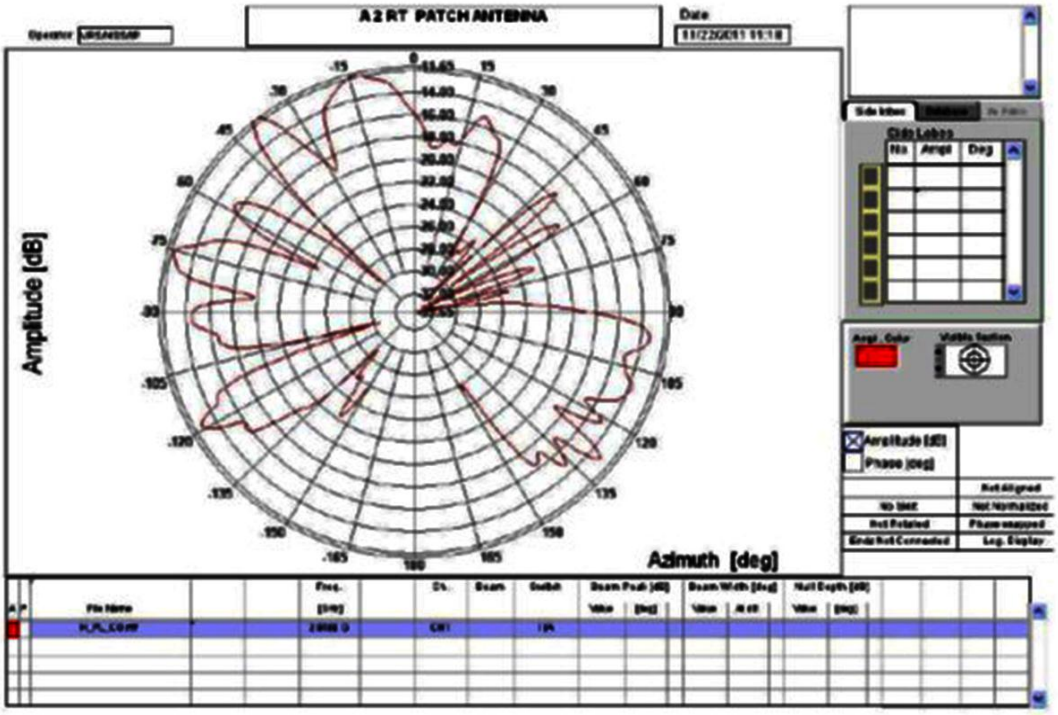

Measured at 2.91 GHz.

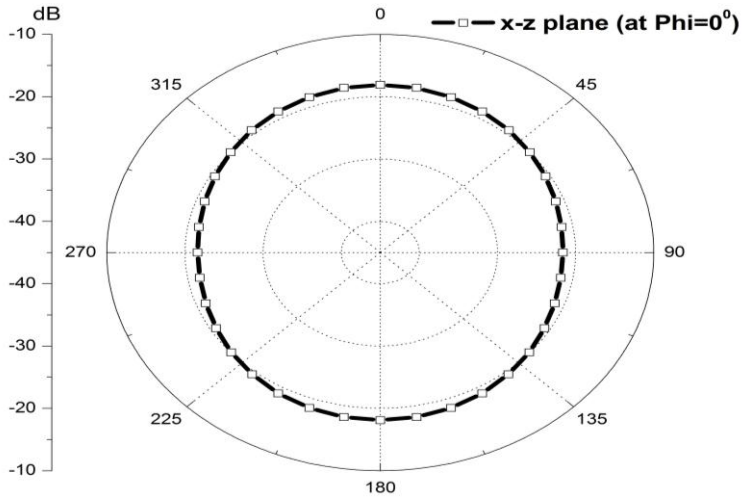

Simulated at 2.73 GHz.

Figure 4.35 (a) H-plane radiation patterns.

In Figure 4.35 (a), an omni-directional H-plane radiation pattern is obtained. It agrees well with the measured E-plane radiation pattern within experimental errors and uncertainties. Signal fluctuations in the main lobe of the measured radiation pattern is more pronounced as frequency decreases. Scattering effects are observed in the measured radiation patterns which may be due to leakage or reflections from RF absorbers.

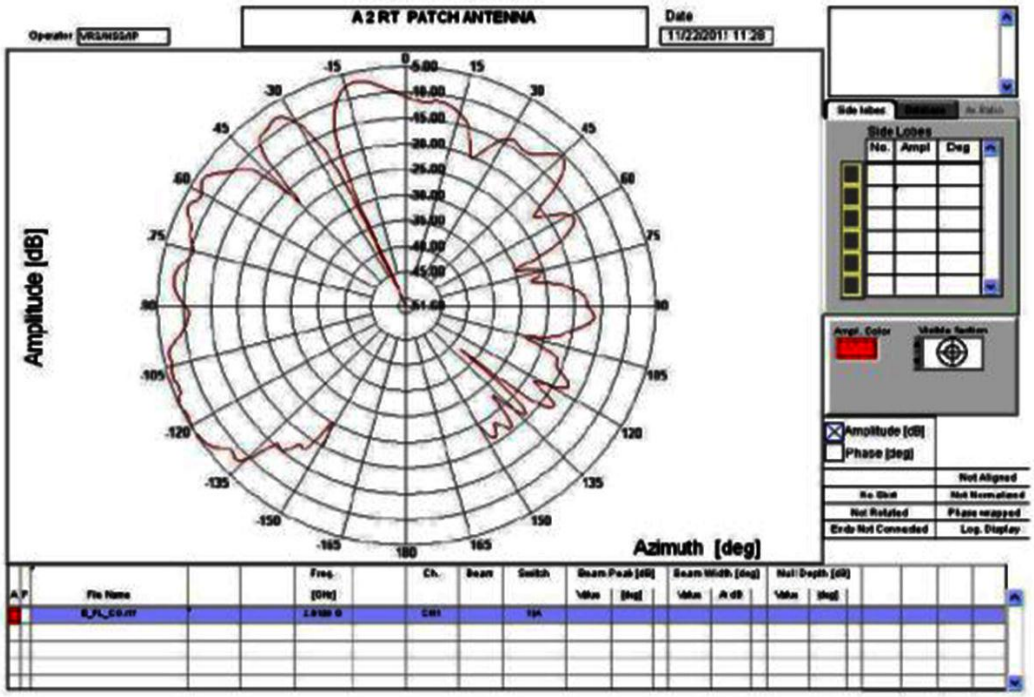

Measured at 2.91 GHz.

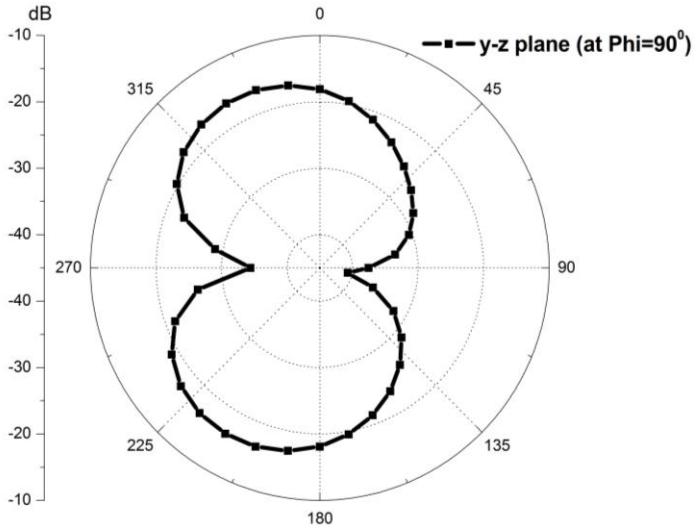

Simulated at 2.73 GHz.

Figure 4.35 (b) E-plane radiation patterns.

In Figure 4.35 (b), a dumb-bell shaped simulated E-plane radiation pattern is obtained and agrees well the measured result within experimental errors and uncertainties. Scattering effect is observed which may be due to etching or fabrication errors.

Table 4.5 Comparison of the simulated and measured performance characteristics of the proposed penta-band antenna at 4.48, 4.19, 3.97, 3.11 and 2.73 GHz.

SIMULATED				MEASURED					
Resonant Freq (GHz)	Reflection Coefficient (dB)	Band-width (%)	Gain (dB)	Resonant Freq (GHz)	Reflection Coefficient (dB)	Band-width (%)	Peak Gain (dBi)	Applications	Radiation Efficiency (%)
4.48	-22.7383	9	4.6074	4.7948	-30.399	7.5		WiMax	83.877
4.19	-13.1860	1	-3.1536					WiMax	44.081
3.97	-31.278	3.28	-1.0195	4.138	-12.347	2	-8.1	WLAN	73.42
3.11	-11.9215	3.53	-2.2901	3.162	-10.410	3		WLAN	81.614
2.73	-23.6767	1.58	-1.619	2.91	-18.664		-4.32	WLAN	50.503

4.4.5. CONCLUSIONS

A new zeroth order resonant antenna implemented by using a combination of open ended spiral and anti-spiral inductors is proposed. The open ended antenna presented here is excited by the shunt mode of resonance. The antenna radiates at five different modes with the zeroth order mode at 3.97 GHz. At 3.97 GHz (3.906 - 4.031) GHz, a bandwidth enhancement of 3.28% is achieved but a low gain of -1.0195 dB is observed whereas at 3.11 GHz (3.058 - 3.168) GHz an improved bandwidth of 3.53% is realised, but a low gain of -2.29 dB acted as a drag. So there is a trade-off between gain and bandwidth. At frequencies 4.19 GHz (4.173 - 4.215) GHz and 2.73 GHz (2.7109 - 2.754) GHz, the antenna exhibited a narrow bandwidth of almost 2%. The bandwidth of the proposed antenna maximizes to almost about 9% at 4.48 GHz (4.38 – 4.79) GHz. Due to the multiband characteristics, the proposed antenna is most suited for modern multiband WLAN systems at 2.73 GHz, 3.97 GHz and 3.11 GHz and WiMax applications at 4.48 GHz and 4.19 GHz.

4.5 Summary

In this chapter, two new structural geometries of CPW fed ZOR antennas are proposed. Here spiral and anti-spiral inductive stubs are introduced to increase shunt inductance L_L. The study showed that with increase in shunt inductance L_L, the bandwidth of the antenna increases to 3.28% with a low gain of -1.0195 dB. So there is a trade-off between gain and bandwidth. As bandwidth increases, gain decreases and vice versa. In the next chapter the focus is laid on increasing the gain without compromising the bandwidth by using an elliptical radiating patch instead of a rectangular one as proposed in this chapter.

Chapter 5

High Gain Elliptical Zeroth Order Resonant Antenna

5.1 Introduction

Low profile antennas with omni-directional radiation pattern are in great demand for modern wireless communication systems that require radiation pattern uniformity due to their large service area.To increase the service area, to improve signal strength and to boost the sensitivity and reliability of wireless communications; high gain omni-directional antennas are essential. This requirement is met with the use of monopole and dipole antennas. However, these devices are too large to meet the demands of compact, portable devices. Metamaterials come handy in resolving this problem as metamaterials are popularly used to design low profile antennas and microwave devices. The composite right/left handed metamaterial transmission lines is an effective method to realize low profile, compact infinite wavelength zeroth order resonant (ZOR) antennas. But these ZOR antennas suffer from narrow bandwidth, low gain or low radiation efficiency. Several methods were employed to improve efficiency and gain but they suffered from certain drawbacks like having a large volume, large ground plane or large frequency ratio.

In the previous chapter focus had been laid on enhancing the bandwidth of a ZOR antenna where the bandwidth of the proposed antenna was successfully enhanced up to about 3.28% but with a low gain of -1.0195 dB at the zeroth mode of 3.97 GHz. In this chapter, the focus is on enhancing the gain of the antenna proposed in chapter 4. To achieve this purpose the area of the radiating patch was reduced by replacing the rectangular patch with an elliptical one to minimize loss due to surface wave thereby enhancing the gain and radiation efficiency of the antenna. This leads to the proposal of a compact high gain monomode elliptical zeroth order resonant antenna. Section 5.3 deals with the parametric and optimization analysis on minor radius of the elliptical radiating patch to achieve maximum bandwidth. It is observed that an antenna can be tuned to a desired working frequency by adjusting the minor radius of the elliptical patch. This is then followed by experimental validation of the proposed design detailed in section 5.4. Finally, the chapter is summarized in section 5.5.

5.2 Antenna Design Methodology

The ZOR antenna proposed in this chapter consists of two elliptical unit cells each of size (6 mm x 7.8 mm). Each unit cell is flanked symmetrically on both sides by a combination of short ended spiral and anti-spiral inductors. A CPW feed line along with a proximity coupled feed network is used to excite the open ended CRLH TL structure to initiate shunt mode of resonance ω_{sh}, with energy being stored in the shunt elements. Figure 5.1 shows pictorial representation of a CPW fed CRLH TL antenna structure consisting of two unit cells. For an open-ended CRLH TL resonator, the fractional bandwidth is given by Equation (4.1).

Bandwidth is directly proportional to the length of these spiral stub inductors (L_L) and inversely proportional to the overall area of the substrate (C_R). By using a combination of short ended spiral and anti-spiral inductors to increase stub inductance (L_L), bandwidth is increased and by using an elliptical radiating patch the surface wave loss is reduced, thereby increasing gain and efficiency of the proposed antenna structure. So by adopting this methodology of elliptical unit cells with spiral and anti-spiral inductors, a ZOR antenna with extended bandwidth, high gain along with improved radiation efficiency is accomplished. As the spiral and anti-spiral inductors are shorted at their ends to the CPW grounds, no vias are needed to simplify the realization of this antenna.

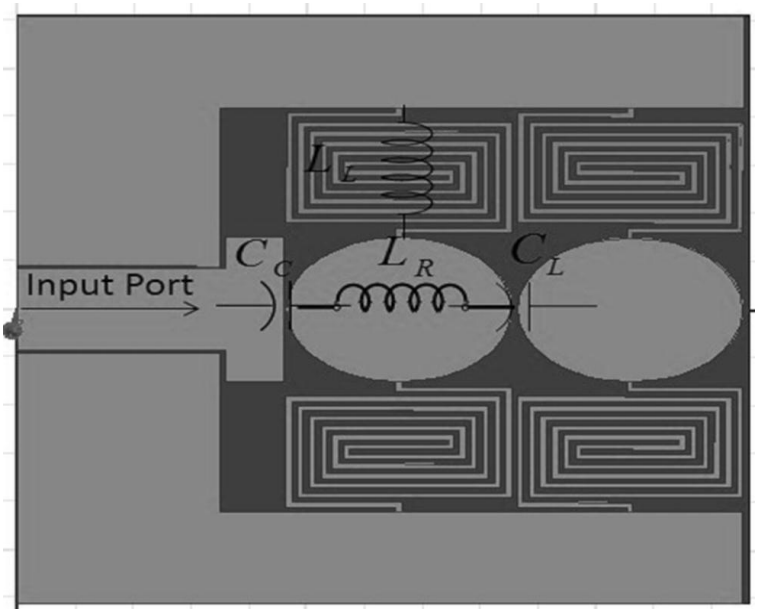

Figure 5.1 Realization of CPW fed CRLH based elliptical resonant antenna.

5.2.1. Generalized Equations for Unit Cell Block Design

In Chapter 4, larger left-handed inductance was achieved by employing spiral and anti-spiral inductors which lead to an enhanced bandwidth. But the proposed antenna suffered from low gain. From Equation (2.30), it can be inferred that for an open circuit zeroth order resonant antenna, the unloaded quality factor Q is dependent only on the loss in the shunt LC tank circuit and not on the loss in the series tank circuit. Since radiation efficiency is inversely proportional to quality factor, so a ZOR antenna with a higher gain and efficiency can be obtained by designing a CRLH unit cell with a lower loss in the substrate and with a larger left-handed inductance. So in this Chapter a CRLH unit cell is designed by adopting the same CRLH topology as used in the previous Chapter but employing an elliptical radiating patch instead of a rectangular patch. This is done to ensure that loss is reduced by suppression of surface waves thereby enhancing gain of the proposed antenna.

Consider the unit cell block of Figure 4.2. Typical guidelines for the design of CRLH TL structure may be the following:

1. Transition frequency at 4.89 GHz is selected as defined by the relation:

$$\omega_0 = \frac{1}{\sqrt[4]{L_R C_R L_L C_L}} = \sqrt{\omega_R \omega_L} = \sqrt{\omega_{se}\omega_{sh}} \quad (5.1)$$

where

$$\omega_R = \frac{1}{\sqrt{L_R C_R}}, \omega_L = \frac{1}{\sqrt{L_L C_L}}, \omega_{se} = \frac{1}{\sqrt{L_R C_L}}, \omega_{sh} = \frac{1}{\sqrt{L_L C_R}} \quad (5.2)$$

2. Applying the matching condition of Equation (2.14) to ports of impedance calculate Z_c using the following equations: 2.15(a) and 2.15(b).

$$Z_R = \sqrt{\frac{L_R}{C_R}} = Z_c \quad (5.3\ (a))$$

$$Z_L = \sqrt{\frac{L_L}{C_L}} = Z_c \quad (5.3\ (b))$$

3. Equations (5.1) and (5.3) consists of four unknowns $L_R, C_R, L_L and C_L$ can be calculated using eigen frequency method detailed in Section 2.3.4.

4. Number of unit cells is set to two.

Once the constitutive lumped element values of the CRLH TL are known, depending on whether RH or LH, it is then multiplied or divided by the length of unit-cell (cell size), to obtain the associated per-unit-length and times unit-length component values:

$$L_R^{'} = \frac{L_R}{p}, C_R^{'} = \frac{C_R}{p}, L_L^{'} = L_L.p, C_L^{'} = C_L.p \quad (5.4)$$

The constitutive parameters extracted for the unit cell in accordance with the procedure given in Section 2.3.4 and Section 4.3 (a) consists of L_L (due to shunt square spiral inductors) =13.69 nH while C_R (between the top patch and the CPW ground) =0.118 pF at f_0=4.89 GHz.

5.3 Antenna Geometry and Simulation Results

The geometrical model of the proposed elliptical antenna is shown in Figure 5.2.The antenna is implemented on a Rogers RT/ Duroid 5880 substrate (ε_r = 2.2) with a size of 30 mm x 32 mm x 1.6 mm. The proposed antenna is designed to have its zeroth order mode at 4.89 GHz by Ansoft High Frequency Structure Simulator (HFSSv12). Antenna parameters are adjusted according to the general design guideline that the electrical size of the unit cell is approximately less than $\lambda_g/4$ where λ_g is the guided wavelength at zeroth order resonance. The electrical size of the unit cell of the antenna is $0.098\lambda_0$ x $0.127\lambda_0$ (6.0 mm x 7.8 mm) at 4.89GHz. The overall area of the radiating aperture is approximately $0.489\lambda_0$ x $0.522\lambda_0$ x

$0.026\,\lambda_0$ (30 mm x 32 mm x 1.6 mm) at 4.89 GHz. Parameters of a short stub provided on top of the substrate is adjusted to achieve good impedance matching. The gap between the stub and the unit cell provides coupling capacitance (C_C) which impedance matches the antenna to 42 ohms.

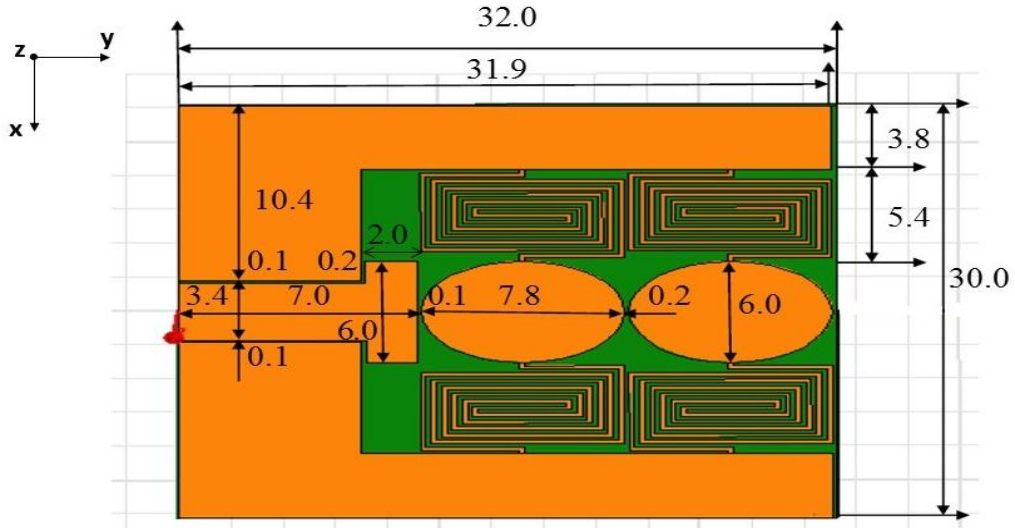

Figure 5.2 Geometry of the proposed CRLH based elliptical resonant antenna. (All dimensions in mm)

From the electric field vector distribution shown in Figure 5.3(a) a constant phase electric field distribution, uniformly vertical to the radiating patch is achieved at 4.89 GHz. From the surface current distribution, shown in Figure 5.3(b), it is observed that current is mostly concentrated in the shunt spiral and anti-spiral inductive lines, as a result, these inductive stubs contribute significantly to antenna radiation. The antenna can be tuned to a desired working frequency by either varying the radius of the elliptical patch or by varying the length and width of these inductive stubs.

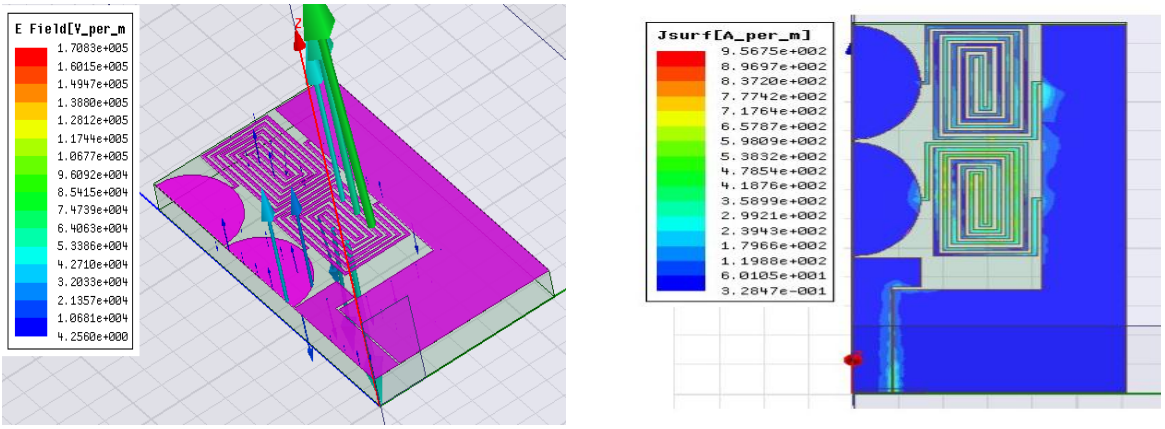

Figure 5.3 (a) E-field vector distributions and (b) Surface current distributions at 4.89 GHz.

Figure 5.4 shows the reflection coefficient for the proposed antenna. The reflection coefficient achieved at this mode is about -26.49 dB with a bandwidth of 5%. The operational

bandwidth obtained at 4.89 GHz ((4.65 – 4.97) GHz) is aptly suited for wireless LAN communications which include the mobile and wireless local area network (WLAN) systems due to their large service area. Figure 5.5 shows the simulated VSWR of the resonant CRLH TL. It is found that the VSWR is less than 2 in each of the resonant frequencies.

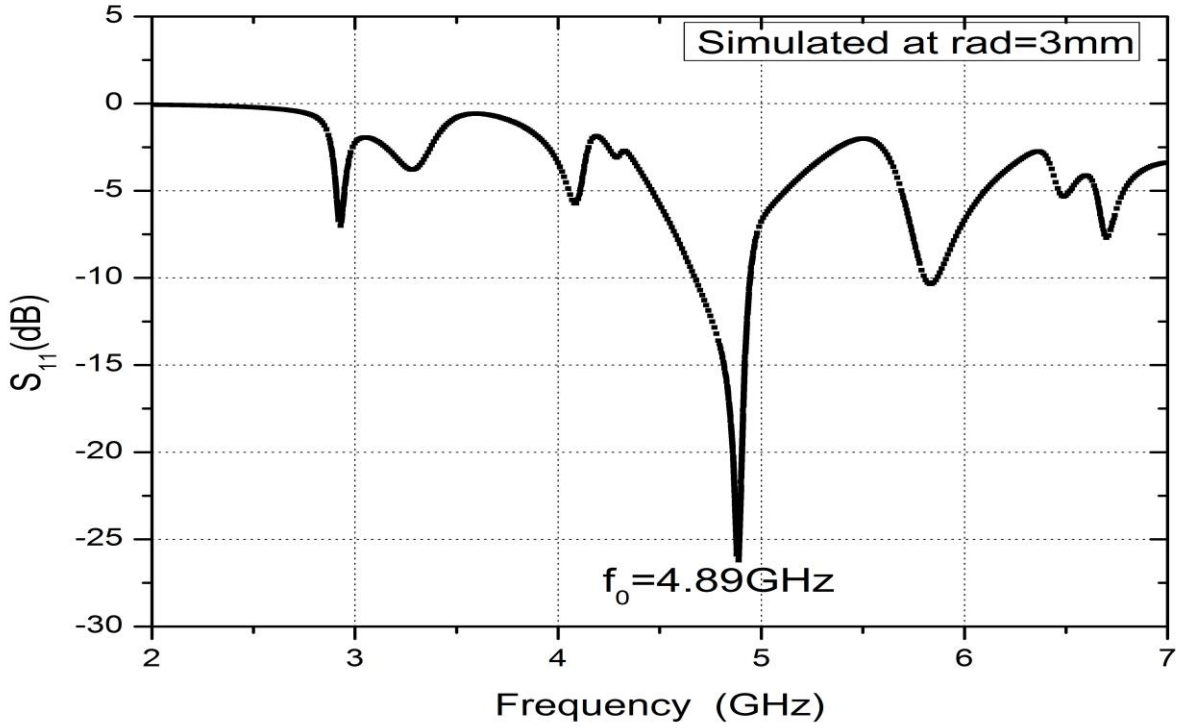

Figure 5.4 Simulated reflection coefficient of the CRLH based resonant antenna.

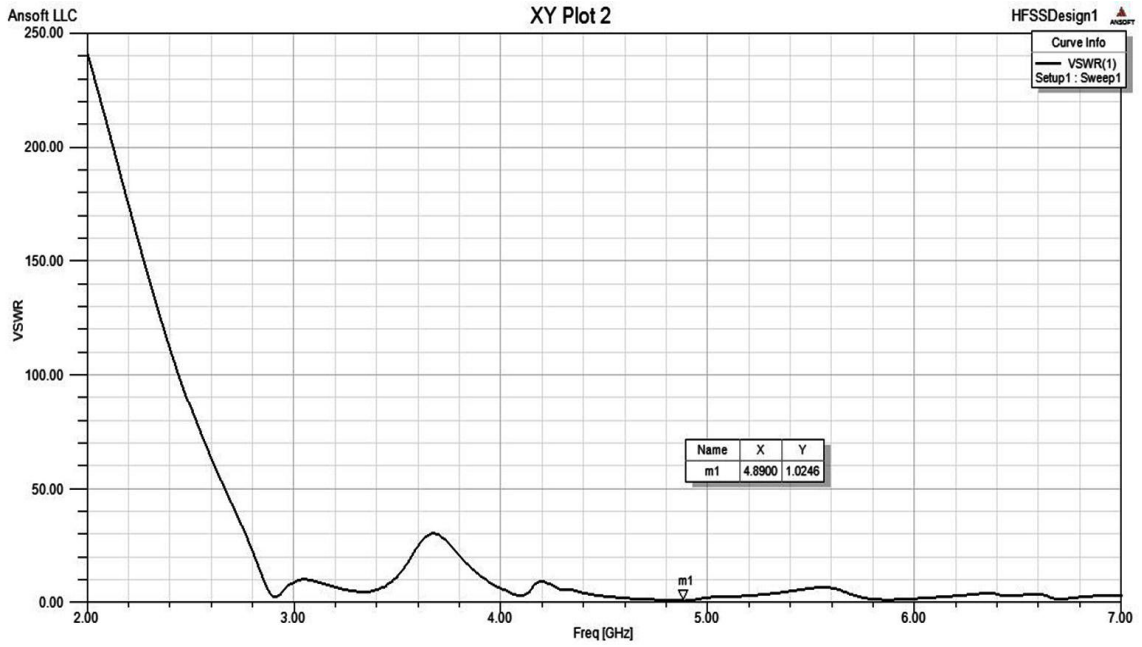

Figure 5.5 VSWR for the proposed structure.

Figure 5.6 shows the simulated 2D radiation pattern and 3D gain pattern at 4.89 GHz for the proposed antenna model shown in Figure 5.2. A monopolar E-radiation pattern along y-z plane and an omni-directional H-radiation pattern along x-z plane is obtained. The antenna exhibits a high gain and efficiency of about 2.2474 dB and 83.094% respectively at the zeroth order mode of 4.89 GHz.

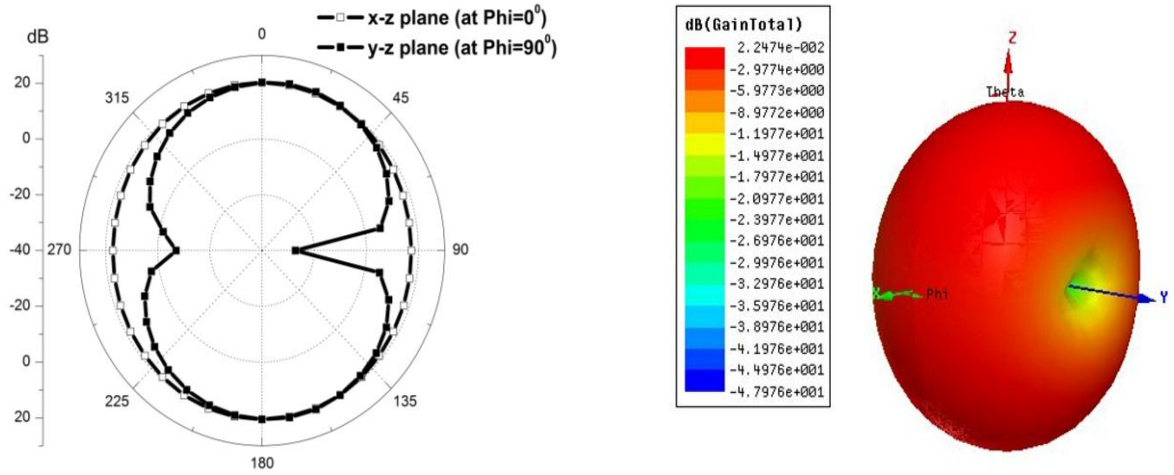

Figure 5.6 Simulated (a) Radiation patterns and (b) 3D Gain for the CRLH based elliptical resonant antenna at 4.89 GHz with minor radius of 3 mm.

5.3.1 Parametric Analysis on Minor Radius

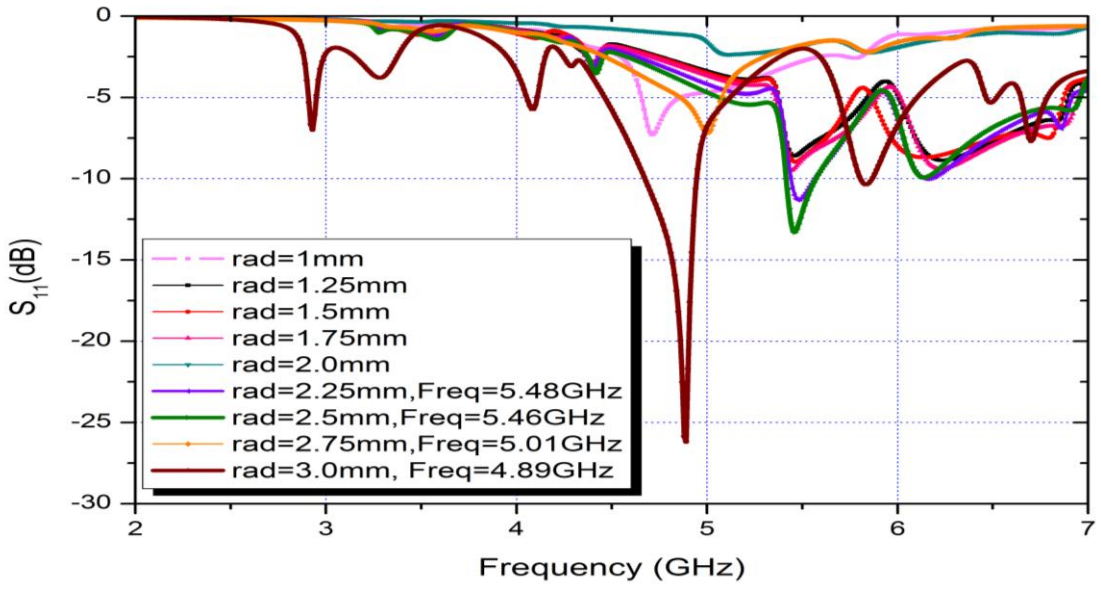

Figure 5.7 Parametric Effect on S_{11} due to change of minor radius.

Figure 5.7 shows the effect of changing minor radius on the zeroth order resonant frequency. The simulated parametric analysis was defined to sweep the value of minor radius from a minimum to a maximum range. The study presented here sweeps the variable with a limit of ±30% about the nominal value. It is observed that with an increase in the minor radius,

multiband functionality of the antenna increases but the resonant frequency decreases. Hence the inductive minor radius can be used as a very suitable element for tuning a given antenna, to a desired operational frequency.

5.3.2 Optimization Analysis to achieve Maximum Bandwidth

Optimization analysis on minor radius parameter is carried out by using HFSS pattern search optimizer to achieve maximum bandwidth. HFSS pattern search optimizer performs a grid-based simplex search, which makes use of simplexes: triangles in 2D space or tetrahedral in 3D space. The cost value is calculated at the vertices of the simplex. The optimizer mirrors the simplex across one of its faces based on mathematical guidelines and determines whether the new simplex provides better results. If it does not produce a better result, the next face is used for mirroring and the pattern continues. If no improvement occurs, the grid is refined. If improvement occurs, the step is accepted and the new simplex is generated to replace the original one.

As shown in Figure 5.8, cost function reduces to an optimized minima for nominal minor radius 3.075 mm. From the optimization analysis shown in Figure 5.9 (a) it is reaffirmed that the best optimized result wherein our objective of maximum bandwidth of 9% is achieved at 4.47 GHz ((4.375 – 4.79) GHz) for an optimum minor radius of 3.075 mm. Additionally, an enhanced bandwidth of 7.6% at 4.76 GHz and 5% at 4.89 GHz is respectively obtained for radius 3.0375 mm and 3 mm. Furthermore, it is observed from Figure 5.9 (b) that tri-band characteristics is achieved for minor radius 3.3375 mm but bandwidth obtained at each of the triband resonant frequencies is quite narrow, which serves as a constraint to our objective. Fabrication with radii of 3.075 mm or 3.0375 mm being phenomenally difficult; so radius with 3.0mm, is chosen for validation of the proposed design.

Finally, Figure 5.10 shows the comparison of the reflection coefficients for optimized antenna design with respect to the simulated antenna model shown in Figure 5.2. The performance characteristic of the antenna at these two radii is tabulated and compared in Table 5.1.

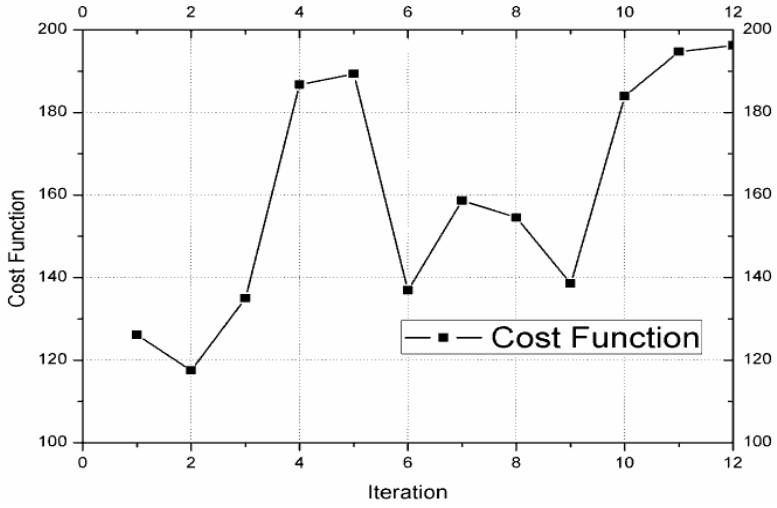

Iteration	Radius	Cost Function
1	3.0375m	126.08
2	3.075mm	117.48
3	3mm	134.95
4	3.3mm	186.7
5	2.7mm	189.34
6	2.85mm	136.88
7	3.15mm	158.65
8	3.375mm	154.53
9	2.775mm	138.51
10	2.925mm	183.93
11	3.225mm	194.69
12	3.1125m	196.22

Figure 5.8 Plot for Cost function Vs No. of iterations using Pattern Search Optimizer.

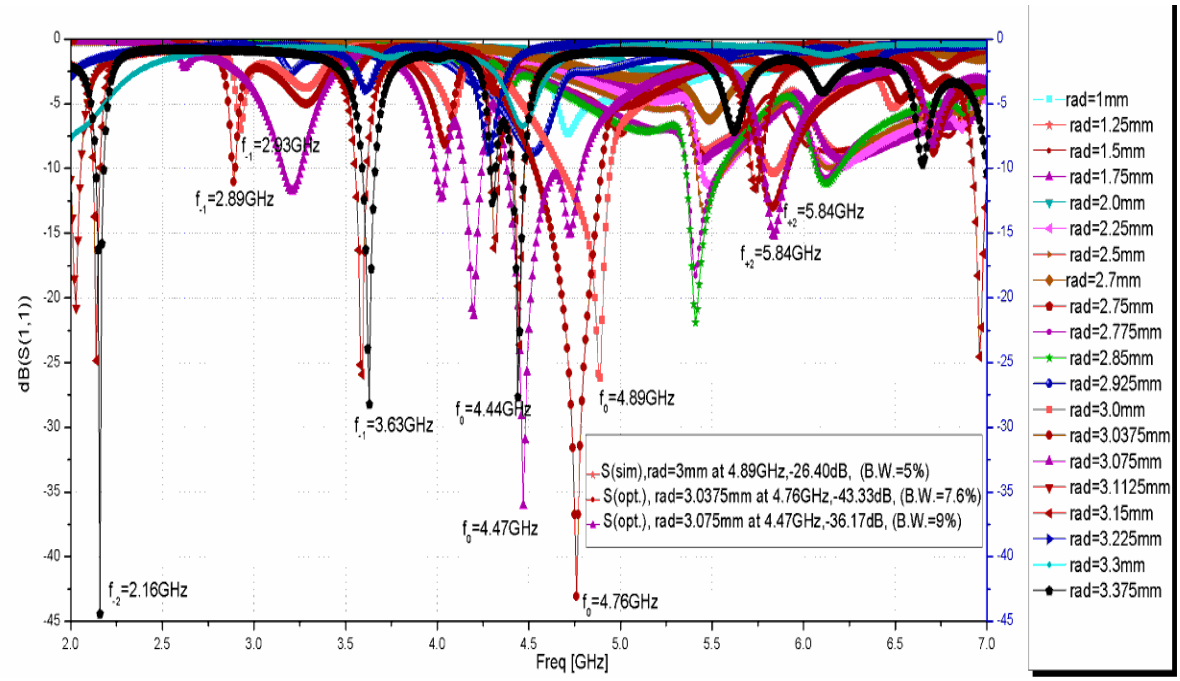

Figure 5.9 (a) Optimization of minor radius for maximum bandwidth at the zeroth mode.

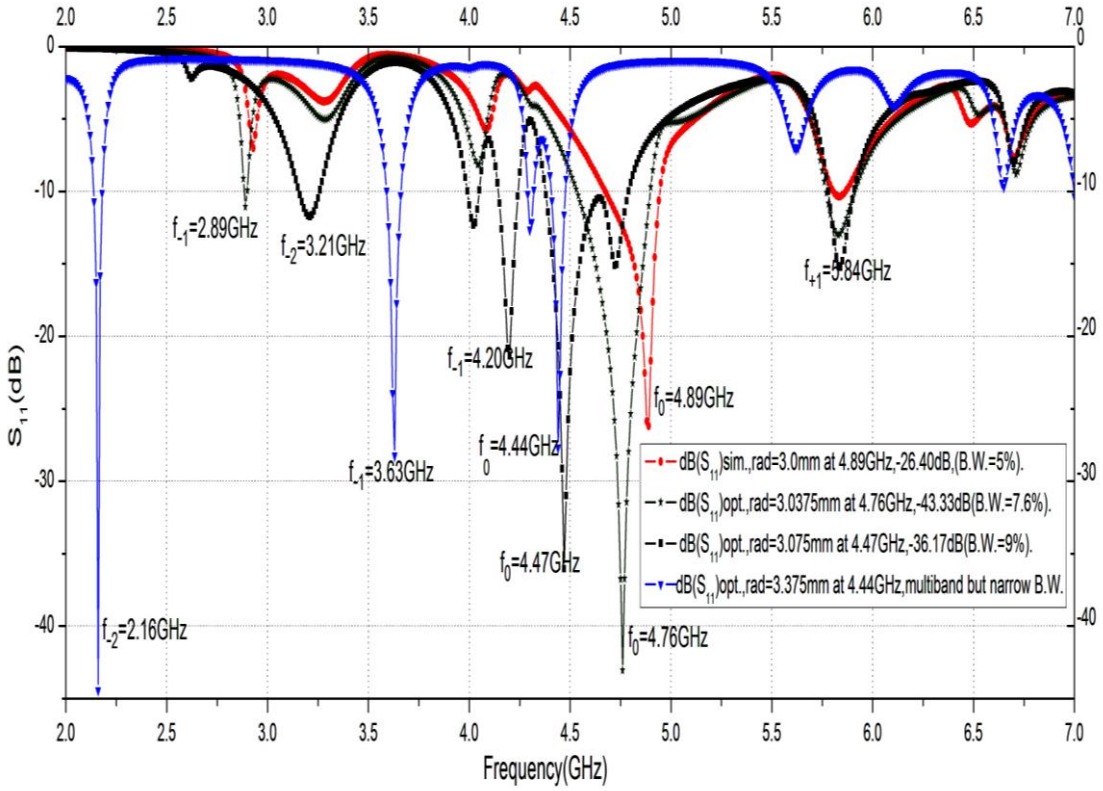

Figure 5.9 (b) Best optimized plot for radius 3mm, 3.075mm, 3.0375mm and 3.375mm obtained from Figure 5.9 (a).

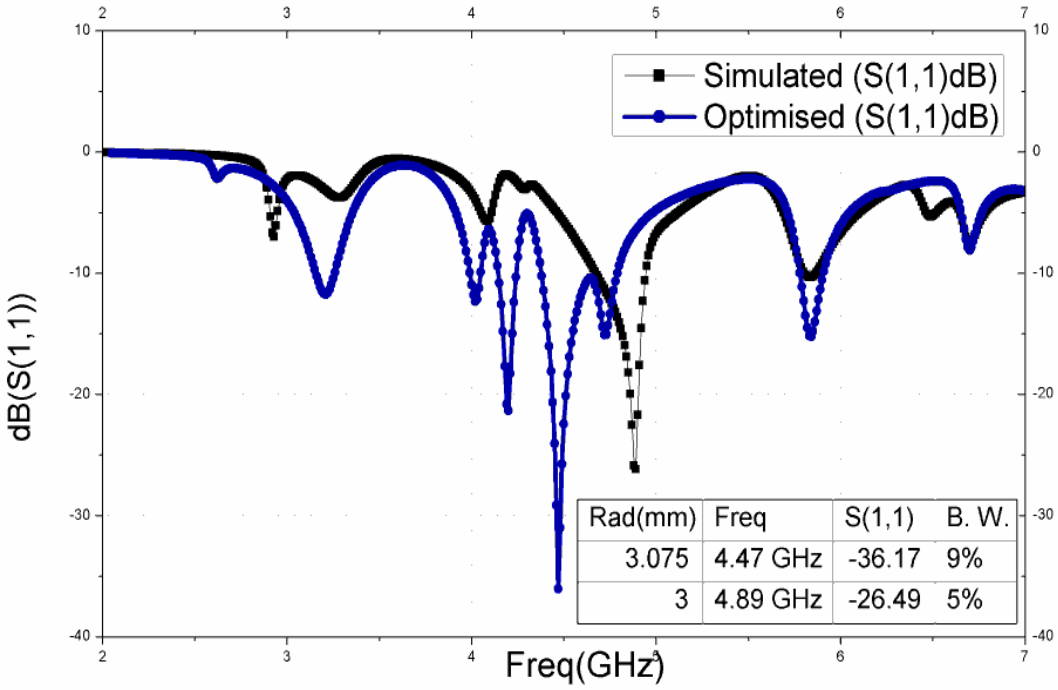

Figure 5.10 Comparison of optimized and simulated reflection coefficient.

Figure 5.11 shows the simulated radiation patterns at E-plane and H-plane and 3D gain pattern at 4.47 GHz for optimal antenna design with minor radius 3.075 mm. A monopolar E-radiation pattern along y-z plane and an omni-directional H-radiation pattern along x-z plane are obtained. A high gain of 3.32 dB with an efficiency of 82.991% is achieved at 4.47 GHz. In Table 5.1, the performance characteristics of the proposed antenna is tabulated.

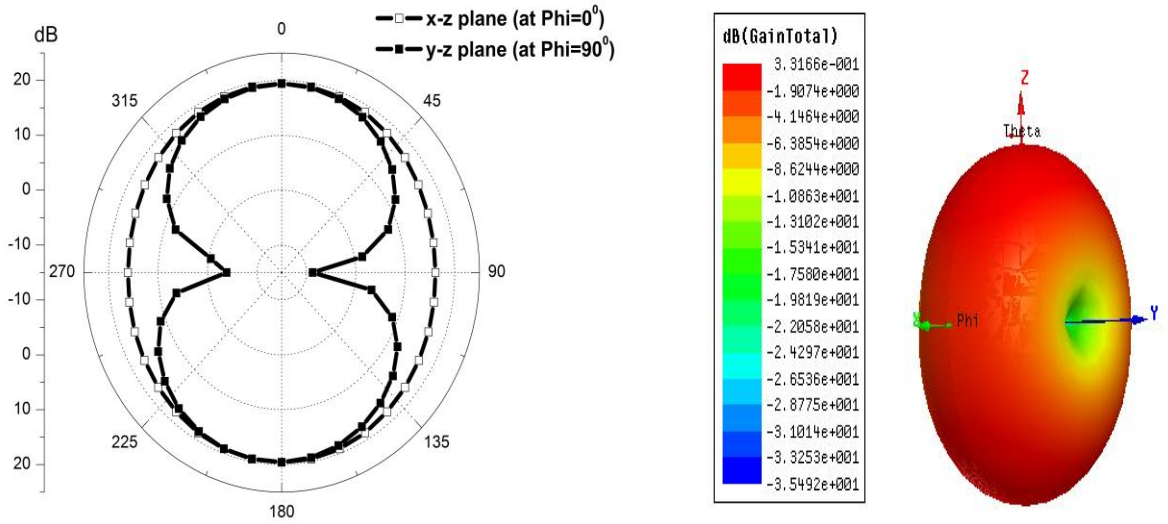

(a) (b)

Figure 5.11 Simulated (a) Radiation patterns and (b) 3D Gain of the proposed antenna at 4.47 GHz for a nominal radius of 3.075 mm.

5.4 Experimental Verification

Figure 5.12 shows the fabricated prototype of the designed antenna. Details of fabrication procedure are mentioned in Appendix A.2. Figure 5.13 shows the comparison of the simulated and measured reflection coefficients of the antenna at 4.89 GHz ((4.65 – 4.97) GHz). A very good agreement between the measured and simulated results is obtained. The slight difference might be due to improper etching and the effect of SMA 50 Ω connectors. Measurements of the proposed antenna are carried out at CUSAT, Kochi, Kerala using Agilent E8363B network analyser.

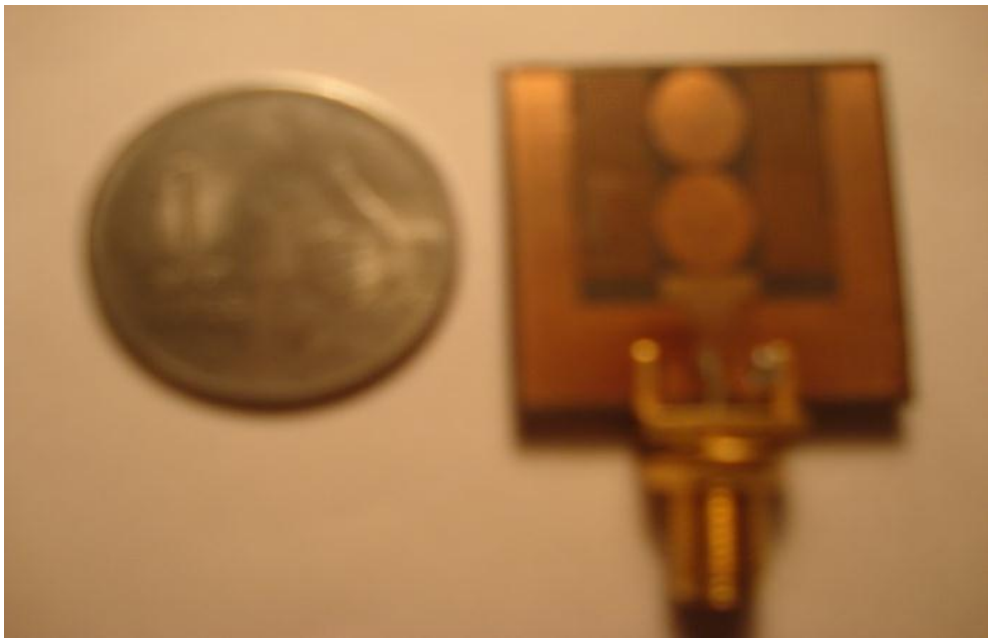

Figure 5.12 Fabricated prototype of the proposed CRLH based Elliptical resonant antenna.

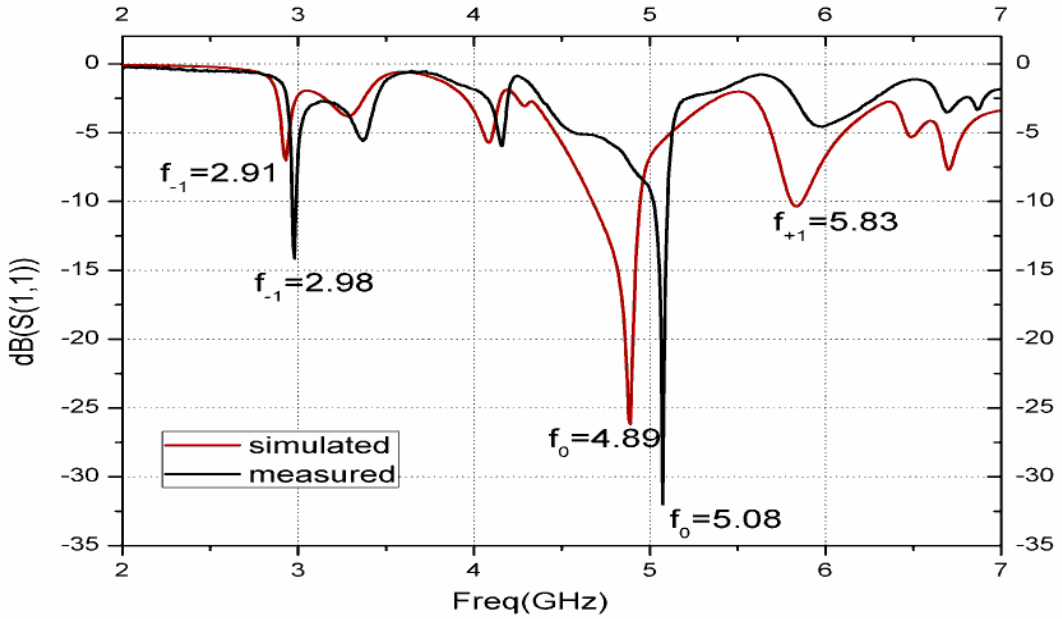

Figure 5.13 Comparison of simulated and measured reflection coefficients of the proposed antenna.

5.4.1 Antenna Gain and Radiation Pattern Measurements

Figure 5.14 shows the measured normalized gain pattern at 2.98 GHz and 5.08 GHz. The measured peak gain of the fabricated antenna at 5.08 GHz is -1 dBi. The gain of the antennas has been measured using Gain comparison method. The experimental setup is similar to the radiation pattern measurement setup. An antenna with known gain is first placed in the antenna positioner and the THRU calibration is done for the frequency range of interest. Standard antenna is then replaced by the AUT and the change in S_{21} is noted. Note that the AUT should be aligned so that the gain in the main beam direction is measured. This is the relative gain of the antenna with respect to the reference antenna. The absolute gain of the antenna is obtained by adding this relative gain to the original gain of the standard antenna.

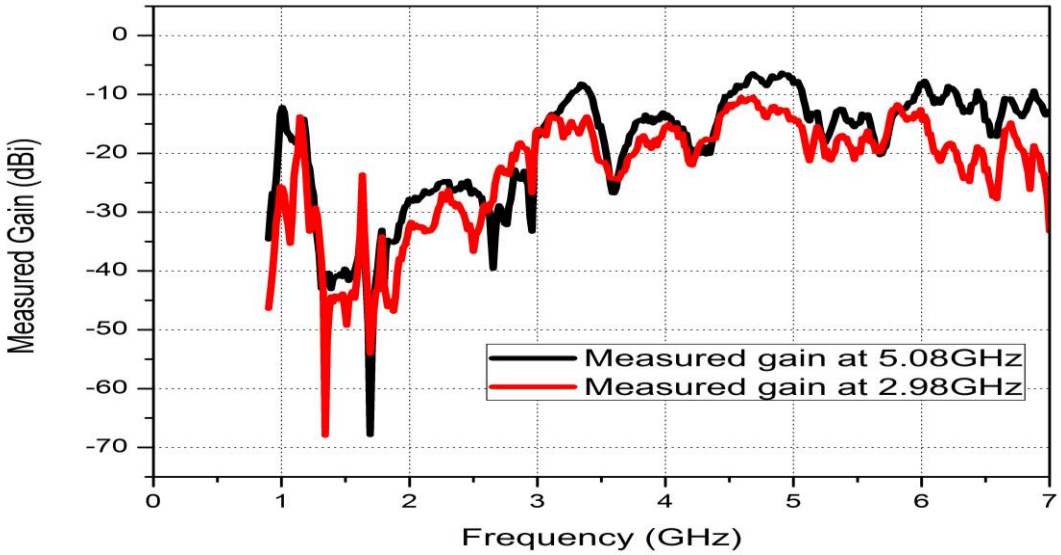

Figure 5.14 Measured normalized gain vs frequency of the proposed antenna at 5.08GHz and 2.98 GHz.

Figures 5.15 and 5.16 show the measured and simulated E-plane (y-z plane) and H-plane (x-z plane) radiation patterns at 5.08 GHz and 2.98 GHz respectively. The test antenna is aligned to a reference wideband horn antenna for radiation pattern measurements. The antenna exhibits a dumb-bell shaped E-radiation pattern and an omni-directional H-radiation pattern at 5.08 GHz and 2.98 GHz. The simulated results are found to be in good agreement with the measured results thus validating the proposed design. The proposed antenna is aptly suitable for IEEE 802.11b/g/n WLAN applications at operational frequencies 2.98GHz and 5.08 GHz.

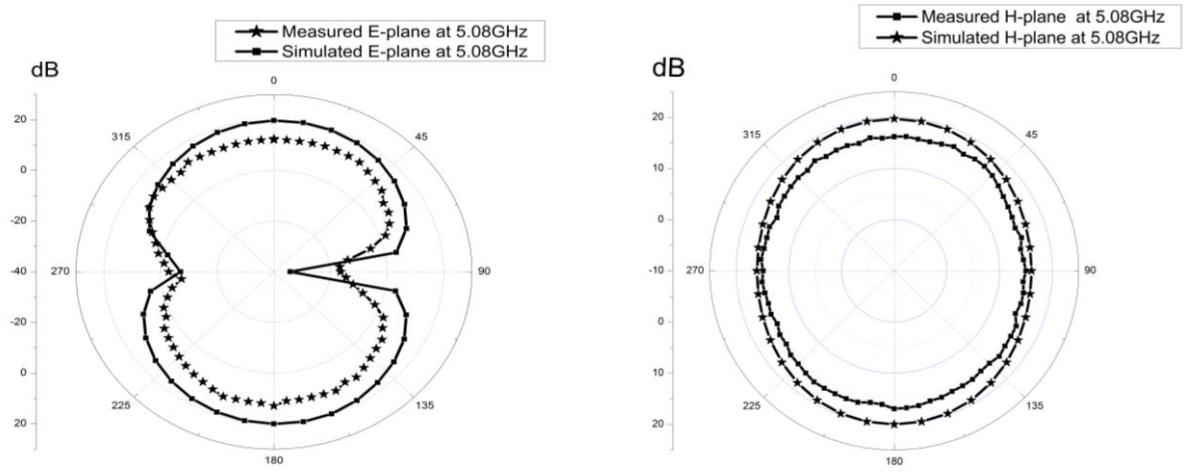

(a) (b)

Figure 5.15 Measured and simulated normalized radiation patterns for (a) E-plane and (b) H-plane at 5.08GHz.

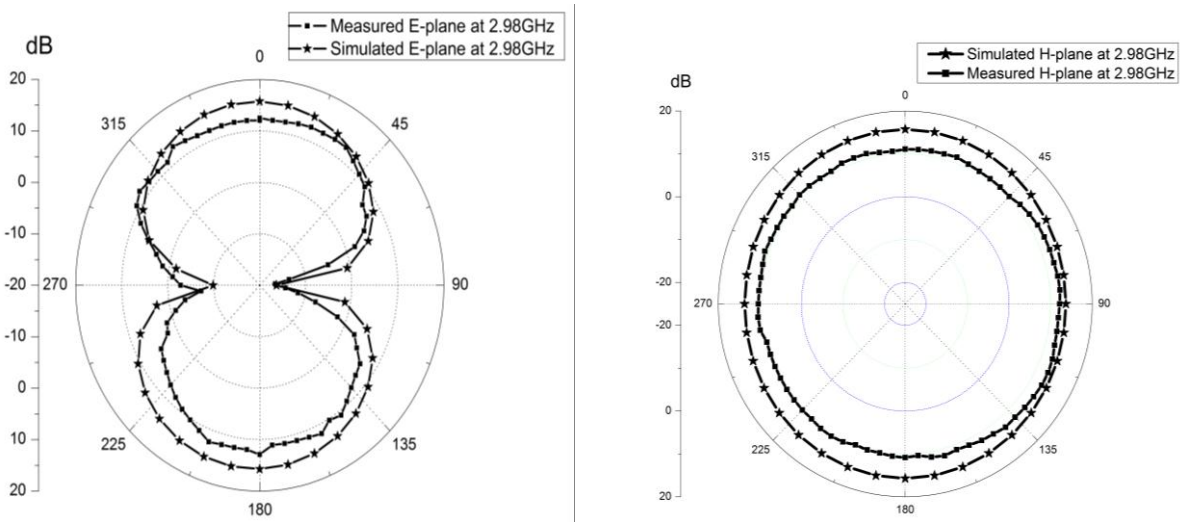

(a) (b)

Figure 5.16 Measured and simulated normalized radiation patterns for (a) E-plane and (b) H-plane at 2.98GHz.

Table 5.1 Comparison of performance characteristics of the proposed CRLH based elliptical resonant antenna at 4.89GHz and 4.47 GHz.

Nominal Radius (mm)	***Frequency (GHz)***	***Bandwidth (%)***	***Maximum Gain(dBi)***	***Efficiency (%)***	***Layers***	***Via process***
3.075	**4.47**(optimal design)	**9**	**3.3166**	**82.991**	**Single**	**Not required**
3.0	**4.89**	**5**	**2.2474**	**83.094**	**Single**	**Not required**

5.5 Summary

A compact, low profile optimized CPW fed ZOR antenna is presented and verified with experimental results. Parametric analysis is used to study the effect of variation in minor radius on the resonant frequency of the frequency independent antenna. The study shows that the zeroth order resonant frequency decreases as the minor radius increases. Through parametric study it is concluded that variation in minor radius can also be used as an extremely suitable element for tuning a given antenna to a desired working frequency. Optimization analysis is then performed on the best parametric result obtained for minimum reflection coefficient and enhanced bandwidth. The open ended antenna presented here is excited by the shunt mode of resonance. The operational frequency is independent of the physical size of the antenna structure, but, is determined by the shunt elements of the unit cell. In this case, the optimized antenna exhibits dumb-bell shaped E- radiation pattern at its fundamental zeroth mode resonant frequency of 4.47 GHz. From the simulated and measured reflection coefficients of the proposed antenna it is found that the measured results varied from the simulated ones at the zeroth order mode by about 0.6% approximately. Good agreement between simulation and experimental data is observed. We achieved the best optimized result with a minor radius of 3.075 mm and 3.0375 mm wherein our objective of enhanced bandwidth of 9% and 7.6% is met. Furthermore, the antenna after designing and optimization; the antenna is analysed and experimentally verified for its performance for IEEE 802.11 standards of wireless LAN applications requiring good radiation characteristics with wide coverage area.

Chapter 6

Conclusion and Future Work

The significant increase in the number of wireless LAN applications with a constraint on component size has made metamaterials an emerging topic of research. An important microwave application of metamaterials is the Zeroth Order Resonator (ZOR) wherein resonance is achieved at the zeroth mode. The major impact of these resonators lies in the fact that its resonance is independent of the physical length of the resonator which makes it theoretically possible to design physically small, multiband resonators with omni-directional radiation characteristic. ZOR antennas notoriously suffer from narrow bandwidth and negative gain. Extremely low gain values do not enable this structure to work efficiently as an antenna. Motivation for this research activity is to explore ways to enhance bandwidth of ZOR antennas without compromising on antenna efficiency and gain. Bandwidth of these resonators depends on the antenna structural design rather than on its material properties. This is the concept that has been used to design the ZOR antenna with extended bandwidth and high gain. New antenna topologies for increasing both bandwidth and gain are presented and proposed (in this study by the finite element method by aid of EM field simulator Ansoft HFSS).

6.1 Conclusion

In this thesis, design of composite right/ left handed based ZOR antennas for WLAN applications has been explored. Simulated results are experimentally verified. A technique for maximizing the bandwidth and gain of a ZOR antenna has been applied to this transmission-line topology. Simulation and measurement results confirm the expected increase in bandwidth and the corresponding gain of the proposed antenna. It is to be noted that it achieves a bandwidth enhancement at the expense of a decrease in gain. This effect has been demonstrated in the maximum-bandwidth ZOR antenna. The work presented in this thesis represents an exploration of a new antenna topology. The goals are to design and realize CRLH-TL based ZOR antennas for bandwidth and gain enhancement and verify their operation through measurement results.

Chapters 2 and 3 are insight into the characteristics of resonant microstrip based CRLH TL antenna structures and lays the foundation for subsequent chapters. One of the major results of this dissertation thesis is the proposal of new types of coplanar waveguide fed zeroth-order mode resonator antennas in chapters 4 and 5. In Chapter 4 the performance of the proposed ZOR antenna is subjected to critical comparison with the reference microstrip fed ZOR monopole antenna shown in Chapter 3. In Chapter 5, methods are implemented to improve the gain of the newly developed CPW fed ZOR antenna structure without compromising on bandwidth and efficiency. Appendix is based on the fabrication technique employed to realize the proposed ZOR antenna structures.

6.2 Limitations

In the present work, slight variations in simulated and measured results are found. Mismatch in measurements may be attributed to fabrication tolerances. Nevertheless some limitations in the present work carried out are

- Influence of both radiation losses and mutual inductance of shunt conductors (spirals and vias) may be taken into account to achieve good input impedance matching.

- Since the CRLH based antenna is a periodic structure consisting of unit cells, this may be regarded as an antenna array where each unit cell represents a CRLH antenna. Several analytical approach such as array factor approach may also be applied to predict radiation patterns of the proposed CRLH based resonant antenna.

6.3 Suggestions for Future Work

Metamaterials can be considered as a transversal topic, involving diverse disciplines and fields, such as acoustics, electromagnetism, RF and microwave engineering, millimeter wave and THz technology, micro and nanotechnology, photonics and optics, and medical engineering, among others. This section will comment on portions of the work presented that could be expanded for future research.

- The work in this doctoral thesis is based on enhancing the bandwidth and gain of zeroth order resonant antennas for wireless LAN applications. In future we may go for higher gain by employing **array configurations**.

- Variations in current topology can be explored including fractal geometries to produce wider bandwidth.

- Use of reactive loadings can be applied to implement frequency or pattern reconfigurability.

- Although still at the prototype stage, LHMs can be efficiently designed, based on the fundamental concepts of Transmission Line theory. This can potentially be applied for optical /microwave applications in Terahertz frequency range.

Appendix A

DESIGN, FABRICATION AND MEASUREMENT OF ANTENNAS

A.1 Techniques for the Design and Optimization of Antennas

This section gives insight into the process involved in the design and optimization of the antennas presented in this thesis are discussed. The ElectroMagnetic simulator used for designing the antennas is the commercial software Ansoft High Frequency Structure Simulator (HFSS). HFSS is the industry-standard simulation tool for 3D full-wave electromagnetic field simulation. HFSS is mainly used in this thesis for evaluating S Parameters, radiation pattern, gain, current distributions, fields, efficiency etc.

A.1.1 High Frequency Structure Simulator

HFSS software automatically generates an appropriate, efficient and accurate mesh for solving the problem using the proven **finite element method (FEM)** (its practical application often known as **finite element analysis** (FEA)) where it is a numerical technique for finding approximate solutions to partial differential equations (PDE) and their systems, as well as (less often) integral equations [102]. This allows solving any arbitrary 3D geometry, especially those with complex curves and shapes, in minimum time. HFSS integrates simulation, modeling, visualization and optimization in a user friendly environment. With adaptive meshing and brilliant graphics HFSS gives an unparalleled performance and complete insight to the actual radiation phenomenon in the antenna. An important and useful feature of this simulator is the availability of different kinds of port schemes such as lumped port, wave port, incident wave scheme etc. The accurate simulation of coplanar and microstrip lines can be done using the port schemes. The parametric set up available with HFSS is highly suitable for an antenna engineer to optimize the desired dimensions.

A.1.2 The Finite Element Method

The Finite Element Method is well-established and widely used for the time-harmonic solution of Maxwell's equations. The unstructured nature of the time domain version of FEM gives a clear advantage over numerical computational methods in modeling complex antenna geometries. FEM is a very powerful tool for solving complex engineering problems, the mathematical formulation of which is not only challenging but also tedious.

The finite element analysis of any problem involves basically four steps [67]:

1. Discretizing the solution region into a finite number of elements
2. Deriving the governing equation for a typical element
3. Assembling of all elements in the solution region, and
4. Solving the system of equations obtained

As mentioned above HFSS uses the FEM technique for the calculation of different parameters. The power behind HFSS lays in the mathematics of the finite element method (FEM) and the integral, proven automatic adaptive meshing technique. In the first step, HFSS divides the geometric model into a large number of small homogeneous pieces or tetrahedral elements (also called as finite elements). The corners of the elements are called nodes. Each tetrahedron is composed of four equilateral triangles and the collection of tetrahedra forms is known as the finite element mesh. This mesh is conformal to the 3-D structure and appropriate for the electromagnetic problem we are solving. The most widely used element for the 3-D electromagnetic problems is the four-node tetrahedron, which is shown in Figure A.1. With HFSS, the physics defines the mesh; the mesh does not define the physics.

The value of a vector field quantity (such as the H-field or E-field) at points inside each tetrahedron is interpolated from those at the vertices of the tetrahedron and/or those at the midpoint of selected edges that are tangential to a face and normal to the edge. A first-order tangential element basis function is used for performing the interpolation. Maxwell's equations are then formulated from the field quantities and are later transformed into matrix equations that can be solved using traditional numerical techniques.As an example, the meshing of a proposed spiral antenna using a tetrahedron in Ansoft HFSS is shown in Figure A.2. FEM is widely used in civil and mechanical engineering to solve material and structural problems. Its major application in electrical engineering is to solve the complex electromagnetic problems such as the antennas.

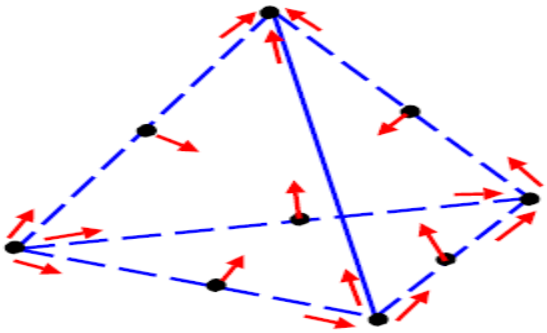

Figure A.1 The tetrahedron element used in finite element analysis.

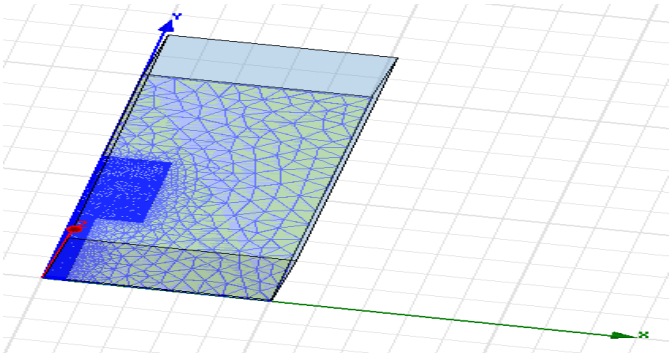

Figure A.2 Meshing of a CRLH based monopole antenna structure in Ansoft HFSS.

FEM has enjoyed a strong interest for electromagnetic analysis. In fact, over the past 10 years, the greatest progress in computational electromagnetic is based on the development and application of partial differential equation (PDE) methods such as the finite difference-time domain (FDTD), finite element (FEM) and methods including hybridizations of these with integral equations and high frequency techniques. The major reasons for the increasing reliance on PDE methods stem from their inherent geometrical adaptability, low memory demand and their capability to model heterogeneous (isotropic or anisotropic) geometries. These attributes are essential in developing general-purpose codes for electromagnetic analysis / design, including antennas and their characterization.

A.2 Antenna fabrication

Global demand for electronic products and the printed circuit boards used to make them continues to rise. Rapid technological advances have permitted the incorporation of more and more functions on ever-smaller printed circuit boards. In addition, improvements in integrated circuit processing have dramatically increased circuit speeds. Both of these phenomena help to fuel the increase in demand for electronic equipment and, in turn, printed circuit boards.

The growth of the electronic equipment industry is driven also by a seemingly insatiable demand for both new and existing products. Examples of new products include interactive multimedia, handheld computers, voice recognition synthesis, image processing, character recognition and artificial intelligence. Coupled with existing products, such as radio, television and computers, these new technologies will demand great quantities of sophisticated electronic equipment and components, including printed circuit boards.

This section provides in-depth information and state-of-the-art technological evaluations for decision making by strategic planners, marketers, forecasters, new product developers, business development managers and presidents in those companies already involved in printed circuit boards, or those companies considering becoming involved in the supply of printed circuit boards to the automotive, business retail, communications, computer, consumer, government/military, industrial electronics and instrumentation markets. Figure A.3 shows the schematic processing flow for fabrication of a single- sided and double-sided (Plated Through Holes).

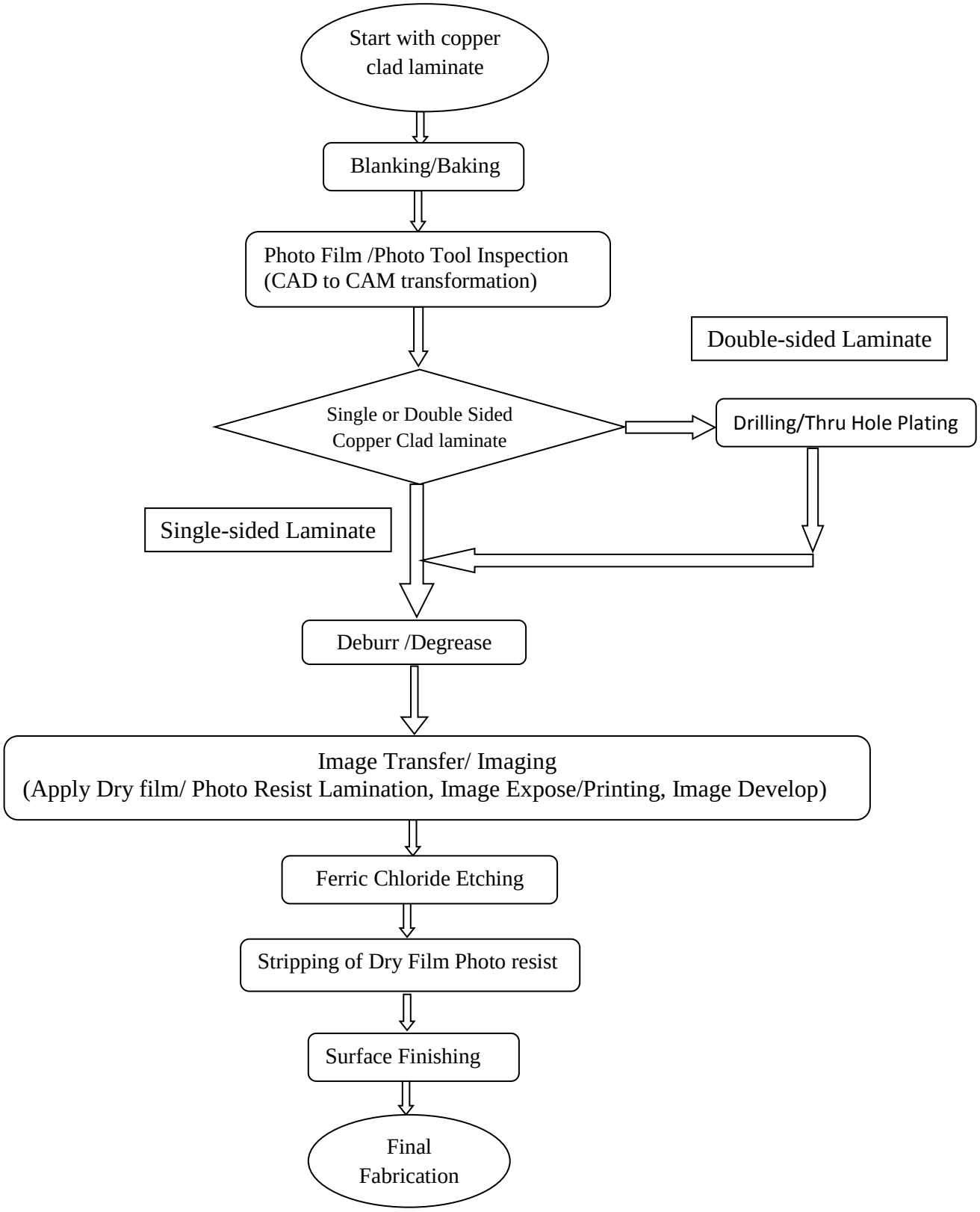

Figure A.3 Schematic showing processing flow for fabrication of a single-sided and double-sided (Plated Through Holes) PCB.

A.2.1 Printed Circuit Board

In hardware terms printed circuit board (PCB) can be defined as a thin board to which electronic components are fixed by solder. Component leads and **integrated circuit** pins may pass through holes ("vias") in the board or they may be surface mounted, in which case no holes are required (though they may still be used to connect different layers).

The simplest kind of PCB has components and wires on one side and interconnections (the printed circuit) on the other. PCBs may have components mounted on both sides and may have many internal layers, allowing more connections to fit in the same board area. Boards with internal conductor layers usually have "plated-through holes" to improve the electrical connection to the internal layers.

The connections are metal strips (usually copper). The pattern of connections is often produced using photo-resist and acid etching. Boards, especially those for high frequency circuits such as modern **microprocessor**s, usually have one or more "ground planes" and "power planes" which are large areas of copper for greater current carrying ability.

A computer or other electronic system might be built from several PCBs, e.g. processor, memory, graphics controller, disk controller etc. These boards might all plug into a **motherboard** or **backplane** or be connected by a ribbon cable.

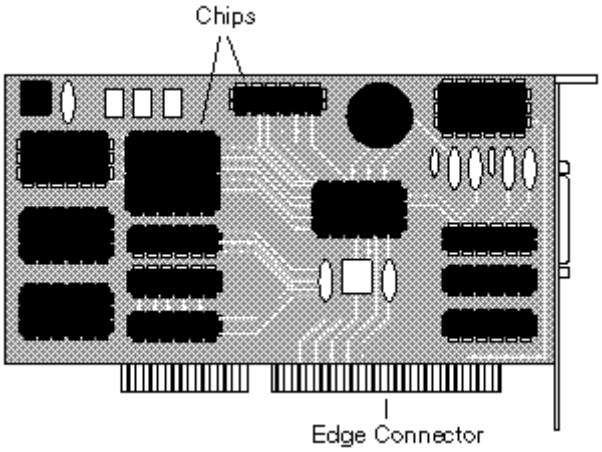

Figure A.4 Printed Circuit Board. *[Courtesy Atlantic Circuits, Hyderabad]*

Sometimes abbreviated *PCB, Printed Circuit Board,* a thin plate on which, **chips** and other electronic components are placed. All the electronic items consist of one or more **boards**, often called **cards** or *adapters*. **Circuit boards** fall into the following categories:

- **Motherboard**: The principal board that has **connectors** for attaching **devices** to the **bus**. Typically, the mother board contains the **CPU**, **memory**, and basic **controllers** for the **system**. On **PCs**, the motherboard is often called the *system board* or *mainboard.*

- **Expansion board**: Any board that plugs into one of the computer's **expansion slots**. Expansion boards include controller boards, **LAN** cards, and **video adapters**.
- **Daughter card:** Any board that attaches directly to another board.
- **Controller board:** A special type of expansion board that contains a controller for a **peripheral device**. When you attach new devices, such as a **disk drive** or graphics monitor, to a computer, you often need to add a controller board.
- **Network Interface Card (NIC):** An expansion board that enables a PC to be connected to a local-area network (LAN).
- **Video adapter:** An expansion board that contains a controller for a **graphics monitor**.
- **Antennas:** Mostly RF Circuits used in wide range of Communication and Defence Related Environments.

Printed circuit boards are also called *cards.*

A.2.1.1 CAD Layout

In order to make a Printed Circuit Board (PCB) with the microstrip antenna on, a mask first need to be made. In order to get an accurate mask, the circuit is first redrawn in AutoCAD. Two patterns need to be drawn, one for each side of the PCB. Furthermore, in order to be able to align the two masks, some markers are added to the design. These markers will later be removed in an intermediate state of the etching production phase. Finally, the two layouts are printed out onto a semi translucent paper.

Printed Circuit Board Types General Description:

1. Single Sided (SS) and Double Sided (DS) circuit boards: A single sided board is made from rigid laminate consisting of a woven glass epoxy or RTD base material clad with copper on one side of varying thickness. Double sided boards are made from the same type of base material clad with copper on two sides of varying thickness. The base material used in this thesis is RT Duroid (RTD) 5880. Double Sided boards are classified as either Double Sided Non Plated Through Hole (DS NPTH) or Double Sided Plated Through Hole (DS PTH).

2. Multi Layer boards (ML): Multi-layer boards are made from the same base material with copper foil on the top and bottom and one or more "inner layer" cores. The number of "layers" corresponds to the number of copper foil layers. Double-sided boards or multi-layer boards use plated-through holes, called **vias**, to connect traces on different layers of the PCB.

3. Multi-Layer Board Fabrication: Multi-layer fabrication begins with the selection of an inner layer core–or thin laminate material (base material) of the proper thickness. Cores can vary from 0.038"to 0.005" thick and the number of cores used will depend upon the board's design. In this thesis core material of thickness 1.6mm is used.

A.2.2 Selection of base materials

Base materials for high performance radiation applications should have low relative permittivity and low dielectric loss to reduce the propagation delay and to increase the signal speed. In addition the materials should have high thermal conductivity for dissipating heat. Other important substrate characteristics include the thickness, homogeneity, isotropicity and dimensional strength of the substrate [5 - 9]. The selection of dielectric constant of the substrate depends on the application of the antenna and the radiation characteristics specifications. High Dielectric constant substrates causes' surface wave excitation and low bandwidth performance. Also as the frequency of operation increases, the loss tangent of the material used for substrates slightly increases, which in turn adversely affects the efficiency of the antenna. Also increasing the thickness of the substrate increases the band width of the antennas at the expense of efficiency owing to increase in surface waves. RT Duroid 5880 substrate with ε_r=2.2 tan δ=.001, h=1.6 mm are used for the study. The final antennas are fabricated on RT Duroid to enhance the antenna efficiency.

Most commonly used base material is FR-4 Grade Glass Epoxy Copper Clad Laminate of indigenous or imported. As it is highly lossy so RTD is preferred.

In General Base Material Thickness (mm) comes in variants of 0.8mm, 1.6mm, 2.4mm and 3.2mm.

Copper Foil Thickness (Microns):

18/0	35/0	70/0	(for Single Sided PCB)
18/18	35/35	70/70	(for Double Sided PCB)

Nowadays Rogers Materials are also widely used in some specific special requirement in Communication and Mostly Defence Sector.

Rogers Materials come in Different Dielectric Constant and Base Material differs accordingly. Some of them are RT Duroid (RTD) 5880, 6006, 6010 etc. The base material used in this thesis is RTD 5880 with a thickness of 1.6mm.

A.2.3 Photo Films Inspection: The Gerber or electronic Computer Aid Design (CAD) software data for the artwork is transformed into customized tools namely photo tools or photo films that depict the traces and pads of the board's design. The photo tools or artwork includes solder mask and legend or nomenclature (fine text) as well as the copper features. This film is then used to place an image on the resist. Proper contact, exposure, emulsion to emulsion, clear glass/ mylar, proper vacuum, no tape dirt etc. is ensured. Edge definition of hoarders, nomenclature identification, and circuit all should have clean ragged edges because ragged edges can cause small piece of polymerized photo resist, which gets displaced and re deposited.

A.2.4 Blanking and Baking: In **blanking** process, the copper clad sheets will be cut to proper sizes as required. If it is single side, blanks will be cut to the correct size and if it is double side (PTH) blanks will be cut to extra size i.e. minimum10mm will be added to each side.

In the process of **baking** the PCB blanks, cut blanks will be kept in the hot air oven for half an hour at 100^0C and then they will be cooled to room temperature and passed on to qc for inspection. For processing of single side PCB's single sided blanks will be sent to screen printing section for circuit print and for double sided PCB's blanks, along with the drill entry (0.25 aluminum) and 1.5mm drill back up sheets, are passed on to drilling section. Drilling for smaller volumes are undertaken by optical pneumatic drilling machine and for higher volumes will done by CNC drilling machine.

A.2.5 Thru hole plating process: The interconnection between the signal trace and the ground lane is done by plating thruholes. In this process, an electrographic film (e.g. Activator-444) is electroplated to the wall of the drill cavity, this allows for galvanisation with copper to occur at a later stage. Activator 444 is a palladium based catalyst in electroless copper plating system for printed circuit boards thru-hole plating. Activator 444 has small particle size of palladium / tin colloid that gives better ability to cover hole surface topography and better adhesion of electroless copper. It has high copper tolerance (upto 5000 ppm) and long bath life.

A.2.6 Degreasing and Deburring: Deburr is an abrasive mechanical process that removes the raised edges of the metal or burrs surrounding the holes that occur during the drilling process. Any debris that may be left in the holes is also removed at this time. Because PCB's must be completely free of grease and dust, they are subjected to rigorous cleaning (e.g. by degreasing and deburring) before proceeding to the next stage.

Laminate Surface Preparation

Copper surface plays a major role in the success or yield of the image transfer process. It demands that the surface should be carefully inspected for pits, drilling burns and any other types of irregularities. So the boards are pre-cleaned and dried. If unacceptable defects are observed, the image transfer process should not be carried out further and the defective material should be rejected straightaway. So, for the image transfer to take place, the cleaning of the copper surface prior to resist application is an essential step for any type of PCB process. The boards are then heated to 50^0C-60^0C in hot air circulation oven for 10-15 minutes.

A.2.7 Image transfer: Image transfer basically involves the transfer of the conductor pattern from the photo film master on to the copper clad base material or any other metal clad laminate. In the fabrication of the PCB, the two methods common for image transfer are:

Photo printing method and Screen printing method.

- Photo Printing: This is an extremely accurate process, which is generally applied to the fabrication of semiconductors and integrated circuits wherein the conductor widths are typically in the region of a few microns. Although such a precision technique is not required in the production of general purpose PCBs but for professional applications, we resort to the photo printing process.
- Screen Printing: Although less precise than the photo printing process, screen printing is a comparatively cheap and simple method. The majority of PCB's produced worldwide are screen printed. In our case we used this method for the fabrication of PCB.

Imaging / Image Transfer for single sided PCB's using Screen Printing process: This process includes three steps: photo resist application, exposing (or printing) and developing.

a) Dry film resist / Photo resist application: Photo resists are available as a dry film and are usually sold in rolls ranging from 2 in. to 60 in. wide and 125 ft. to 1,000 ft. long. It is applied with heat and pressure to the surface of the panel. Photo resist was done at $100^0 C \pm 5^0 C$ at 1.0 to 1.5 Mt. / min and air pressure was set to 1.5-2.0 Bar. This can be done with a hot-roll or cut sheet laminator.

b) Image Expose (or printing): Printing is done by aligning the film phototool between the panel to image and a high intensity UV light source (3.0 kW) for 30secs each respectively for negative and positive print using screen printing method. Clear areas or exposed area of the photo tool allow light to pass through and polymerize (harden) the film resist thus creating an image of the circuit panel (similar to a negative of a photograph). The exposed PCB's are then held for (15-20) min. before being developed in a conveyorised developing machine.

c) Image Develop: Image developing is performed in a developer solution (consisting of water-1000 cc, sodium carbonate -100 gms (1% -2%), antifoam-10-15 ml) at 30º C. The developer removes the resist from the unexposed areas (those which were under opaque areas of the photo tool), revealing the copper layer underneath whereas the exposed (clear areas) polymerized areas remain intact. The board is then rinsed with water and dipped in 10% sulphuric acid and again thoroughly rinsed with water.

A.2.8 Etching Process: Etching is one of the major steps in the chemical processing of the subtractive PCB process. By this process, the final copper pattern (signal trace) is achieved by selective removal of all the unwanted copper (areas not covered by the dry film resist) to retain the desired antenna patterns. The copper which is not protected by an etch resist is removed by the etching process. Etching is performed with conveyorized equipment that typically includes a main spray chamber, an etchant flood rinse, and several cascading water rinses. Long conveyorized units that include developing, etching, and film stripping are common only in large production shops.

The conveyor speed was set to achieve complete etching in one feed. Free rotation of rollers and blocked nozzles are checked. Adequate water spray was ensured. Etchant (ferric chloride solution) sprayed onto the surface of the panel removes the exposed copper, but cannot significantly dissolve the copper residing under the resist. In this way, a copper circuit is formed. The etching should be uniform throughout the circuit board. Any left out copper at edges, should be removed by hand etching. The boards are then cleaned thoroughly under running water. The etched boards are dipped in 5% HCl solution before being rinsed with water.

The antenna is produced on a single sided PCB. The dielectric chosen was a 1.6mm RTD 5880. The pattern of the antenna and the ground plane were first printed on translucent paper, where black areas represent areas that are supposed to be metal. Then, these two patterns are placed around the PCB and put inside a UV under perfect vacuum exposure unit for 45-50 sec (5 kW), where a vacuum is used to ensure the patterns and PCB is in close contact. Then, the UV light will shine through the unpainted parts of the translucent paper and expose the photo sensitive layer of the PCB. Afterwards, the exposed parts are then washed away with a NaOH (150 gms Sodium hydroxide / 1000cc water) solution, allowing for some last adjustments to be done before the metal is etched away. For example, the boards were inspected thoroughly for cuts, shorts, under etch/over etch, plated through hole (PTH) failures etc. Finally, the board is put inside the etching machine, which removes all uncovered metal areas and results in the final product.

A.2.9 Resist stripping of dry film or printing ink: The photoresist is stripped after etching. Stripping was done as a batch process in a stripping tank. The etched boards are dipped in sodium hydroxide ((150 gms NaOH / 1000cc water) solution for 5-10 min. The boards were then removed and cleaned with water and dried. The final fabricated PCB thus obtained is then inspected thoroughly for cuts, shorts, under etch/over etch, plated through hole (PTH) failures etc. The various steps involved in the fabrication process are illustrated in Figure A.3

A.3 Antenna Measurements

One of the most important things to achieve after the antenna is designed and fabricated is an accurate characterization of the antenna concerned. This section deals with the techniques used for the accurate measurement of antennas under study.

A.3.1 E8363B Programmable Network Analyzer (PNA)

The microwave PNA Series instruments are integrated vector network analyzers equipped with a built-in S-parameter test set, synthesized source, hard and floppy disk drives, and LCD display. The Agilent E8363B Vector Network Analyzer is a member of the PNA Series Network Analyzer platform and provides the combination of speed and precision for high frequency measurements [103]. The operation range is from 10 MHz to 40 GHz. For antenna measurements it provides exceptional results with more points and faster measurement speed. It has 16,001 points per channel with < 26 μsec /point measurement speed and 32 independent measurement channels. Windows operating system and user interface mouse

makes measurement procedure much easier. Embedded help system with full manual, extensive measurement tutorials, and complete programming guide helps to carry out accurate measurement of antenna characteristics promptly.

A.3.2 Reflection coefficient and Bandwidth Measurements

The calibration of the port is done for the frequency range of interest using the standard open, short and matched load. The calibrated instrument including the port cable is now connected to the antenna under test. The return loss characteristic of the antenna is obtained by connecting the antenna to any one of the network analyzer port and operating the VNA in S_{11}/S_{22} mode. The frequency for which the return loss value is the minimum is taken as resonant frequency of the antenna. The range of frequencies for which the return loss value is within the -10dB points is usually treated as the bandwidth of the antenna [84]. The bandwidth of an antenna is defined as "the range of usable frequencies within which the performance of the antenna, with respect to some characteristic, conforms to a specified standard". In other words, there is no unique characterization of the bandwidth and the specifications are set to meet the needs of each particular application. The reason for this qualitative definition is that all the antenna's parameters change with frequency. The bandwidth can be the range of frequencies on either side of the center frequency where the antenna characteristics, like the input SWR (equivalent return loss), are confirmed to a specified standard (e.g. SWR=2). For example, the antenna bandwidth is usually expressed as percentage of bandwidth, which is defined as the percentage of the frequency difference over the centre frequency i.e.

$$\%Bandwidth = \frac{f_u - f_l}{f_c} * 100 \qquad \textbf{(}\text{A.1)}$$

Where, f_u denotes the higher-10 dB point, f_l denotes the lower -10 dB point and f_c the centre frequency having the minimum return loss value. At -10dB points, the VSWR is ~2. The above bandwidth is sometimes referred to as 2:1 VSWR bandwidth or -10 dB bandwidth.

A.3.3 Anechoic Chamber

Radiation pattern measurements for the proposed antennas is performed at Space Application Centre, ISRO, Ahmedabad, India in an Anechoic Chamber having size of 13m x 8m x 8m (L x W x H) respectively. It is used for characterizing feed system and electrically small antennas radiation pattern measurement at very low power levels in far field configuration. The Anechoic chamber has a quiet Zone of $1m^3$ and has been designed for the frequency range of 1.0 GHz to 40 GHz. Currently it can cater to the frequency range of up to 60 GHz. This chamber is equipped with an antenna measurement test set up procured from M/s Microwave Instrument Technologies (USA) and M/s Orbit/Fr (Israel). The set up does data acquisition, data analysis, and data presentation as well as data storing. The anechoic chamber is semi shielded and lined with Microwave Absorbers procured from M/s Emerson and Cuming. The anechoic chamber provides a quite zone, free from all types of EM distortions. All the antenna characterizations are done in an Anechoic chamber to avoid reflections from nearby objects. It is a very big room consisting of microwave absorbers fixed

on the walls, roof and the floor to avoid the EM reflections. A photograph of the anechoic chamber along with its axis definition used for the study is shown in Figure A.5.

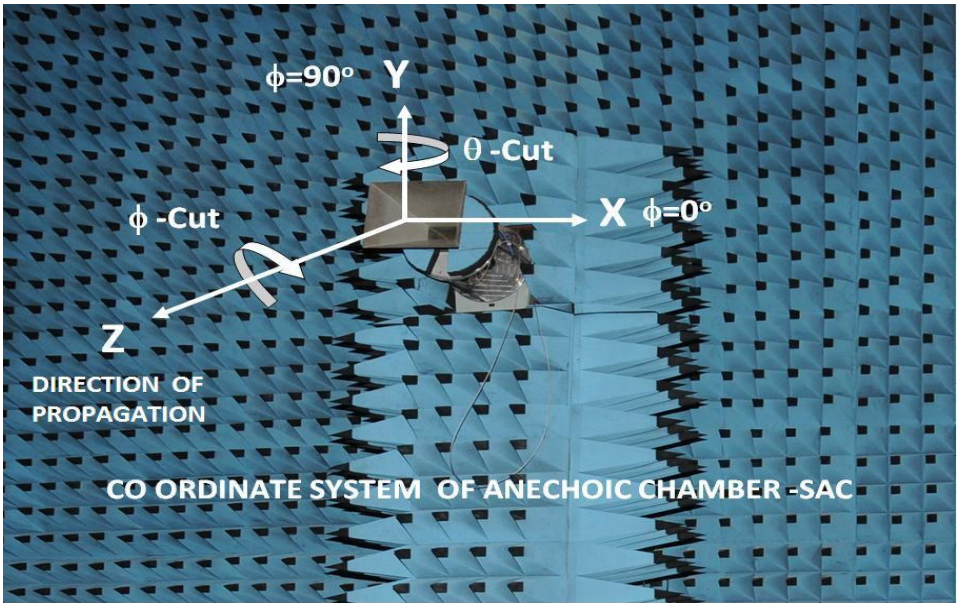

Figure A.5 Photograph showing axis definition in the Anechoic chamber. For clarity, a coordinate system has been superimposed on the picture.

It is equipped with an along-track linear slide to allow the measurement range to be varied from 3.0 to 8.0m. The chamber is shielded using aluminum foil mounted on marine-grade plywood panels and is internally lined with RF absorbers. The AUT and test horn towers are also lined with absorbers to preclude measurement errors. Measurement is performed by an automated acquisition system with a precision test horn radiating down range towards the AUT. A microwave test receiver receives the signal from the AUT which is oriented using an azimuth positioner. For rotating the plane of measurement, both the test horn and the AUT mounts are equipped with a roll positioner. The acquired data may be plotted and/or post-processed with a variety of features. Set up for radiation pattern measurement is shown in Figure A.6.

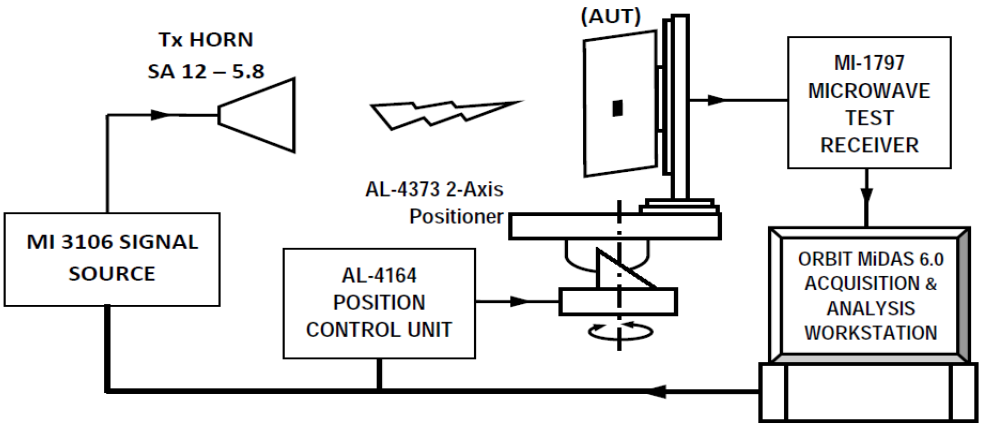

Figure A.6 Set-Up for Radiation Pattern Measurements.

A.3.4 Antenna Pattern Measurement and Gain Measurement

Pattern measurement is the relative power density of the electromagnetic wave transmitted by the antenna in a given direction [82]. Pattern measurement is done to view and validate the radiation pattern of an antenna in far field region of free space. It is accomplished keeping in mind the radiation pattern expected of an antenna, and the simulated and measured results are compared for accuracy and similarity based on the application desired. Radiation pattern of an antenna is defined as "a mathematical function or a graphical representation of the radiation properties of the antenna as a function of space coordinates, which in most cases is determined in the far field region and is represented as a function of directional coordinates" [82, 85]. Thus to measure the radiation pattern, the Antenna Under Test (AUT) is kept in the far field range for that antenna. The Far-Field measurements can be performed in outdoor or indoor ranges. In general, there are two basic types of Far-Field antenna ranges: reflection and free space ranges. In the reflection range, we create in the region of the AUT, a constructive interference between the direct rays from the transmitting antenna and the specular reflection from the ground. In the free space ranges the reflections from the ground are minimized. There are three different types of free space ranges:

- Elevated Ranges,
- Slant Ranges and
- Compact Ranges.

The measurement type used for measuring the AUT in this thesis is the Compact Far Field Test Range measurements. Gain is one of the most important parameters to define the performance of an antenna. Gain of an antenna (in a given direction) is defined as the ratio of the intensity in a given direction, to the radiation intensity that would be obtained if the power accepted by the antenna were to be radiated isotropically [85].

$$Gain = 4\pi \frac{RadiationIntensity}{TotalInputPower} \tag{A.2}$$

Gain measurement is thus important as it is related to both efficiency and directivity of the antenna. Gain calculation in simulation of AUT is straight forward and most of the new tools do it while simulating the antenna, but in measurement for an AUT it can be only done after the pattern measurement is done and the highest amplitude values are known. Two of the methods used to do gain measurement for an AUT are:

- Gain Comparison Measurement,
- Direct Gain Measurement.

The reported antenna gain is 4π times the ratio of the power radiated per unit solid angle in that direction to the net power delivered to the antenna by a 50Ω generator. The gain of the antennas used in this thesis has been measured by using Gain comparison method. The experimental setup for determining the gain is similar to the radiation pattern measurement setup. The measurement is performed in a free space. The gain of the AUT is measured relative to the power levels detected by a known reference antenna. Reference antenna used

here is a standard Horn antenna. In order to measure the gain of AUT, the standard horn antenna is mounted on the turntable and a thorough calibration is performed at bore sight direction. The AUT is carefully mounted over the turntable and extreme care is taken for the exact alignment. The relative power level is obtained from the analyzer and this provides the gain relative to the standard antenna. The gain of the standard antenna is added to the relative gain to obtain the gain of the AUT. The gain measurement method basically based on Friis transmission formula as given by Equation (A.3) [82].

$$(G_t + G_r)_{dB} = 20\log_{10}\left(\frac{4\pi R}{\lambda} + 10\log_{10}\left(\frac{P_r}{P_t}\right)\right) \tag{A.3}$$

where,

$(G_t)_{dB}$ = gain of the transmitting antenna (dB),
$(G_r)_{dB}$ = gain of the receiving antenna (dB),
P_r = received power (W),
P_t = transmitted power (W),
R = antenna separation (m),
λ = operating wavelength (m).

If the transmitting antennas and the receiving antennas are equal, $((G_t)_{dB} = (G_r)_{dB})$ then the Equation (A.3) can be written as

$$(G_t + G_r)_{dB} = (G_r)_{dB} = 10\log_{10}\left(\frac{4\pi R}{\lambda} + 10\log_{10}\left(\frac{P_r}{P_t}\right)\right) \tag{A.3}$$

By measuring R, λ and $\frac{P_r}{P_t}$, the gain of the antenna can be calculated from Equation (A.3).

Bibliography

1. N. Herscovici, Z. Sipus and P. S. Kildal, "The Cylindrical Omnidirectional Patch Antenna," *IEEE Trans. Antennas Propagat.*, vol. 49, no.12, pp.1746-1753, 2001.

2. R. Porath, "Theory of miniaturized shorting-post microstrip antennas," *IEEE Transactions on Antennas and Propagation*, vol. 48, no. 1, January 2000, pp. 41-47.

3. J. H. Lu and K. L. Wong, "Slot-loaded meandered rectangular microstrip antenna with compact dual frequency operation," *Electronic Letters*, vol. 34, May 1998, pp. 1048-1050.

4. D. H. Schaubert, D. M. Pozar and A. Adrian, "Effect of microstrip antenna substrate thickness and permittivity," *IEEE Transactions on Antennas and Propagation*, vol. 37, no. 6, June 1989, pp. 677-682.

5. D. Sievenpiper, L. Zhang, R. Broas, N.G. Alexopolous, and E. Yablonovitch, "High impedance electromagnetic surfaces with a forbidden frequency band," *IEEE Transactions on Microwave Theory and Techniques*, vol. 47, no. 11, Nov. 1999, pp. 2059–2074.

6. R. A. Shelby, D. R. Smith, and S. Schultz, "Experimental verification of a negative index of refraction," *Science*, vol. 292, 2001, pp. 77-79.

7. J. B. Pendry, A. J. Holden, D. J. Robbins, W. J. Stewart, "Magnetism from conductors and enhanced nonlinear phenomena," *IEEE Transactions on Microwave Theory and Techniques*, vol. 47, No. 11, Nov 1999, pp. 2075-2084.

8. A. Grbic and G. V. Eleftheriades, "Overcoming the diffraction limit with a planar left-handed transmission lines," *Physical Review Letters*, vol. 92, no. 11, March 2004, pp. 117 403 1 – 117 4034.

9. C. Caloz and T. Itoh, *Electromagnetic Metamaterials: Transmission Line Theory and Microwave Applications*, John Wiley &Sons, Piscataway, New Jersey, 2006.

10. G. V. Eleftheriades and K. G. Balmain, *Negative Refraction Metamaterials: Fundamental Principles and Applications*, IEEE Press-John Wiley & Sons, New York, 2005.

11. R. W. Ziolkowski, P. Jin and C.-C. Lin, "Metamaterial-Inspired Engineering of Antennas," *Proc. IEEE*, 99, 10, 2011, pp. 1720-1731.

12. John D Kraus and Ronald J Marhefka, Antennas and Wave propagation, Tata McGraw Hill, 2010.

13. Tapan K Sarkar, "History of Wireless", John Wiley and Sons.

14. Binu Paul, *Development and Analysis of microstrip antennas for dual band microwave communication*. Ph.D Thesis, Cochin University of Science and Technology.

15. Sujith R, *Design and development of compact coplanar waveguide fed antennas for wireless applications*. Ph.D Thesis, Cochin University of Science and Technology.

16. IEEE-SA. IEEE 802.11n-2009-Amendment 5: Enhancements for Higher Throughput. Technical report, 2009.

17. Qualcomm: http://qualcomm.com/technology, Retrieved 30 August 2011.

18. Motorola. Long Term Evolution (LTE). Technical report, Retrieved 12 August 2011.

19. Qi Luo, *Design synthesis and miniaturization of multiband and reconfigurable microstrip antenna for future wireless applications*. Ph.D. Thesis. FEUP, Porto, Portugal, 2012.

20. Ge, Y., K. Esselle, and T. Bird, "Compact triple-arm multiband monopole antenna," Proc. IEEE Int. Workshop: Antenna Technology Small Antennas and Novel Metamaterials , 172-175, March 2006.

21. T. H. Lam, M. J. Milicic Jr and D. M. Pritchett, "Dipole Antenna having Co-axial Radiators and Feed," U. S. Patent 5 387 919, Feb. 7, 1995.

22. T. E. Koscica and B. J. Liban, "Simplified Stacked Dipole Antenna," U. S. Patent 6 014 112, Jan. 11, 2000.

23. Kuo, Y. L. and K. L. Wong, "Printed double-T monopole antenna for 2.4/5.2 GHz dual-band WLAN operations," IEEE Trans. Antennas Propag. , Vol. 51, No.9, 2187-2192, 2003.

24. Eleftheriades, G. V., A. Grbic, and M. Antoniades, "Negative- refractive index transmission-line metamaterials and enabling electromagnetic applications," IEEE Antennas and Propagation Society Int. Symp. Digest, 1399-1402, June 2004.

25. Erentok, A. and R. W. Ziolkowski, "Metamaterial-inspired efficient electrically small antennas," IEEE Trans. Antennas Propag., Vol. 56, No. 3, 691-707, 2008.

26. Malik, J. and M. V. Kartikeyan, "A stacked equilateral triangular patch antenna with Sierpinski gasket fractal for WLAN applications," Progress In Electromagnetics Research Letters, Vol. 22, 71-81, 2011.

27. L.-M. Si and X. Lv, "CPW-fed multi-band omni-directional planar microstrip antenna using composite metamaterial resonators for wireless communications," Progress In Electromagnetics Research, Vol. 83, pp.133-146, 2008.

28. Seol, K., Jung, J., and Choi, J., "Multi-band monopole antenna with inverted U-shaped parasitic plane," Elect. Lett., vol.42, No. 15, pp. 844–845, 2006

29. Dahele, J. S., K. F. Lee, and D. P. Wond, "Dual frequency stacked annular ring microstrip antenna," IEEE Trans. Antennas Propag., Vol. 35, 1281-1285, 1987.

30. Long, S. A. and M. D. Walton, "A dual frequency stacked circular disk antenna," IEEE Trans. Antennas Propag. Soc. Int. Symp. Dig., Vol. 27, 270-273, 1979.

31. Sappan, A., "A new broadband stacked two layered microstrip antenna," IEEE Trans. Antennas Propag. Soc. Int. Symp. Dig., Vol. 22, 251-254, 1984.

32. Tan, Y. M., Y. K. Chan, V. C. Koo, and M. T. Islam, "A novel wideband antenna for dual band WLAN application," IEEE International Conference on Communication Systems (ICCS), 97-100, 2010.

33. Behdad, N., Sarabandi, K., "A wide-band slot antenna design employing a fictitious short circuit concept," IEEE Transactions on Antennas and Propagation, vol. 53, No. 1, pp. 475–482, Aug. 2005.

34. Y.-C. Lee and J.-S. Sun, "compact printed slot antennas for wireless dual- and multi-band operations," Progress In Electromagnetics Research, Vol. 88, pp.289-305, 2008

35. Li Zhang, Yong-Chang Jiao; Kun Song and Fu-Shun Zhang, "Compact dual-frequency double t-shaped slot antenna for RFID application," Microwave and Optical Technology Letters, vol 51, No 7, pp. 1755-1757, 2009.

36. C.-J. Wang and S.-W. Chang, "Studies on dual-band multi-slot antennas," Progress In Electromagnetics Research, Vol. 83, pp.293-306, 2008

37. S. M. Zhang, F. S. Zhang, W. M. Li, W. Z. Li, and H. Y. Wu, "A multi-band monopole antenna with two different slots for WLAN and WIMAX applications," Progress In Electromagnetics Research Letters, Vol. 28, pp.173-181, 2012

38. P. Xu, Z. H. Yan, and C. Wang, "Multi-band modified fork-shaped monopole antenna with dual L-shaped parasitic plane," *Electron. Lett.*, Vol. 47, No. 6, 364-365, 2011.

39. Abaga Abessolo, M. A., A. El Moussaoui, and N. Aknin, "Dual-band monopole antenna with omega particles for wireless applications," *Progress In Electromagnetics Research Letters*, Vol. 24, 27-34, 2011.

40. S. C. Kim, S.H. Lee and Y.-S. Kim, "Multi-band monopole antenna using meander structure for handheld terminals," Electronic Letters, vol.44, No. 5, pp. 331–332, 2008

41. IEEE Standard 802.11: "Wireless LAN medium access control (MAC) and physical layer (PHY) specifications," 1997.

42. W. S. Chen and K. Y. Ku, "Band-rejected design of the printed open slot antenna for WLAN/WiMAX operation," IEEE Trans. Antennas Propag., Vol. 56, No. 4, 1163-1169, 2008.

43. W. Hu, Y. Z. Yin, P. Fei, and X. Yang, "Compact triband square-slot antenna with symmetrical L-strips for WLAN/WiMAX applications," IEEE Antennas Wireless Propagat. Lett. , Vol. 10, 462-465, 2011.

44. Song, K., Y. Z. Yin, and B. Chen, "Triple-band open L-slot antenna with a slit and a strip for WLAN/WiMAX applications," Progress In Electromagnetics Research Letters, Vol. 22, 139-146, 2011.

45. Chen, J. S., "Dual-frequency annular-ring slot antennas fed by CPW feed and microstrip line feed," IEEE Trans. Antennas Propag. , Vol. 53, No. 3, 569-571, 2005.

46. Gai, S., Y. C. Jiao, Y. B. Yang, C. Y. Li, and J. G. Gong, "Design of a novel microstrip-FED dual-band slot antenna for WLAN applications," Progress In Electromagnetics Research Letters, Vol. 13, 75-81, 2010.

47. J. C. Bose, "On the rotation of plane of polarization of electric waves by a twisted structure," Proc. Roy. Soc., vol. 63, pp. 146–152, 1898.

48. H. Lamb, "On Group-Velocity," Proc. London Math. Soc., Ser. 2, 1, 1904, pp. 473-479.

49. W. Kock, "Metal-lens antennas," *IRE Proc.*, pp. 828-836, 34 November 1946.

50. W. Kock, ''Metallic delay lenses,'' Bell Syst. Tech. J., Vol. 27, pp. 58-82, 1948.

51. G. Veselago, "The electrodynamics of substances with simultaneously negative values of permittivity and permeability," *Soviet Physics Uspekhi*, vol. 10, no. 4, 509-514, Jan., Feb., 1968.

52. Pendry, J.B, Holden, A.J., Robbins, D.J., Stewart, W.J., "Low frequency plasmons in thin-wire structures," *J. Phys. Condens. Matter*, vol. 10, pp. 4785-4809, 1998.

53. A. A. Houck, J. B. Brock and I. L. Chuang, "Experimental observations of a left-handed material that obeys Snell's Law," *Physical Review Letters*, vol.90, pp. 137-401, April 2003.

54. C. R. Simovski, P. A. Belov and H. Sailing, "Backward wave region and negative material parameters of a structure formed by lattices of wires and split-ring resonators," *IEEE Transactions on Antennas and Propagation*, vol. 51, pp. 2582-2591, October 2003.

55. E. Ozbay, K. Aydin, E. Cubukcu and M. Bayindir, "Transmission and reflection properties of composite double negative metamaterials in free space," *IEEE Transactions on Antennas and Propagation*, vol. 51, pp. 2592-2595, October 2003.

56. R. W. Ziolkowski and A. D. Kipple, "Application of double negative materials to increase the power radiated by electrically small antennas," *IEEE Transactions on Antennas and Propagation*, vo. 51, pp. 2626-2640, October 2003.

57. C. Caloz, H. Okabe, T. Iwai and T. Itoh, "Transmission line approach of left-handed (LH) materials," in proceedings USNC/URSI National Radio Science Meeting, San Antonio, Texas, June 2002, vol. 1. pp.39.

58. A. Sanada, C. Caloz, and T. Itoh, "Planar distributed structures with negative refractive properties," *IEEE Trans. Microwave Theory Tech.*, vol. 52, pp. 1252–1263, Apr. 2004.

59. I. Lin, C. Caloz, and T. Itoh, "A branch-line coupler with two arbitrary operating frequencies using left-handed transmission lines," presented at IEEE-MTT Int. Symp. Dig., Philadelphia, PA, 2003.

60. S. Lim, C. Caloz, and T. Itoh, "Metamaterial-based electronically controlled transmission line structure as a novel leaky-wave antenna with tunable radiation angle and beamwidth," *IEEE Trans. Microwave Theory Tech.*, vol. 52, Dec. 2004.

61. S. H. Lee, C. M. Park, Y. M. Seo, and C. K. Kim, "Reversed Doppler effect in double negative metamaterials", Phys. Rev. B., vol. 81, pp. 241102:1-4, 2010.

62. D. Braaten, R. P. Scheeler, M. Reich, R. M. Nelson, C. Bauer-Reich, J. Glower, G. J. Owen, "Compact Metamaterial-Based UHF RFID Antennas: Deformed Omega and Split-Ring Resonator Structures," *Applied Computational Electromagnetics Society (ACES) Journal*, vol. 25, no. 6, pp. 530-542, June 2010.

63. J. C. Liu, W. Shao, B. Z. Wang, "A Dual-Band Metamaterial Design using Double SRR Structures," *Applied Computational Electromagnetics Society (ACES) Journal*, vol. 26, no. 6, pp. 459-463, June 2011.

64. M. Tang, S. Xiao, D. Wang, J. Xiong, K. Chen, B. Wang, "Negative Index of Reflection in Planar Metamaterial Composed of Single Split-Ring Resonators," *Applied Computational Electromagnetics Society (ACES) Journal*, vol. 26, no. 3, pp. 250-258, March 2011.

65. L. Brillouin. Wave Propagation in Periodic Structures, McGraw-Hill, 1946.

66. J. R. Pierce. Traveling-Wave Tubes, D. Van Nostrand, 1950.

67. S. Ramo, J.R. Whinnery, and T. Van Duzer. *Fields and Waves in Communication Electronics*, Third Edition, John Wiley & Sons, 1994.

68. J. A. Kong. *Electromagnetic Wave Theory*, Second Edition, EMW Pub., 2000.

69. C. Caloz and T. Itoh, "Application of the transmission line theory of left-handed (LH) materials to the realization of a microstrip LH transmission line," in *Proceedings IEEE-AP-S USNC/URSI National Radio Science Meeting*, vol. 2, San Antonio, Texas, pp. 412-415, June 2002.

70. A. Lai, C. Caloz and T. Itoh, "Transmission line based metamaterials and their microwave applications," *IEEE Microwave Mag.*, vol. 5, no., pp.34-50, Sept. 2004.

71. A. A. Oliner, "A planar negative-refractive-index medium without resonant elements," in *URSI Digest, IEEE-AP-S USNC/URSI National Radio Science Meeting*, San Antonio, Texas, June 2002, pp.41.

72. A. Grbic and G. V. Eleftheriades, "A backward-wave antenna based on negative refractive index L-C networks," in *Proc. IEEE-AP-S USNC/URSI National Radio Science Meeting*, San Antonio, Texas, June 2002, vol. 4, pp.340-343.

73. L. Liu, C. Caloz and T. Itoh. "Dominant mode (DM) leaky-wave antenna with backfire-to-endfire scanning capability," *Electron. Lett.*, vol. 38, no. 23, pp. 1414–1416, Nov. 2002.

74. C. Caloz and T. Itoh, "Novel microwave devices and structures based on the transmission line approach of meta-materials", *IEEE-MTT Int'l Symp.*, vol. 1, pp. 195-198, Philadelphia, PA, Jun. 2003.

75. S. Lim, C. Caloz and T. Itoh. "Metamaterial-based electronically-controlled transmission line structure as a novel leaky-wave antenna with tunable radiation angle and beamwidth," *IEEE Trans. Microwave Theory Tech.,*, vol. 53, no. 1, pp. 161–173, Nov. 2005.

76. K. K. Bhan, S. Ghosh, and G. P. Srivastava. "Study of control of beamwidth of radiation pattern of a waveguide using inclined slotted flanges," *IEEE Trans. Antennas Propagat.*, vol. 2, no. 3, pp. 447–450, May 1978.

77. I. A. Korisch and B. Rulf, "Antenna beamwidth control using parasitic sub-arrays," in *Proc. IEEE AP-S Intl. Symp. Dig.*, pp. 117–120, Nov. 2000.

78. L. C. Van Atta. "Electromagnetic reflector," U.S. Patent 2908002, Oct. 1959.

79. S. Lim, C. Caloz, and T. Itoh. "A reflecto-directive system using a composite right/left-handed (CRLH) leaky-wave antenna and heterodyne mixing," *IEEE Microwave Wireless Compon. Lett.*, vol. 14, no. 4, pp. 183–185, April 2004.

80. C. Y. Pon, "Retrodirective array using the heterodyne technique," *IEEE Trans. Antennas Propagat.*, vol. 22, no. 2, pp. 176–180, March 1964.

81. R. Y. Miyamoto, Y. Qian, and T. Itoh. "An active integrated retro directive transponder for remote information retrieval-on-demand," *IEEE Trans. Microwave Theory Tech.*, vol. 49, no. 9, pp. 1910–1919, Sept. 2001.

82. C. A. Balanis. *Antenna Theory, Analysis and Design,* Second Edition, John Wiley & Sons, 1997.

83. D. F. Sievenpiper, J. H. Schaffner, H. J. Song, R. Y. Loo, and G. Tangonan. "Two-dimensional beam steering using an electrically tunable impedance surface," *IEEE Trans. Antennas Propagat.*, vol. 51, no. 10, pp. 2713–2722, Oct. 2003.

84. C. A. Allen, K. M. K. H. Leong, C. Caloz, and I. Itoh. "A two-dimensional edge excited metamaterial-based leaky-wave antenna," *IEEE-MTT Int'l Symp.,* pp. 301–304, June 2004.

85. D. Verba and M. Polivka, "Improvement of the radiation efficiency of the metamaterial zero-order resonator antenna" *Radio engineering",* April, vol. 18, pp. 1-8, 2009.

86. A. Sanada, C. Caloz and T. Itoh, "Zeroth order resonance in composite right/left handed transmission line resonators," in proceedings Asia-Pacific Microwave Conf., vol. 3, pp. 1588-1592, Seoul Korea, 2003.

87. F. J. H. Martinez, V. G. Posadas, F. I. Villacorta and D. S. Vargas, "Low-cost approach based on an eigenfrequency method to obtain the dispersion diagram in CRLH structures", *IEEE Microwave and Wireless Components Letters*, Jan. 2007, vol. 17, no. 1, pp. 13-15.

88. C. Caloz and T. Itoh, " Transmission line approach of left-handed (LH) structures and microstrip realization of a low-loss broadband LH filter," *IEEE Trans. Antennas Propagat.,* vol. 52, no. 5, May 2004.

89. C. Caloz, A. Sanada and T. Itoh, "Microwave applications of transmission-line based negative refractive index structures," *in Proc. Of Asia-Pacific Microwave Conf.,* Seoul, Korea, vol. 3, pp.1708-1713, Nov. 2003.

90. A. Sanada, K. Murakami, I. Awai, C. Caloz and T. Itoh, " A planar zeroth-order resonator antenna using a left-handed transmission line," in proceedings European Microwave Conf., pp. 1341-1344, Amsterdam, Netherlands, April 2004. 2003.

91. A. Sanada, K. Murakami, S. Aso, H. Kubo and I. Awai, " A via-free microstrip left-handed transmission line," *IEEE- MTT International Symposium,* Fort Worth, TX, pp. 301-304, June 2004.

92. C. J. Lee, K. M. K. H. Leong, and T. Itoh, "Composite right/left-handed transmission line based compact resonant antennas for RF module integration," *IEEE Trans. Antennas Propag.*, vol. 54, pp. 2283–2291, Aug. 2006.

93. A. Sanada, C. Caloz, and T. Itoh, "Novel zeroth-order resonance in composite right/left-handed transmission line resonators," in *Proc.Asia-Pacific Microwave Conf.*, Seoul, Korea, Nov. 2003, vol. 3, pp. 1588–1592.

94. A. Lai, K. M. K. H. Leong, and T. Itoh, "Infinite wavelength resonant antennas with monopole radiation pattern based on periodic structures," *IEEE Trans. Antennas Propag.*, vol. 55, no. 3, pp. 868–875, Mar. 2007.

95. F. Qureshi, M. A. Antoniades, and G. V. Eleftheriades, "A compact and low-profile metamaterial ring antenna with vertical polarization," *IEEE Antenna Wireless Propag. Lett.*, vol. 4, pp. 333–336, 2005.

96. C. J. Lee, K. M. K. H. Leong, and T. Itoh, "Broadband Small Antenna for Portable Wireless Application," *iWat*, pp. 10–13, Mar. 2008.

97. J. Zhu and G. V. Eleftheriades, "A compact transmission line metamaterial antenna with extended bandwidth," *IEEE Antenna Wireless Propag. Lett.*, vol. 8, pp. 295–298, 2009.

98. A. Lai, C. Caloz, and T. Itoh , "Composite right/left-handed transmission line metamaterials," *IEEE Microwave Mag.*, vol. 5, no. 3, September", pp. 34–50, 2004.

99. T. Jang, J. Choi and S. Lim, "Compact Coplanar Waveguide (CPW)-Fed Zeroth-Order Resonant Antennas With Extended Bandwidth and High Efficiency on Vialess Single Layer," *IEEE transactions on antennas and propagation,* vol. 59, no. 2, 363-372, February 2011.

100. S. Jenei, B. K. J. C. Nauwelaers and S. Decoutere, "Physics-based closed form inductance expression for compact modelling of integrated spiral inductors," *IEEE Journal of Soild-State Circuits*, January2002, vol. 37,no. 1,pp. 77-80.

101. M. E. Goldfarb and R. A. Pucel, "Modeling via hole grounds in microstrip," *IEEE Microwave and Guided Wave Letters*, June 1991, vol. 1, no. 6, pp. 135-137.

102. Agilent High-Frequency Structure Simulator User's Guide, 2000.

103. http://www.home.agilent.com

Dissemination of the Work

RESEARCH PUBLICATIONS IN REFEREED JOURNALS:

1. Sheeja K.L., S.K. Behera and P.K. Sahu, "***Bandwidth Improvement of a Zeroth Order Resonant Antenna for WiMax Applications***", *International Journal of RF and Microwave Computer-aided Engineering*, vol. 22, no. 4, pp. 569-574, July 2012, DOI 10.1002/mmce. 20647.

2. Sheeja K.L., P. K. Sahu, S. K. Behera and Nabil Dakhli, "***Compact Triband Metamaterial Antenna for Wireless Applications***", *Applied Computational Electromagnetics Society (ACES) Journal*, vol. 27, no. 11, pp. 947 – 955, Nov. 2012.

3. Sheeja K.L., P.K. Sahu and S.K. Behera, "***Design and Optimization of a Zeroth Order Resonant antenna along with Experimental Verification for Wireless Applications***", *International Journal of Signal and Imaging Systems Engineering (IJSISE),* Inderscience Publishers. (**Online Published July, 2012**)

RESEARCH PUBLICATIONS IN CONFERENCES

[1] **Sheeja K.L.,** P.K. Sahu and S.K. Behera**, "*Modeling of Zeroth Order Resonant Antennas for Multiband Wireless Applications",*** 6th annual conference ATMS India-2013, 11th -13th Feb., Kolkata, India, 2013. (**Best Paper Award**)

[2] **Sheeja K. L.**, P. K. Sahu, S. K. Behera and Nabil Dakhli, "***Compact pentamode, tri-band metamaterial antenna for wireless applications***", IEEE International Symposium on Antennas and Propagation and USNC/URSI Radio Science Meeting, **Chicago, Illinois**, **USA**, July 8th – 14th, 2012. (**DST Funded**).

[3] **Sheeja K. L.** and P. K. Sahu, "***CPW fed Eliptical zeroth order resonant antenna for WiMax applications***", IEEE International Symposium on Antennas and Propagation and USNC/URSI Radio Science Meeting, **Chicago, Illinois, USA**, July 8th – 14th, 2012. (**DST Funded**).

[4] **Sheeja K.L.**, P.K. Sahu and S.K. Behera, "***A bandwidth enhanced elliptical metamaterial antenna***", Progress in electromagnetic research symposium (PIERS), Kaula Lumpur, Malaysia, March 27th – 30th, 2012.

[5] Chandra Kandula, P.K. Sahu , P. Panda and **Sheeja K.L.**, "***Micro Strip Line Fed I-shaped Dielectric Resonant Antenna for Millimeter Wave Applications***", Progress in electromagnetic research symposium(PIERS), Kaula Lumpur, Malaysia, March 27th – 30th, 2012.

[6] **Sheeja K.L.**, P.K. Sahu and S.K. Behera, "***Comparative study of a CRLH TL based zeroth order resonant antenna***", 18th national conference on communications (NCC), IIT Kharagpur, Kolkata , India, Feb.3rd – 5th , 2012.

[7] **Sheeja K.L.**, P.K. Sahu and P. Panda, "***Elliptical antenna based on zeroth order resonance****",* 5th annual conference ATMS India-2012, 2nd -3rd Feb., Mumbai, India, 2012.

[8] **Sheeja K.L.**, S.K. Behera, P.K. Sahu, "***Electromagnetic parameter retrieval of a Split Ring Resonator****",* International Conference on Electronic Systems(ICES-2011), N.I.T. Rourkela, Orissa Jan 7th -9th, 2011.

[9] **Sheeja K.L.**, P.K. Sahu, G. Gangadhar and S.K. Behera ***"Parametric Retrieval of a Split Ring Resonator metamaterial****",* International Conference on Microwaves, Antenna, Propagation and Remote sensing (ICMARS-2010), Jodhpur, Rajasthan, Dec14th –17th , 2010.

[10] **Sheeja K.L.** and P.K. Sahu, *"****Decision feedback equalization using RBF networks and MLP****",* 2nd Vaagdevi international conference on information technology for real world problems (IEEE VCON' 2010), Warangal, Andhra Pradesh Dec.9th – 11th, 2010.

[11] **Sheeja K.L.**, Nabil Dakhli, P.K. Sahu and S.K. Behera, "***Resonant Antenna based on CRLH TL***", 13th international conference on Mathematical Methods in Electromagnetic Theory, (MMET-10), Kyiv, Ukraine, Sept 6th – 8th, 2010.
